ARMY RESEARCH LABORATORY

Rechargeable Lithium Battery with Solid Electrolyte

D. Peramunage
D. M. Pasquariello
K. M. Abraham

ARL-CR-269 May 1996

prepared by
EIC Laboratories, Inc.
111 Downey Street
Norwood, MA 02062
under contract
DAAL01-93-C-3355

NOTICES

Disclaimers

The findings in this report are not to be construed as an official Department of the Army position, unless so designated by other authorized documents.

The citation of trade names and names of manufacturers in this report is not to be construed as official Government endorsement or approval of commercial products or services referenced herein.

REPORT DOCUMENTATION PAGE

Form Approved
OMB NO. 0704-0188

1. AGENCY USE ONLY (*Leave Blank*)	2. REPORT DATE	3. REPORT TYPE AND DATES COVERED
	May 1996	Final Report: Apr 93 to Jul 95

4. TITLE AND SUBTITLE
RECHARGEABLE LITHIUM BATTERY WITH SOLID ELECTROLYTE

5. FUNDING NUMBERS
C: DAAL01-93-C-3355

6. AUTHOR(S)
D. Peramunage, D. M. Pasquariello, K. M. Abraham

7. PERFORMING ORGANIZATION NAME(S) AND ADDRESS(ES)
EIC Laboratories, Inc.
111 Downey Street
Norwood, MA 02062

8. PERFORMING ORGANIZATION REPORT NUMBER
C-92055

9. SPONSORING/MONITORING AGENCY NAME(S) AND ADDRESS(ES)
US Army Research Laboratory (ARL)
Physical Sciences Directorate
ATTN: AMSRL-PS-CC (M. Salomon)
Fort Monmouth, NJ 07703-5601

10. SPONSORING/MONITORING AGENCY REPORT NUMBER
ARL-CR-269

11. SUPPLEMENTARY NOTES

12a. DISTRIBUTION/AVAILABILITY STATEMENT
Approved for public release; distribution is unlimited.

12b. DISTRIBUTION CODE

13. ABSTRACT *(Maximum 200 words)*

The work carried out under this contract had its primary goal, the development of a polymer electrolyte-based rechargeable battery with the rate capability and cycle life required by batteries for the Army's communication devices. In particular, the battery is to perform over the temperature range of 239 to 343 K. The cell being developed has the configuration: Li/solid polymer electrolyte (SPE)/$LiMn_2O_4$.

Polyacrylonitrile (PAN) based electrolytes with improved low temperature conductivity can be prepared with the use of carefully selected plasticizer compositions from ternary solvent mixtures consisting of propylene carbonate (PC), ethylene carbonate (EC) and butylene carbonate (BC), or from mixtures of PC, EC and 3-methyl-2-oxazolidinone (MEOX). All of the polymer electrolytes were prepared as free-standing films with a thickness of ~4.5 mil. Their conductivities were of the order of 0.003 S/cm at 298 K and 0.00011 S/cm at 233 K. They exhibited good stability to oxidation with oxidative currents of the order of 0.5 microamps per square centimeter at 4.2V *versus* a metallic lithium reference electrode on aluminum.

14. SUBJECT TERMS
Batteries; lithium batteries; rechargeable lithium batteries; metallic lithium anodes; lithium intercalating anodes; metal oxide cathodes; lithium intercalating cathodes; electrolytes; solid electrolytes; liquid electrolytes; polymer electrolytes; aprotic solvents.

15. NUMBER OF PAGES
89

16. PRICE CODE

17. SECURITY CLASSIFICATION OF REPORT	18. SECURITY CLASSIFICATION OF THIS PAGE	19. SECURITY CLASSIFICATION OF ABSTRACT	20. LIMITATION OF ABSTRACT
Unclassified	Unclassified	Unclassified	UL

TABLE OF CONTENTS

TABLE OF CONTENTS (continued)

LIST OF ILLUSTRATIONS

LIST OF ILLUSTRATIONS (continued)

LIST OF ILLUSTRATIONS (continued)

LIST OF ILLUSTRATIONS (continued)

LIST OF ILLUSTRATIONS (continued)

LIST OF ILLUSTRATIONS (continued)

LIST OF ILLUSTRATIONS (continued)

LIST OF TABLES

EXECUTIVE SUMMARY

The work carried out under this contract had its primary goal, the development of a polymer electrolyte-based battery with the rate capability and cycle life required by batteries for the Army's communication devices. In particular, the battery is to perform over the temperature range of -34 to 70°C. The cell being developed has the configuration,

Li//Solid Polymer Electrolyte (SPE)//$LiMn_2O_4$

PAN-based electrolytes with improved low temperature conductivity can be prepared with the use of carefully selected plasticizer compositions from ternary solvent mixtures consisting of propylene carbonate (PC), ethylene carbonate (EC) and butylene carbonate (BC) or PC, EC and 3-methyl-2-oxazolidinone (MEOX). All of the polymer electrolytes were prepared as free-standing films with a thickness of ~4.5 mil. Their conductivities were of the order of 3×10^{-3} ohm^{-1} cm^{-1} at 25°C and 1.1×10^{-4} ohm^{-1} cm^{-1} at -40°C. They exhibited good stability to oxidation with oxidative currents of the order of 0.5 $\mu A/cm^2$ at 4.2V *vs.* Li^+/Li on Al.

Rechargeability of a variety of Li and Li-ion cells utilizing these electrolytes was investigated. Li//SPE//$Li_{1.0}Mn_2O_{4.7}$ (3V) cells yielded more than 200 full-depth discharge/charge cycles when cycled between 3.75V and 2V at 0.1 mA/cm^2 at room temperature. The cell capacity decreased from ~0.8 Li/Mn_2 at the second cycle to ~0.4 Li/Mn_2 at the 200th cycle. A $Li/Li_xMn_2O_4$ cell based on the spinel $Li_{1.1}Mn_2O_4$ (4V) cathode cycled within the potential range from 4.2V to 3.0V at 0.1 mA/cm^2, showed a cycle life in excess of 130 cycles in MEOX-containing electrolytes. In almost all cells containing Li anodes, cycle life failure occurred from internal "soft shorts", caused by Li dendrites. Rechargeability of commercially available carbons such as graphite petroleum coke and acetylene black was demonstrated in a variety of electrolytes.

Graphite exhibited a reversible capacity of ~1 Li/C_6 while the other carbons yielded ~0.5 Li/C_6. Graphite/SPE/$LiMn_2O_4$ and Petroleum Coke/SPE/$LiMn_2O_4$ cells, discharged at the C/3 rate and charged at the C/6 rate at room temperature, were characterized as low capacity fade rates of ~0.1% and <0.05% per cycle, respectively. The graphite anode cell yielded more than 170 cycles while the coke anode cells underwent about 75 cycles before cycling was terminated. The specific energy of the graphite/SPE/$LiMn_2O_4$ cell was close to 106 Wh/Kg at the C/3 discharge rate and it approached 140 Wh/Kg at the C/30 rate.

1.0 INTRODUCTION

The aim of this program has been the development of a polymer electrolyte-based rechargeable battery that exhibits rate capability and cycle life suitable for the Army's communication devices. In particular, the battery is to perform over the temperature range of -34 to 70°C. The battery can be represented as

Li or Carbon//PAN-based solid polymer electrolyte//$Li_xMn_2O_4$

We have conducted detailed investigations on electrolyte and electrode materials and on the performance of cells fabricated with them. Our findings are discussed below. In particular, we have

i) identified and optimized polyacrylonitrile (PAN)-based solid polymer electrolytes containing mixtures of three or more plasticizer solvents which are highly conductive at low ambient temperatures,

ii) developed a rechargeable Li//PAN-based solid polymer electrolyte//$Li_xMn_2O_4$ cell that exhibits satisfactory rate capability and cycle life at ambient temperatures,

iii) investigated the Li intercalation capacity and cycling performance of commercially available graphite (Alfa Graphite) in Li//PAN-based solid polymer electrolyte//carbon cells,

iv) studied of the rechargeability of Li-ion cells of the configuration Carbon//PAN-based solid polymer electrolyte//$Li_xMn_2O_4$,

v) studied the use of alternative anode materials and electrode fabrication techniques in rechargeable Li and Li-ion cells containing PAN-based solid polymer electrolytes.

Lithium ion conductive plasticized polymer electrolytes such as those based on polyacrylonitrile (PAN) and poly(vinyl chloride)(PVC) have provided room temperature conductivity $>10^{-3}ohm^{-1}\ cm^{-1}$, enabling the development of solid state Li and Li-ion batteries with performance reminiscent of their liquid electrolyte counterparts.[1-3] These freestanding thin-film electrolytes have adequate dimensional stability to serve as the separators in these batteries. Their high conductivity results from the presence of solutions of lithium salts in low molecular weight organic solvents such as ethylene carbonate (EC), propylene carbonate (PC), butylene carbonate (BC), dipropyl carbonate (DPC), γ-butyrolactone (γ-BL), 3-methyl-2-oxazolidinone (MEOX) and mixtures thereof. Conductivity of the solid electrolyte is dependent upon the concentration and the mobility of the charge carriers derived from the Li salt, which in turn is dependent upon the fluidity of the ionic environment. This requirement tends to be very critical at subambient temperatures where freezing of the plasticizer could drastically affect the ionic motion. Thus, development of a solid polymer electrolyte-based ionic conductor suitable for subambient temperatures requires mixtures of high permittivity polar plasticizers that can produce low melting eutectics of ionic solvates formed between the lithium salt and the plasticizers, providing a more fluid environment for ionic motion.

During Phase I of this program, the importance of optimizing the ratio of EC and PC in binary plasticizer compositions and the beneficial effect of incorporating BC to form ternary plasticizers, were demonstrated. The Phase II program called for a more extensive study to identify and optimize electrolytes based on mixtures of three or more plasticizer solvents which are highly conductive at subambient temperatures. Specific aspects of the electrolyte development included the construction of composition diagrams to determine electrolyte compositions with the best low temperature conductivity, measurement of conductivity at ambient temperatures as low as -40°C, determination of the electrochemical stability window in the potential region between -0.3 and 5.0 V *vs.* Li^+/Li relative to Pt, Ni, Al and carbon electrodes, and evaluation of the properties of the interface between Li and the electrolyte. The study also involved a detailed investigation on the rechargeability of Li and Li-ion cells utilizing these PAN-based solid electrolytes.

2.0 EXPERIMENTAL

2.1 Material

Polyacrylonitrile (PAN) of Mw = 10^5 (Polysciences) was dried under vacuum at ~50°C for 24 hours. Propylene carbonate (PC) (anhydrous, Grant Chemicals), Ethylene carbonate (EC) (anhydrous, Grant Chemicals) and, Dipropyl carbonate (DPC) (anhydrous, Grant Chemicals) were used as-received. Butylene carbonate (BC) (Mitsubishi Chemicals, Japan), 3-methyl-2-oxazolidinone (MEOX) (99%, Aldrich) γ-butyrolactone (γ-BL) (+99%, Aldrich) were dried over molecular sieves and distilled at around 100°C under Ar at reduced pressure. All the solvents were stored in the glove box over activated Linde-4Å molecular sieves prior to use. Lithium hexafluoroarsenate ($LiAsF_6$, Lithco) and Lithium hexafluorophosphate ($LiPF_6$, Lithco) were used as-received.

2.2 Synthesis of Lithiated Manganese Dioxide $Li_xMn_2O_4$

$Li_xMn_2O_4$ was prepared by heating LiOH (99.9%, Cerac) with electrolytic manganese dioxide (EMD, >90%, Aldrich) at 450°C in air. A well-ground mixture of the reactants was fired in an alumina boat first for 48 hours. After grinding the mixture again, it was fired for another 12 hours. The product was repeatedly ground to obtain a particle size of smaller than 20 μm. Two samples were prepared from mixtures containing initial LiOH to EMD ratios of 1:2 and 1:2.3 and the compositions were $Li_{0.9}Mn_2O_{4.2}$ and $Li_{1.0}Mn_2O_{4.7}$, respectively. The high voltage (4V) lithiated manganese oxides were prepared by heating a 1:1.2 mixture of LiOH and EMD at 750°C for about 60 hours in two steps, first at 48 hours followed by grinding and then re-heating the mixture for another 48 hours. The resulting material was ground again to an average particle size of 20 μm

2.3 Synthesis of Polymer Electrolytes (SPE)

Polymer electrolytes were prepared by heating a weighed and thoroughly mixed slurry of PAN, Li salt and plasticizers in a Pyrex bottle at 140°C in the glove box for about 30 minutes. The transparent, viscous melt was placed between stainless steel shims covered with FEP films and rolled between slip rollers to form SPE film. Upon cooling, mechanically strong films of typical thickness between 50-75 μm were formed. Preparation of precursor mixtures, their processing and rolling of SPE films were carried out in a Vacuum Atmospheres Corporation (Hawthorne, CA) glove box purged with Argon.

2.4 Conductivity Measurements

Ionic conductivity of the polymer electrolyte membrane was determined using impedance spectroscopy. This procedure involved the use of an EG&G PAR (Model 273) potentiostat/galvanostat and EG&G lock-in analyzer (Model 5208) in the frequency range of 0.1 Hz to 100 KHz to apply a 5 mV AC modulation across the conductivity cell. The phase and amplitude of the current response to this applied voltage was used to calculate the real and imaginary components of the impedance. Acquisition and analysis of the data as well as the operation of the potentiostat/galvanostat and the lock-in amplifier were software controlled from an IBM-PC. Conductivity measurements are done in duplicate using electrolyte films of known

thickness sandwiched between two cylindrical (1.27 cm^2) stainless electrodes. Schematic of the set up used to measure electrolyte impedance is given in Figure 1. The data were collected at +25°C, +10°C, -10°C, -25°C and -40°C after thermostating the conductivity cell in a Tenney Jr. environmental chamber.

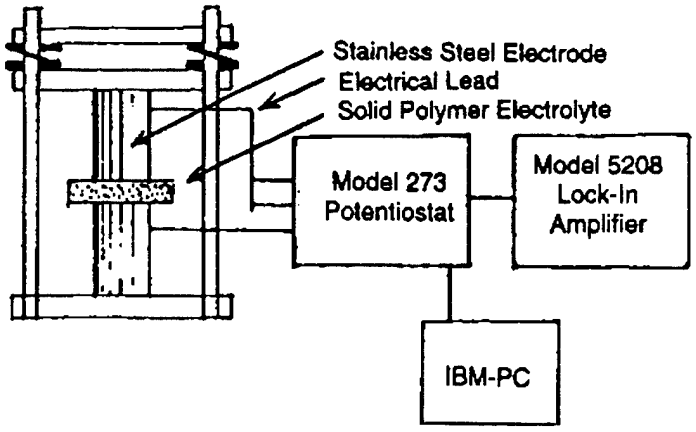

Figure 1. Schematic of the setup used to measure impedance of solid polymer electrolyte.

AC modulation gives rise to a current inversely proportional to the electrolyte impedance Z according to equation [1].

$$I = V/Z \qquad [1]$$

where, impedance Z = Z (Real) + Z (imaginary). The Z (real), which is the real part of the impedance include the bulk resistance of the electrolyte. Z (imaginary) includes impedance due to the RC coupling of parallel resistance (R) and capacitance (C) elements included in the network representing the SPE//stainless steel interface. Since Z (imaginary) = $1/\omega C$, where ω is the frequency of the modulation, typical impedance measurement involves scanning the frequency at a constant applied potential. In the present case scanning is limited to the range of 500 kHz to 5 Hz, while the applied potential is maintained at zero.

Impedance data are typically displayed as a graph of Z (real) *vs.* Z (imaginary) called a Cole-Cole plot, from which bulk resistance R_b can be readily obtained as the first high frequency intercept on the Z (real) axis. The conductivity of SPE is calculated from the relationship give in equation [2].

$$\sigma = l/(R_b \times A) \qquad [2]$$

where, σ is the conductivity, A is the active contact area, l is the thickness of the SPE film, and R_b is the bulk resistance.

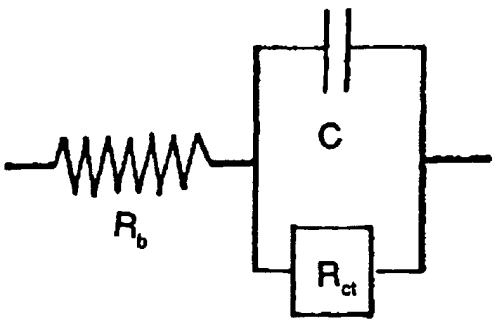

Figure 2a. Equivalent circuit for the solid polymer electrolyte (SPE)//stainless steel interface, where R_b is the bulk resistance of the SPE, R_{ct} is the charge transfer resistance, C is the interfacial capacitance.

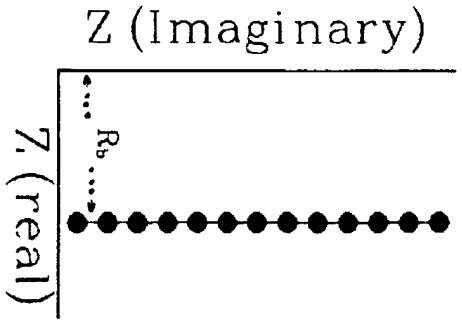

Figure 2b. Impedance plot for the equivalent circuit shown in Figure 2a (R_{ct} is assumed to be infinit).

The equivalent circuit which describes the impedance of SPE is shown in Figure 2a where, R_b is the SPE bulk resistance, C is the interfacial capacitance and R_{ct} is the charge transfer resistance. The two stainless steel electrodes act as blocking electrodes to cationic as well as anionic charge carriers present in the electrolyte. Consequently, the charge transfer resistance can be considered infinitely high and the resulting Cole-Cole impedance plot typically appears as a line vertical to the Z (real) axis (actually, a semicircle with an infinitely high radius) offset from the origin by the bulk resistance, as shown in the Figure 2b. Typical impedance plots for SPE usually do not show a perfect vertical line expected for an ideally blocking type interface. The less-than-ideal behavior may be due to rough surface of the electrode or impurity related charge transfer at the SPE/stainless steel interface. The high frequency intercept on the real axis of the Cole-Cole plots of the impedance data gave the electrolyte resistance

2.5 Electrochemical Stability Measurements

Electrochemical stability measurement was performed by using a Schlumberger S1286 Electrochemical Interface. Schematic of the cell used for this measurement is shown in Figure 3.

Pt, Ni, Al were cut to 0.25 cm^2 size, cleaned with soap and water and degreased with pentane. Pt and Ni were etched with concentrated HNO_3 and 50% aqueous HCl, respectively, followed by washing with distilled water. Carbon electrodes (0.25 cm^2) were made by dip coating from a homogenized suspension of 2% polyethylene, 1% PTFE and 97% carbon (Conoco) onto an Al foil followed by air drying and then hot pressing at 150°C for 30 seconds under a load of 10 tons The cell was fabricated by sandwiching the polymer electrolyte between an oversized Li counter electrode and a 0.25 cm^2 working electrode. A Li electrode contacting the SPE in proximity (<1 mm) to the working electrode served as the reference electrode. The whole assembly is positioned between two glass plates and secured with metal clips. Cyclic voltammetry experiments were done under software control from an IBM-PC in the potential region between -0.3 and 5.0V *vs.* Li^+/Li on Pt, Ni, Al and carbon electrodes. Following a series of preliminary experiments, a 0.5 mV/sec scanning rate was chosen for all the cyclic voltammetry experiments.

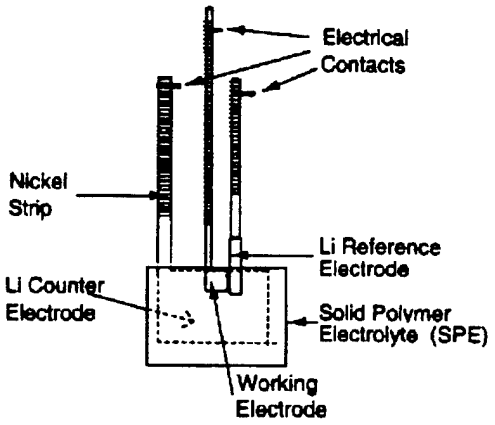

Figure 3. Schematic of the cell used for cyclic voltammetric measurement on solid polymer electrolytes.

2.6 Fabrication and Cycling of Li/$Li_xMn_2O_4$ Cell

The prototype test cells, with the configuration Li//SPE//$Li_xMn_2O_4$, typically contained rolled cathode laminates. The cathode composition based on either of the two low voltage materials was close to 51 w/o $Li_xMn_2O_4$:8 w/o Carbon:41 w/o binder. The composition of the binder was related to the SPE used in a test cell but with reduced contents of PAN and $LiAsF_6$. For example, the SPE typically used in cells containing the low voltage (3V) cathode material had 32.1 w/o EC:30.6 w/o PC:12.6 w/o MEOX:12.1 w/o PAN:12.7 w/o $LiAsF_6$ whereas, the corresponding cathode binder had 36.4 w/o EC:34.7 w/o PC:14.3 w/o MEOX:7.3 w/o PAN:7.3 w/o $LiAsF_6$. Rolling the cathode mixture was done under conditions identical to that of solid polymer electrolytes. These electrodes are typically identified in the text as ***hot-rolled*** electrodes. Li/$Li_xMn_2O_4$ solid state cells were fabricated by sandwiching the polymer electrolyte laminate (100-125 μm thickness) between the Li foil anode and the $Li_xMn_2O_4$ cathode laminate (approximately 100 μm). The cathode had an active area of 10 cm^2. Al foil served as the cathode current collector and Ni strips were used as electrode leads. The sandwich was vacuum-packed in an aluminized polyethylene bag. A computer controlled ARBIN 24-channel battery cycler was used to cycle the cells. A schematic diagram of a sold state cell is shown in Figure 4.

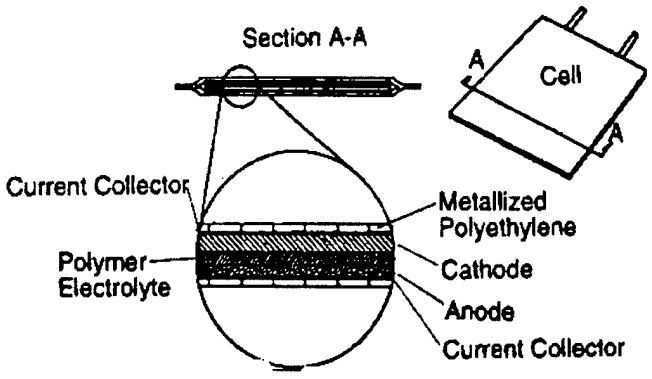

Figure 4. Schematic of the cell used in studies of the rechargeability of Li or Li-ion cells.

2.7 Fabrication and Cycling of Carbon/$Li_xMn_2O_4$ Cells

A high voltage (4V) lithiated manganese dioxide cathode in conjunction with a carbon composite anode was used to fabricate Li-ion cells. The cathodes were laminates of a composite typically ***hot-rolled*** on to an Al film. They usually comprised of $Li_xMn_2O_4$ (4V), polymer electrolyte and Chevron black at the proportions of 53.2:38.8:8.0 by weight. Carbon anodes were similarly rolled on to Ni foil and a typical graphite composite for example, contained Alfa graphite, and polymer electrolyte blended together at the proportions of 51:49 by weight. In cases where Al powder was included in the graphite composites, a composition with Alfa graphite 38.4 w/o:Al powder 12.8 w/o:Chevron black 1.3 w/o:polymer electrolyte 47.5 w/o was used. Two other procedures were used to prepare electrodes. These were: *i*) a process involving no heating, in which the binder was introduced as a concentrated solution of a polymer (e.g., poly(vinyl chloride-co-vinyl acetate (COP) in THF. After rolling the composite laminate the low boiling solvent was evaporated at a temperature slightly above the ambient leaving high boiling plasticizers in the composite. A typical composition expressed in w/o included 49.3 Graphite:14.6 Al:1.5 carbon:7.4 COP:14.7 EC:14.4 BL:3.4 $LiAsF_6$. The electrodes made by this process is referred to as ***solvent-cast*** electrodes in the text. *ii*) spreading a homogenized slurry made of the dry precursors such as carbon or $Li_xMn_2O_4$, and a polymeric binder in N-methyl pyrrolidine (NMP) on a current collector (Al mesh for the cathode and Cu mesh for the carbon anode), evaporating off the solvent at 100°C under vacuum and finally, hot-pressing the resulting dry laminates at 150°C under a load of 10 tons. Polyethylene (PE) and poly(vinyledene fluoride) (PVDF) were used as the binders for the $Li_xMn_2O_4$ and carbon electrodes, respectively. The term ***hot-pressed*** is used in the text to describe this type of electrodes. These electrodes were impregnated with a liquid electrolyte prior to use in cells.

3.0 RESULTS AND DISCUSSION

3.1 Development of Solid Polymer Electrolytes Suitable for Subambient Temperatures

3.1.1 Physical Properties of Plasticizers. The plasticizers used in this study have the following structures and some of their physical properties are given in Table 1.

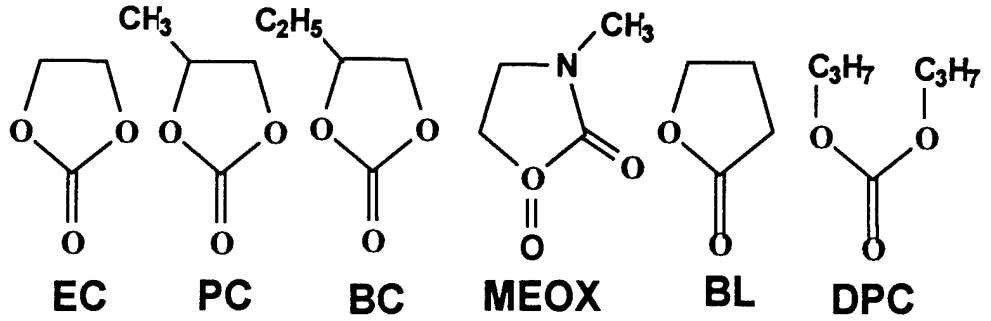

Table 1. Physical Properties of Solvents.

Component	Dielectric Constant	Viscosity (CP)	Boiling Point (°C)	Melting Point (°C)
Ethylene carbonate (EC)	89.6	1.85 (40°C)	238	36.5
Propylene carbonate	63.8	2.53	240	-55
Butylene carbonate	53	3.2	240	-53
3-Methyl-2-oxazolidinone (MEOX)	78	2.5	87-90/1 mm	15
γ-Butyrolactone			89-93/5 mm	-45
Dipropyl carbonate			167-168	

The high boiling points and low vapor pressures (except DPC) of these solvents make them desirable as plasticizers for the preparation of electrolytes with good dimensional stability and minimal changes in the composition from solvent evaporation during storage. They also have high dielectric constants which should allow the preparation of high conductivity electrolytes. All of these solvents have been previously used in liquid electrolyte-based primary and secondary Li batteries.[4] However, it was necessary to identify specific solvent mixture compositions with which homogeneous solid electrolyte phases having high conductivity over a wide temperature range could be prepared with PAN and $LiAsF_6$.

3.1.2 Effect of SPE Thickness on the Conductivity Measurement. SPE samples used for the conductivity measurement were made in small batches using a pair of manually controlled slip rollers and as a result, precise control of the SPE thickness was not feasible. Therefore, it was of interest to find out the effect, if any, of the SPE thickness on the conductivity of the sample.

The data in Figure 5 demonstrate that the conductivity of SPE increases with thickness and reaches a plateau (prominent at low temperature) as the thickness is increased further. We may explain this in the following way. When the SPE sample is held between two stainless steel electrodes it gets compressed under the pressure of springs. As the thickness (l) decreases, if the

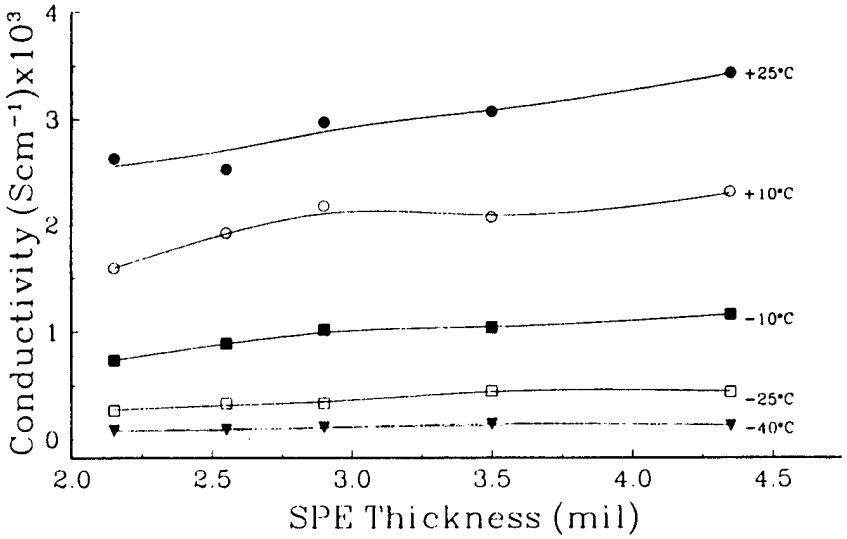

Figure 5. Solid polymer electrolyte conductivity as a function of the SPE thickness at various temperatures.

resistance R also decreases proportionately, the conductivity σ will be overestimated since the original thickness is used in calculating the conductivity (equation [2]). However, if some liquid electrolyte in the SPE plasticizer is squeezed out of the electrode contact area due to compression, R may actually go higher than the original value (overestimated). The result would be a lower apparent conductivity. The thinner the sample the higher will be the difference between the real and the apparent values of R and the lower will be the conductivity. In all further studies efforts were made to maintain the SPE thickness in the vicinity of 3.5 mil so that, comparison of conductivity among different SPE samples (compositions) was possible.

3.1.3 Composition Diagrams for Solid based on Ternary Solvent Mixtures as Plasticizers. Dimensionally stable, PAN-based polymer electrolytes have been prepared from ternary plasticizers containing mixtures of EC and PC along with either BC or MEOX. Only certain mixtures of the three solvents led to homogeneous free-standing films. These are presented in the form of composition diagrams. Since there are five components in each electrolyte including the three solvents, $LiAsF_6$ and PAN, a full representation of each electrolyte requires a five component composition diagram even when the temperature is fixed and only one Li salt is considered. Obviously, a task of this proportion involves the preparation and conductivity measurement of a very large number of electrolytes. However, in the present study this task was simplified by fixing the amounts of PAN and $LiAsF_6$ at 21 m/o and 8 m/o, respectively, and focusing attention primarily on the three-component plasticizer mixture. This approach was considered reasonable for several reasons. A principal role of PAN is to provide dimensional stability to the electrolyte laminate and our previous work with PC- and EC-containing electrolytes indicated that 21 m/o of PAN was sufficient to provide adequate

dimensional stability. The Li salt content of 8 m/o was close to the optimum for the highest conductivity. Since the plasticizer solvent formed 71 m/o of the electrolyte composition, its interaction with the Li salt to form the eutectic solvate can be considered as the most important factor that determines the conductivity of the electrolyte. $LiAsF_6$ was the preferred salt in this study because it forms highly conductive solutions with organic solvents and it is the salt desired for high efficiency cycling of the Li anode.[5] Preliminary experiments involved a series of ternary plasticizers chosen randomly to identify the area of the ternary composition diagram desirable for SPE formation and to locate the region where electrolytes with high conductivities at low temperature are found. Following this initial survey, a series of electrolytes with systematically varying ternary plasticizer compositions, which included these regions of high conductivity, was designed.

Three such electrolyte series (L, M, N) in the EC/PC/BC composition diagram are depicted in Figure 6.

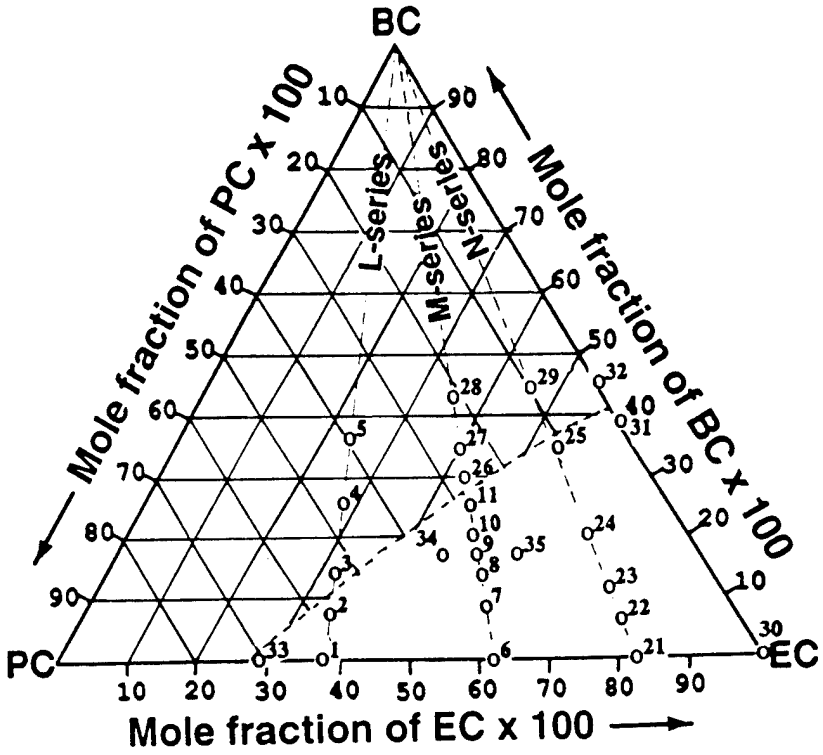

Figure 6. Region of the EC-PC-BC composition diagram favorable (not hatched) for solid polymer electrolyte formation with PAN and $LiAsF_6$.

Each series includes compositions with varying BC content which fall on the same straight line connecting the BC apex and a particular point on the PC/BC axis. As a result, as the location of any composition moves from the PC/EC axis towards the BC apex, EC and PC are proportionately reduced and BC is substituted to make up for the deficit. The electrolytes incorporating these ternary plasticizers had the general composition of 21 m/o PAN, 71 m/o plasticizer and 8 m/o $LiAsF_6$.

Table 2 contains the compositions of some M-series electrolytes. As mentioned earlier, homogeneous solid polymer electrolytes (SPE) are possible only for certain combinations of the plasticizers. For example, all compositions which are located inside the hatched area failed to form a homogeneous melt, upon heating, that could be rolled into a transparent thin laminate and, are, therefore, considered to be unsuitable.

Table 2. Conductivities of M-Series (Figure 6) Electrolytes.

	Electrolyte	Conductivity x 10^5 (ohm^{-1} cm^{-1}) at:				
No.	PAN:EC:PC:BC:$LiAsF_6$ m/o	+25°C	+10°C	-10°C	-25°C	-40°C
BC6	**21.0:44.2:26.8:0.0:8.0**	**237**	**153**	**56**	**16**	**3**
BC7	21.0:40.5:24.5:6.0:8.0	231	156	61	18	3
BC8	21.0:38.3:23.2:9.5:8.0	232	162	68	19	4
BC9	**21.0:36.7:22.3:12.0:8.0**	**252**	**186**	**88**	**27**	**6**
BC10	21.0:35.5:21.5:14.0:8.0	203	139	65	20	4
BC11	21.0:33.0:20.0:18.0:8.0	154	117	48	15	3

Since the region desirable for SPE formation is located towards the EC corner of the composition diagram, EC can be considered an indispensable component of the plasticizer mix. Note that, of the three plasticizer solvents, EC has the highest dielectric constant which may be necessary to form a gel with a considerable amount of the polar polymer host and, at the same time, to solvate high concentration of the Li salt. Desirable binary compositions between EC and BC include those with no more than 40 m/o BC (relative to the total of EC and BC). On the other hand, in binary compositions consisting of EC and PC, as high as 70 m/o PC (relative to the total of EC and PC) can be used in the plasticizer mixture. The L-series compositions with high PC content (Figure 6) incorporate only about 6 m/o of BC before they become unsuitable for SPE formation, whereas M-series compositions can accommodate as much as 24 m/o of BC. In the latter case, the high permittivity of EC may have compensated for the low permittivity of BC, thereby maintaining high overall permittivity of the mixture.

As depicted in Figure 7, different areas of the PC-EC-MEOX composition diagram was systematically surveyed not only to isolate the region where mechanically strong electrolyte formation was possible, but also to identify possible candidates for low ambient temperature use. The basis for selecting the various test compositions on the ternary composition diagram was the same as described above for EC-PC-BC-based electrolytes. As Figure 7 indicates, MEOX content in the Q-series electrolytes varies from zero electrolyte (MX1) upwards and all these compositions have a common EC/(EC+PC) ratio equal to 0.55. A few compositions which we investigated are given in Table 3.

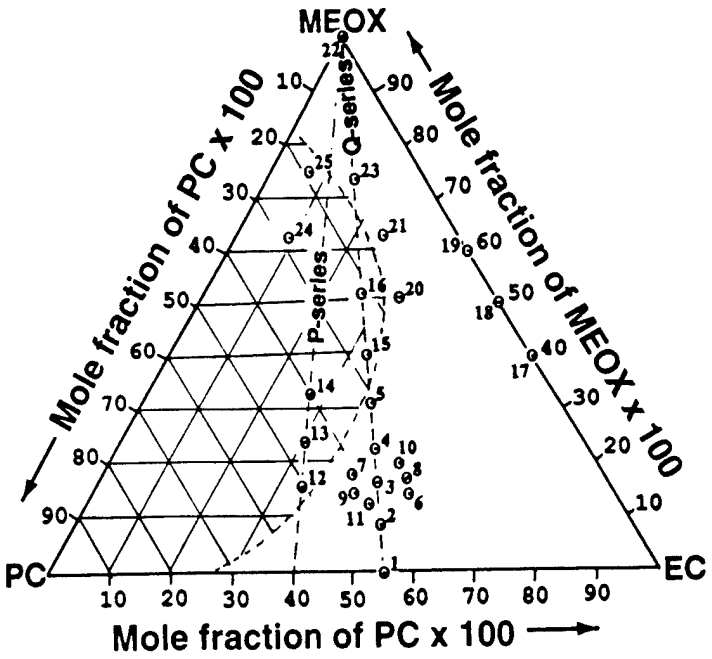

Figure 7. Region of the EC-PC-MEOX composition diagram favorable (not hatched) for solid polymer electrolyte formation with PAN and $LiAsF_6$.

Table 3. Conductivities of Electrolytes MEOX containing Ternary Compositions.

	Electrolyte	Conductivity x 10^5 (ohm^{-1} cm^{-1}) at:				
No.	PAN:EC:PC:MEOX:$LiAsF_6$ m/o	+25°C	+10°C	-10°C	-25°C	-40°C
MX1	21.0:40.2:32.9:0.0:6.0	213	167	82	27	7
MX3	**21.0:33.8:27.7:11.5:6.0**	**298**	**218**	**102**	**39**	**11**
MX5	21.0:27,8:22.7:22.5:6.0	275	204	98	44	8
MX6	21.0:37.5:25.0:10.5:6.0	249	196	93	39	10
MX8	21.0:36.3:24.2:12.5:6.0	261	187	89	34	10
MX9	21.0:31.1:31.1:10.7:6.0	283	209	100	38	10
MX10	21.0:34.4:23.9:14.7:6.0	279	197	101	37	11
MX23	**21.0:10.8:8.7:53.4:6.0**	**310**	**237**	**115**	**45**	**16**
MX22	21.0:0.0:0.0:73.0:6.0	321	234	126	11	0.5
Base line	21.0:61.0:13.0:0.0:5.0	150 (20°C)	-	50	-	1

All MEOX containing SPE had a total plasticizer mixture of 73.0 m/o with 21.0 m/o PAN and 6.0 m/o $LiAsF_6$. The reason for the use of 6 m/o Li salt as opposed to 8 m/o in the BC containing electrolytes will become clear later. The compositions that appear in the hatched area in Figure 7 represent plasticizer mixtures not suitable for SPE formation. Again, the region desirable for SPE formation is located towards the EC corner. It is interesting to note that, while PC-EC binary compositions can successfully incorporate up to 30 m/o PC, only 10 m/o PC is possible with PC/MEOX mixtures. On the other hand, the whole range of MEOX/EC mixture is suitable for SPE formation. This suggests that the order of plasticizing ability of individual solvent is EC>MEOX>>>PC. Data given in Table 3 indicate that compositions suitable for low temperature applications can be found in high MEOX (Electrolyte MX23) as well as low MEOX (MX3) regions of the ternary composition diagram. These two domains are flanked by a region representing compositions undesirable for SPE formation. One may speculate that there can be other EC-PC-MEOX compositions that leads to SPEs with superior low temperature conductivity. The potential of such compositions in this or any other ternary system may not be realized, however, unless they are capable of forming a gel with PAN. Therefore, gel formation itself seriously limits the choices one has for plasticizer mixtures suitable for SPE preparation.

3.1.4 Conductivity of Ternary Electrolytes. Conductivities of SPEs based on M-series plasticizers (Figure 6) in the temperature range of -40 to 25°C are given in Table 2. In this series of electrolytes, the composition with 12 m/o BC electrolyte (Electrolyte BC9) has shown the highest conductivity over the whole temperature range. In relation to the data given in Table 2, Figure 8 illustrates SPE conductivity as a function of BC mole fraction of the ternary plasticizer at different temperatures.

Evidences discussed below show that the highest conductivity of the BC9 electrolyte is consistent with the formation of a low melting eutectic of ionic solvates formed between $LiAsF_6$ and the plasticizers. If the conductivity at a particular temperature (ref. Table 2) for each composition is normalized against the highest value observed for BC9 at that temperature and plotted as a function of BC mole fraction, one obtains the result shown in Figure 9. At room temperature, as X_{BC}, BC mole fraction of the ternary plasticizer x 100, is increased from zero (Electrolyte BC6) through 17 (Electrolyte BC9), no substantial variation of conductivity is evident. For example, the ratio of SPE conductivities corresponding to 17 X_{BC} and 5 X_{BC} is close to 1.1 as shown in Figure 9.

This is expected since, $LiAsF_6$ containing liquid electrolytes with 5 X_{BC} and 17 X_{BC} compositions are in the liquid state at room temperature. Yet, for -40°C, the same ratio becomes greater than 20. Assuming that 17 X_{BC} leads to a low melting eutectic of solvates of the Li salt, this SPE should retain a more fluid environment and show higher conductivity at low temperature. In comparison, SPE originating from a non-eutectic composition should result in a substantially lower conductivity. Thus, the disparity between the conductivities of the 5 X_{BC} and 17 X_{BC} compositions can be explained in terms of the formation of Li salt-solvent eutectics. The eutectic nature of the 17 X_{BC} plasticizer composition was further investigated by measuring the conductivity of liquid electrolytes in solvent mixtures corresponding to 5 X_{BC} and 17 X_{BC} compositions (i.e., mixtures without PAN). The conductivity data as a function of temperature are given in Figures 10 and 11.

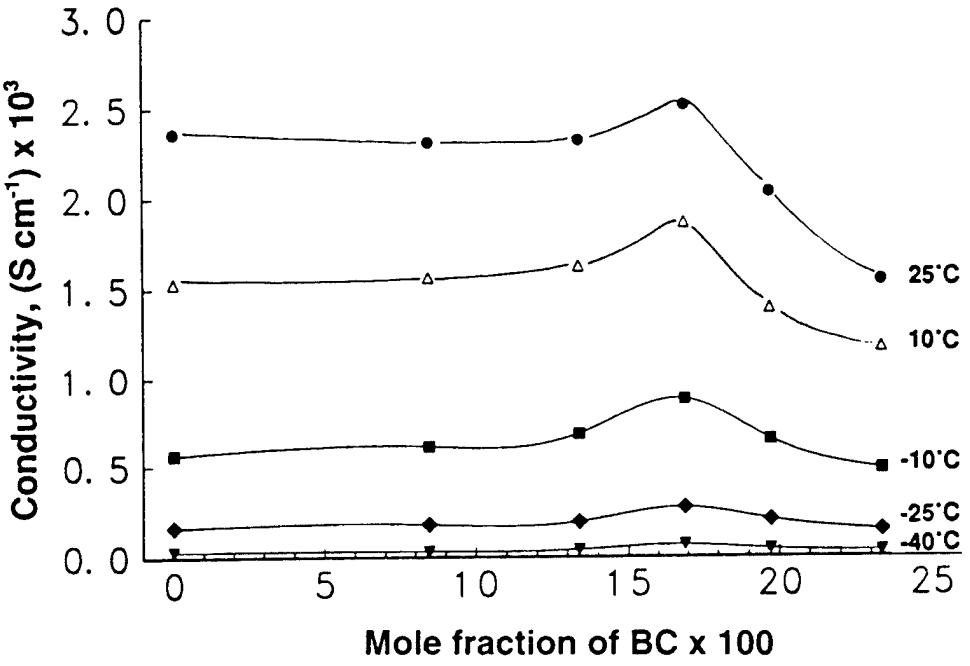

Figure 8. Solid polymer electrolyte conductivity as a function of the mole fraction of BC in the EC-PC-BC liquid ternary plasticizer, at various temperatures.

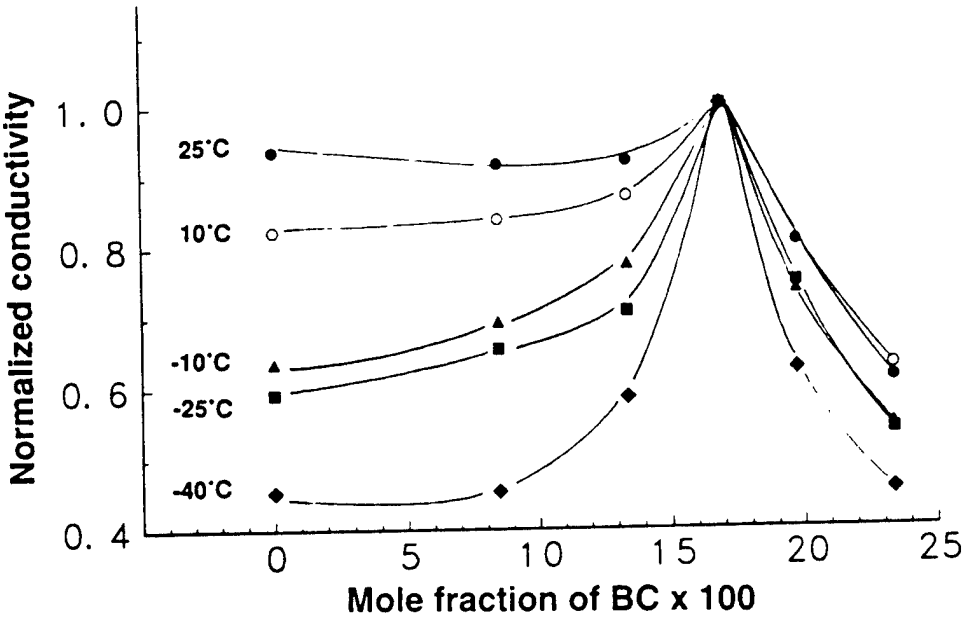

Figure 9. Normalized solid polymer electrolyte conductivity observed at a particular temperature as a function of the mole fraction of BC in the EC-PC-BC liquid ternary plasticizer.

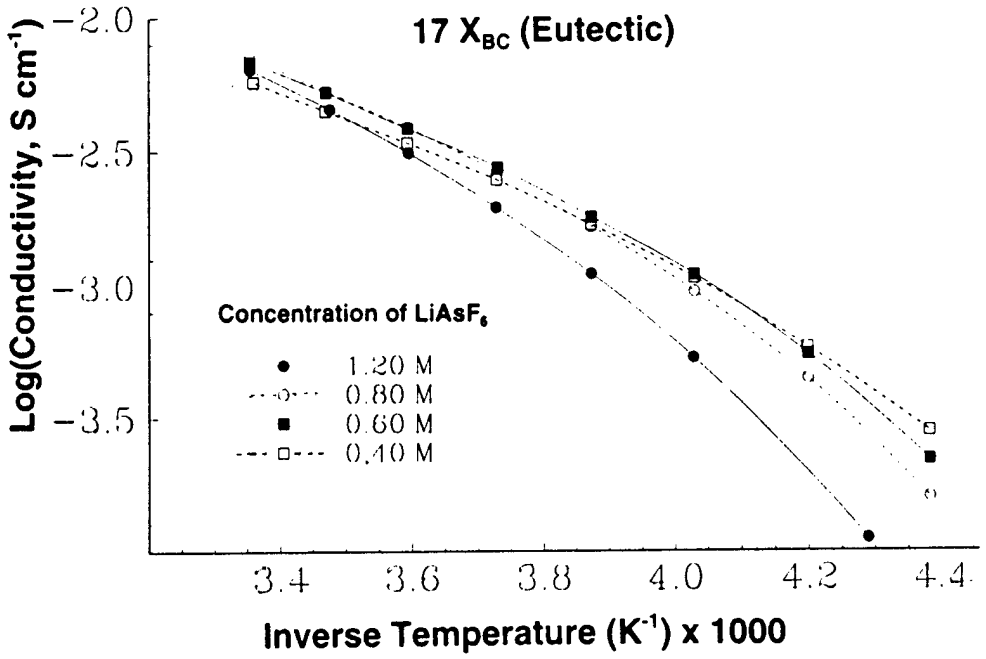

Figure 10. Conductivity *vs.* temperature of several different concentrations of $LiAsF_6$ in the EC-PC-BC liquid ternary plasticizer containing 17 X_{BC}.

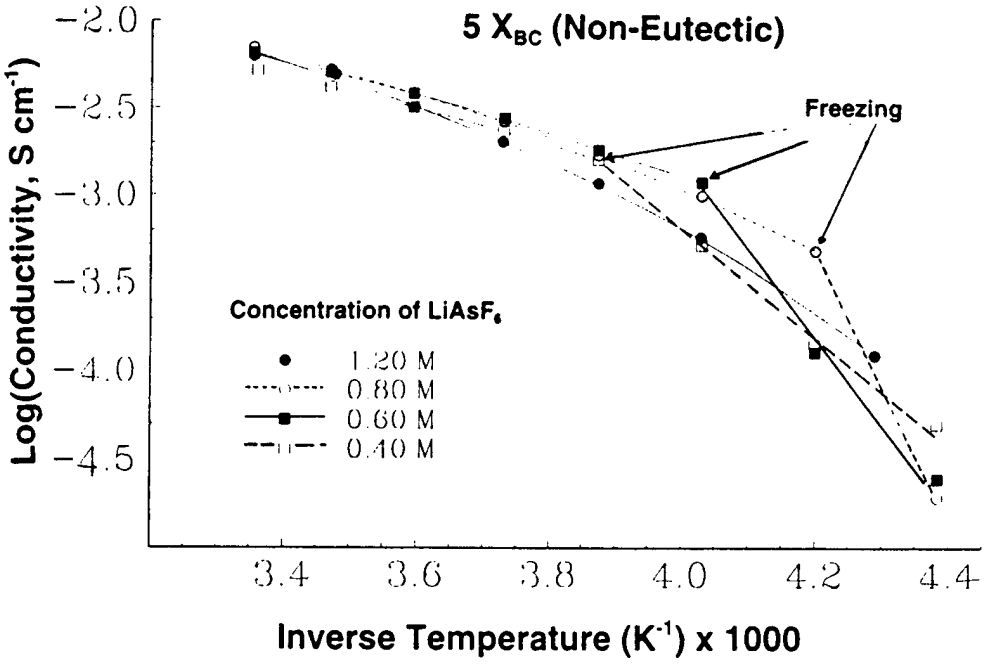

Figure 11. Conductivity *vs.* temperature of several different concentrations of $LiAsF_6$ in the EC-PC-BC liquid ternary plasticizer containing 5 X_{BC}.

The non-Arrhenius behavior of the temperature-dependent conductivity of ternary electrolytes with X_{BC} = 17 can be seen in the log(σ) *vs.* 1/T plots in Figure 10. None of these solutions was frozen at -45°C, the lowest temperature at which data were taken. On the other hand, for solutions with X_{BC} = 5 in Figure 11, a discontinuity is evident at a certain temperature for concentrations below 1.2M. Visual observations confirmed that the solutions were frozen below this temperature. In the SPE compositions tested so far, concentration of the Li salt relative to the ternary plasticizer mixture alone falls within 1-1.2M. Inclusion of the polymer in the gel phase should make the actual salt concentration in the SPE even lower. Therefore, data shown in Figures 9 and 10 strongly suggest the possibility of phase separation in the SPE at low ambient temperatures when the BC mole fraction in the ternary plasticizer mixture corresponds to 5 X_{BC}, which leads to a low conductivity. This situation should be common to any plasticizer other than the eutectic composition and as a result an SPE with a non-eutectic composition should yield lower conductivity at subambient temperatures as already seen in Figure 9. A number of ternary mixtures around the most favorable 17 X_{BC} (BC9) composition were tested for SPE formation and also for conductivity. In close proximity to BC9 they all showed comparable conductivities and, therefore, the SPE with this particular amount of BC was chosen for further study.

3.1.5 Effect of Li Salt Content on Conductivity. As illustrated in Figure 12 and Table 4, variation of SPE conductivity with temperature as a function of $LiAsF_6$ molality reveals dependence of the conductivity on $LiAsF_6$ content.

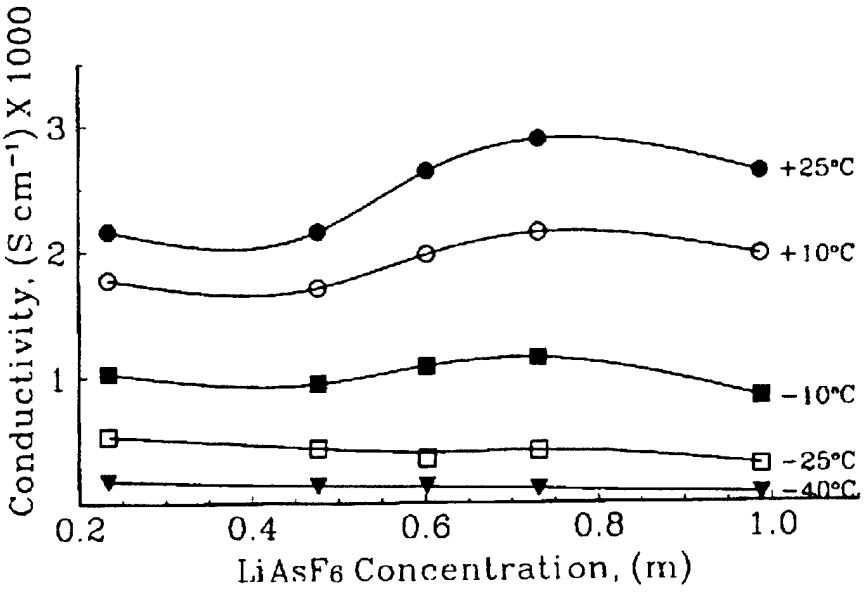

Figure 12. Conductivity *vs.* $LiAsF_6$ molality for SPE with EC-PC-BC liquid ternary plasticizer containing 17 X_{BC}.

Table 4. Conductivities of Solid Polymer Electrolytes with Different $LiAsF_6$ Content.

Electrolyte		Conductivity x 10^5 (ohm^{-1} cm^{-1}) at:				
No.	PAN:EC:PC:BC:$LiAsF_6$ m/o	+25°C	+10°C	-10°C	-25°C	-40°C
BC12	21.0:39.8:24.1:13.0:2.0	216	177	103	53	17
BC13	21.0:38.8:23.5:12.7:4.0	215	170	94	43	13
BC14	21.0:38.3:23.2:12.5:5.0	263	197	108	35	13
BC15	**21.0:37.8:22.9:12.3:6.0**	**288**	**214**	**114**	**41**	**11**
BC9	21.0:36.7:22.3:12.0:8.0	262	196	38	29	07

The SPE compositions investigated are based on the (EC-PC-BC/$LiAsF_6$) liquid plasticizer compositions corresponding to 17 X_{BC} and they all have a common PAN/plasticizer ratio of 0.30, and an EC/(EC + PC) ratio of 0.62. Assuming that PAN functions as a 'polymer solvent' along with the plasticizer, the combined weight of the polymer and the ternary electrolyte was used in calculating the salt molality. As $LiAsF_6$ concentration is increased, e.g., at 25°C, the conductivity goes through a maximum. The appearance of a conductivity maximum may indicate the interplay of increasing charge carrier concentration, viscosity and ion pairing effects. Morphological changes in the gel phase that occur at high salt concentration may also have a negative influence on conductivity. The BC15 composition with high overall conductivity corresponds to 6 m/o of the $LiAsF_6$ salt. As the temperature approaches -40°C, the conductivity increases with decreasing salt content and this may be due to the increasing mobility of charge carriers with decreasing salt content or perhaps, dominance of the ion pairing effect when the liquid phase supporting the conductance becomes too viscous at low temperature.

3.1.6 Effect of the Type of Salt. Type of salt used in the solid polymer electrolyte affects the SPE conductivity as shown in Table 5. A common composition of 37.8 m/o EC:22.9 m/o PC:12.3 m/o BC:21.0 m/o of PAN:6.0 m/o salt corresponding to 17 X_{BC} plasticizer was used in this study.

Table 5. Effect of the Type of Salt on SPE Conductivity.

No.	Li salt	Conductivity x 10^5 (ohm^{-1} cm^{-1}) at:				
		+25°C	+10°C	-10°C	-25°C	-40°C
BC15	$LiAsF_6$	288	214	114	41	11
BC16	$LiPF_6$	216	177	103	53	17
BC17	$LiN(CF_3SO_2)_2$	215	170	94	43	13

Substitution of $LiPF_6$ for $LiAsF_6$ in the Electrolyte BC15 (Table 5) formed SPEs with similar conductivities. The higher molecular weight of the $LiN(CF_3SO_2)_2$ salt (No. BC17) prevents formation of a SPE with 6 m/o of that salt as it was over 17 w/o of the composition

3.1.7 SPE containing EC-γ-BL Binary Plasticizers. Work related to optimizing the ratio of EC to γ-BL in the plasticizer was undertaken and the results are presented in Figure 13. The composition with the highest overall conductivity contains about 0.6 mole fraction of γ-BL. Conductivity of the corresponding SPE reached 3.8×10^{-3} S cm^{-1} at 25°C and 1.7×10^{-4} S cm^{-1} at -40°C.

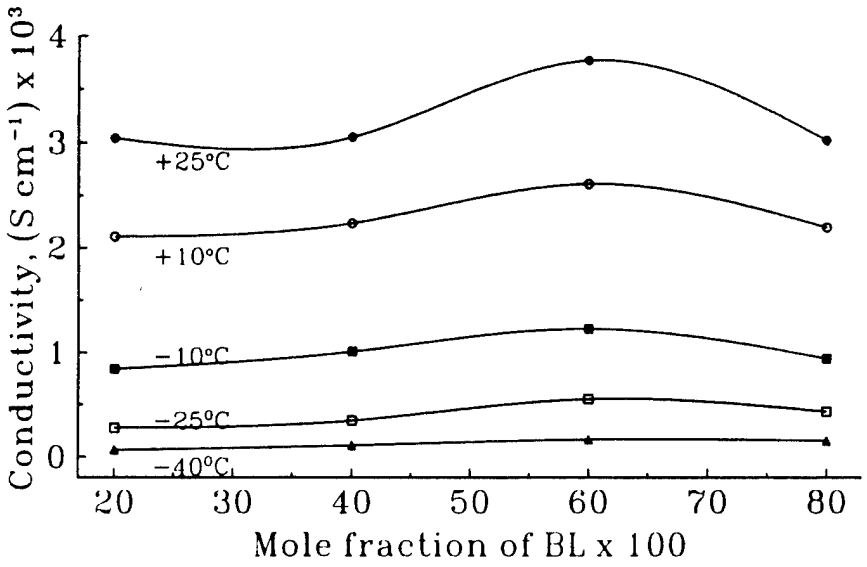

Figure 13. SPE conductivity as a function of the mol fraction of γ-BL in the EC-γ-BL liquid binary plasticizer at various temperatures.

3.1.8 Electrochemical Stability of Solid Polymer Electrolytes. Since a laminate of SPE in a solid state Li cell remains in contact with both Li anode and a composite cathode, chemical compatibility is always an important parameter that determines the usefulness of the cell. Since Li is the most electronegative element towards which any other material is thermodynamically unstable, long term chemical stability at Li/SPE interface is achieved through a passivation phenomenon. During operation of a cell, electrochemical reactions at the anode occur close to 0V *vs.* Li^+/Li while the cathode reactions take place at potentials as positive as 4.5V depending on the cathode material. Ideally, polymer electrolytes should exhibit stability within these potential boundaries and their usefulness in a secondary Li cell would be severely limited unless high conductivity is complimented by favorable electrochemical properties. Assessment of the electrochemical stability of SPEs has been the subject in a number of recent studies. Generally, the cathodic limit of a SPE is determined by the reduction of the anion or the plating of metallic Li, while the anodic limit is defined either by the oxidation of the current collector, the salt or the solvent. In the present study, electrochemical response on Al, Ni, Pt and Teflon-bonded Conoco coke was investigated in different regions between -0.3V to 4.2V in polymer

electrolytes. Whenever appropriate, results are compared with electrolytes containing a single plasticizer or a binary plasticizer mixture. An important objective of this study was to identify anode and cathode current collectors suitable for use with these electrolytes. Pt is the most anodically stable electrode of this group. At low potentials, however, Pt alloys with Li.[6] In order to investigate the effect of individual components of the EC-PC-BC ternary solvent mixture on the cyclic voltammetric (CV) characteristics of the SPE containing them, a proper strategy would have been to use each plasticizer separately to prepare solid polymer electrolytes. However, BC or PC alone does not produce mechanically strong electrolytes with PAN and $LiAsF_6$. Consequently, the SPEs shown in Table 6 were selected for CV work to maximize the effect of the individual plasticizer solvent on the SPE's electrochemical behavior.

Table 6. Solid Polymer Compositions chosen for CV Measurements.

	Electrolyte	
No.	PAN:EC:PC:BC:$LiAsF_6$ m/o	PAN:EC:PC:BC:$LiAsF_6$ w/o
BC18	21.0:73.0:0.0:0.0:6.0	12.8:73.7:0.0:0.0:13.5
BC19*	21.0:45.5:27.6:0.0:6.0	12.2:44.0:30.9:0.0:12.9
BC20*	21.0:33.9:20.6:18.5:6.0	11.7:31.4:22.0:22.6:12.3

*Both solid polymer electrolyte compositions, BC19 and BC 20, have a ratio EC/(EC+PC) = 0.62 and therefore belong to the M-series of compositions in Figure 6. The BC content in BC20 is close to the maximum amount that can be accommodated without disrupting the gel electrolyte formation process.

The CV observations on Pt, Ni, Al, and C electrodes for the three electrolytes given in Table 6 are presented in Figures 14 through 16. All potentials are expressed with respect to the Li^+/Li couple. Figure 14 depicts the CV response of Al and Pt between 2.5V and 4.2V.

Aluminum exhibits the lowest overall current response in all three electrolytes and it appears that it can be the material of choice for the cathode current collector. The similarity between the CV profiles for Al and Pt at high anodic potentials indicate that Al like Pt is resistant to oxidation, presumably due to its Al_2O_3 passivated surface. Comparison of the response of Al in Electrolytes BC18 and BC19 suggests that the PC-containing electrolyte is more susceptible to oxidation. The BC in BC20 electrolyte seems to retard the oxidation of PC. Pt seems to have a cathodic response, albeit with low currents, at the lower end of the potential window. This response is close to the onset potentials of the $LiAsF_6$ reduction[7]. Significant decrease of the current response, especially on Al, during the second CV cycle may be either related to a passivation phenomenon or simply the removal of electrolytic impurities within the first cycle. CV response of all four electrodes between 2.5 and 5.0V in the Electrolyte BC19 is depicted in Figure 15.

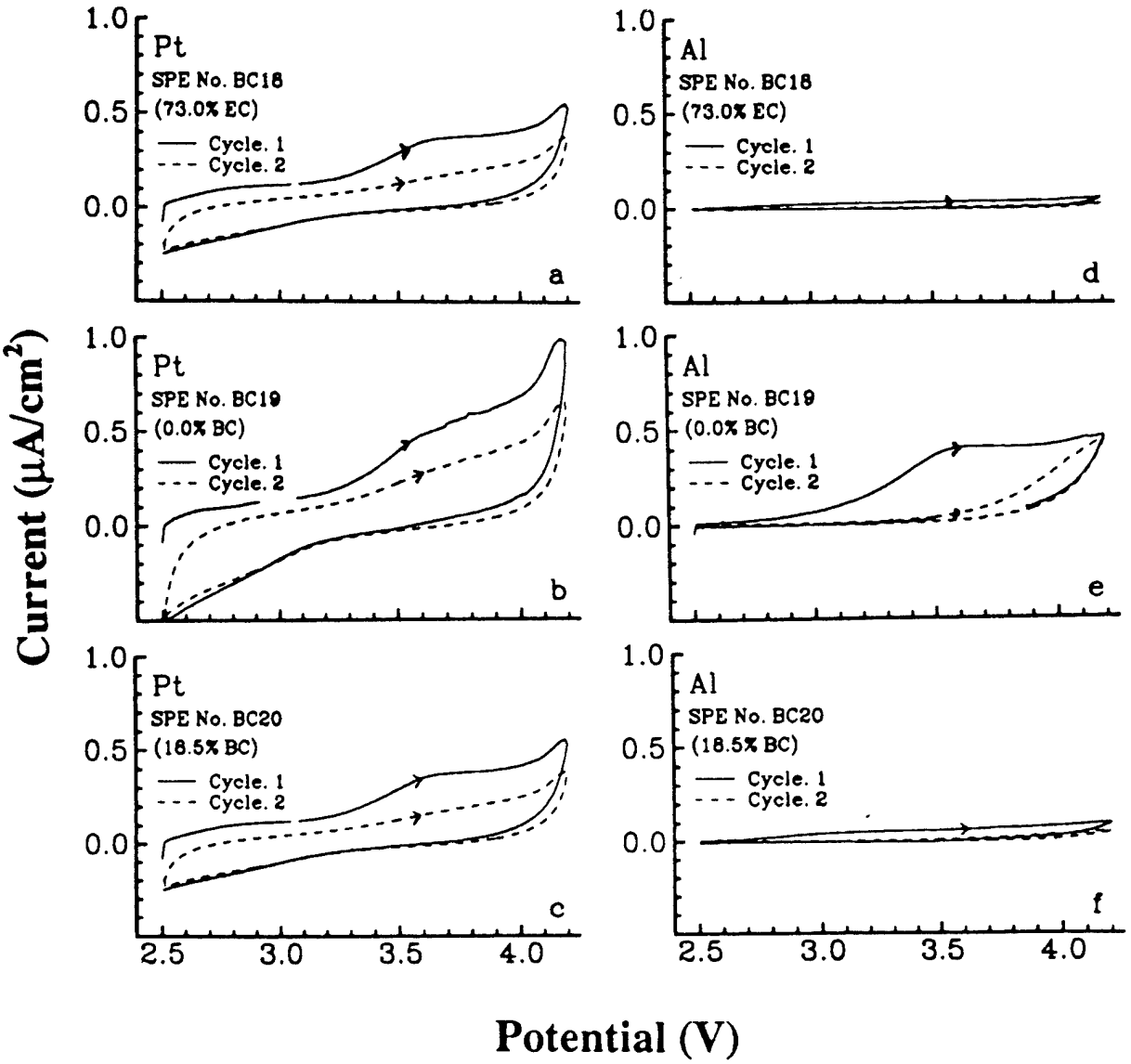

Figure 14. Cyclic voltammograms on Al and Pt from 2.5 and 4.2V of the solid polymer electrolytes given in Table 6. Sweep rate was 0.5 mV/s.

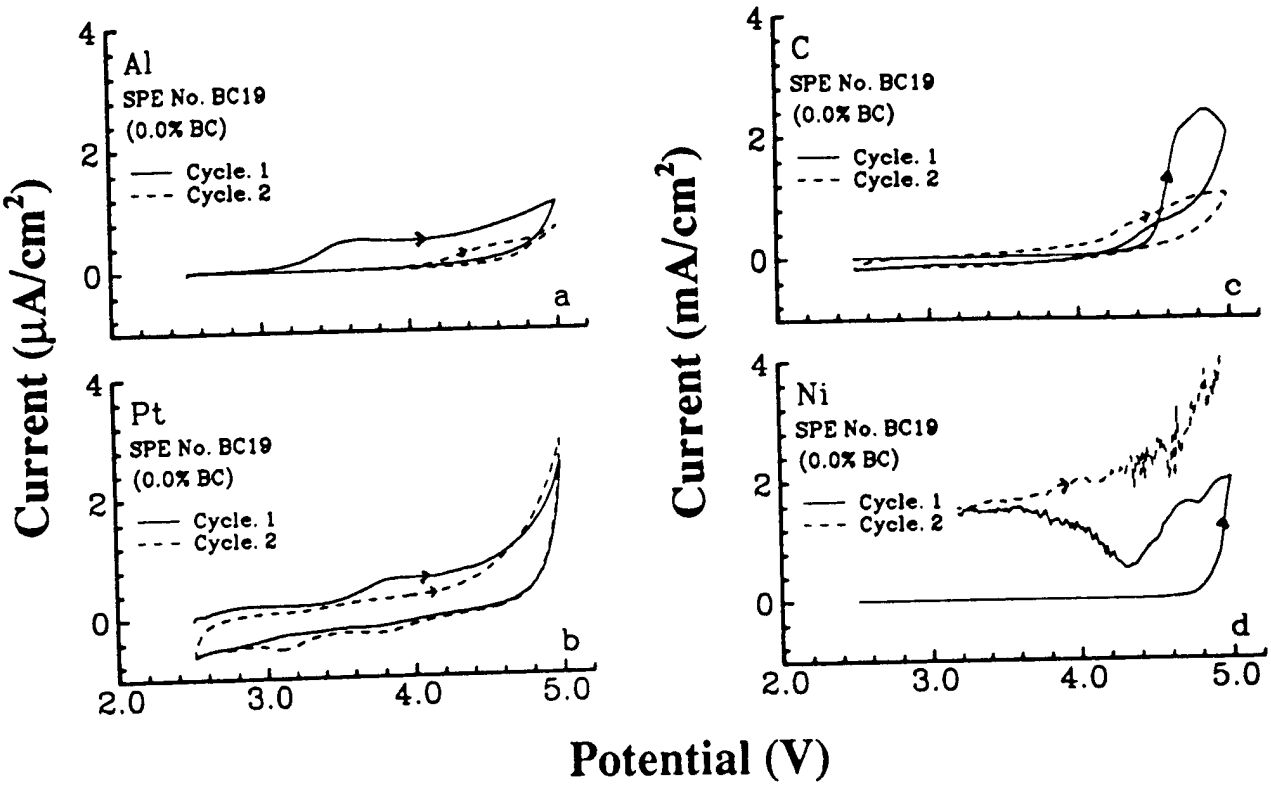

Figure 15. Cyclic voltammograms on Al, Pt, Ni, and carbon from 2.5 to 5.0V of the solid polymer Electrolyte BC19 given in Table 6. Sweep rate was 0.5 mV/s.

Higher anodic limit may mimic the situation in which a secondary battery is subjected to an overcharge. Again, in the case of Al anodic response observed around 3.2V during the first cycle becomes insignificant until above 4.2V during the second cycle. This illustrates the favorable response of an Al cathode current collector towards overcharge. In contrast, the oxidation currents on Ni, as shown in Figure 15d, began to increase substantially beyond 4.5V and continued upwards during the reverse scan, and also in the second cycle. A highly corroded electrode surface suggested oxidation of Ni itself. CV response for the Pt (Figure 15b) and carbon electrodes (Figure 15c) indicate that electrolyte oxidation occurs around 4.5V in both cases. The difference between the effective surface areas of Pt and carbon (about 1500 cm^2) correlates with the relative magnitudes of their current responses.

Figure 16 illustrates the CV response on all four electrodes of the SPE BC18 within a potential span of 2.5V to -0.3V.

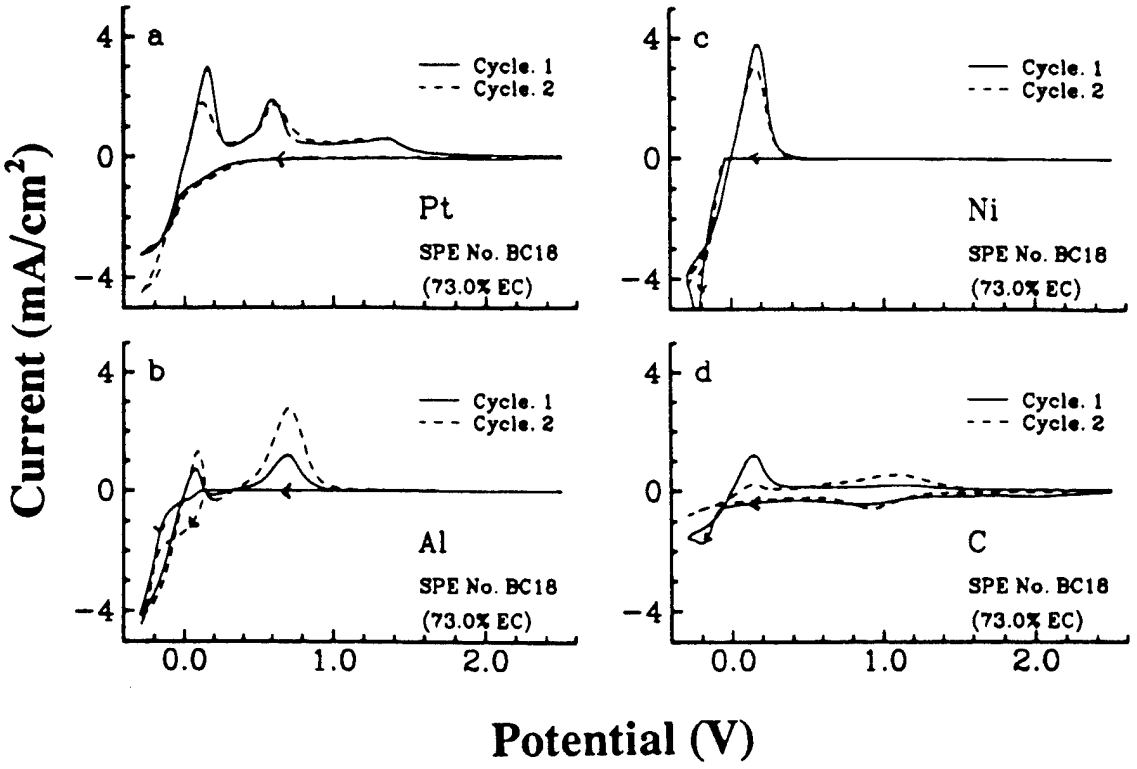

Figure 16. Cyclic voltammograms on Al, Pt, Ni, and carbon from 2.5 to -0.3V of the solid polymer Electrolyte BC19 given in Table 6. Sweep rate was 0.5 mV/s.

Formation of Li-Al alloys has been well documented.[6,8] As can be seen in Figure 16b, Li alloying on Al begins about 0.15V and proceeds at a high rate in the cathodic direction. Lithium deposition and alloy formation take place simultaneously around 0V and cross-over in the voltammogram relates to a nucleation and growth phenomenon. Delithiation of the alloy take place at around 750 mV. In the case of Ni, a simple Li deposition/stripping process took place with nearly 100% charge efficiency. Since no alloy formation was observed, Ni is the material of choice for the anode current collector as being used traditionally in many Li cells. Platinum, which also has the ability to form Li alloys, behaved similar to Al. In this case, three peaks for Li de-alloying located at 0.2, 0.75 and 1.38V are visible in Figure 16a. Unlike the other electrodes, the carbon electrode showed a distinct cathodic peak for Li intercalation at 1.0V with a corresponding peak centered around 1.2V for the reverse process. This intercalation process has been well documented.[9] The peaks located around 0V are for Li deposition and stripping processes. Nearly identical observations with SPE BC20 suggest that BC is indifferent to the cathodic processes.

Similar investigations were also carried out to determine the electrochemical stability of Electrolytes MX3, MX22, MX23 (Table 3) on different electrode surfaces. Electrolyte MX22 allowed us to study the electrochemical effect of MEOX plasticizer individually. Figure 17 depicts the CV response of Al and Ni from 2.5V to 4.2V.

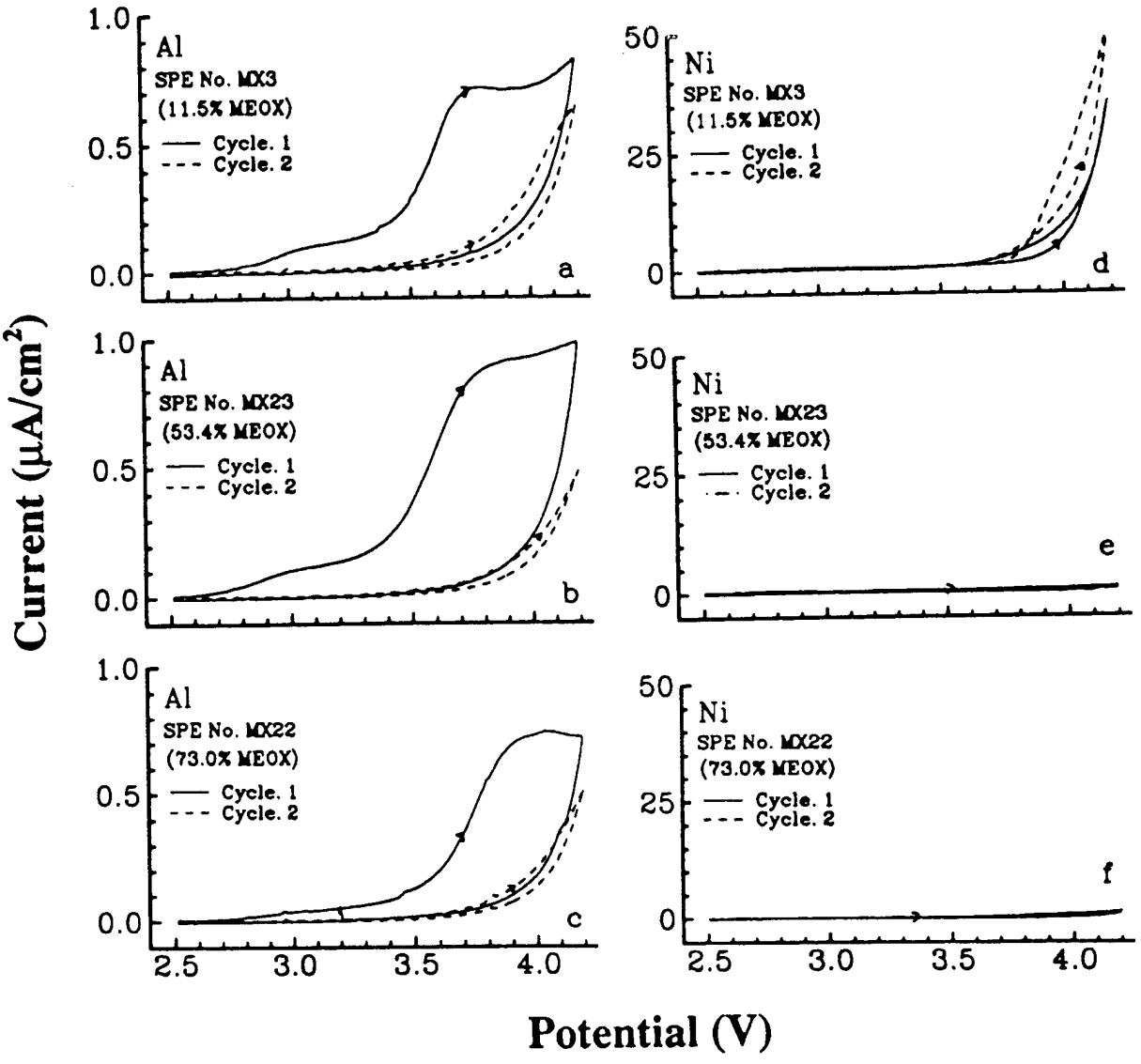

Figure 17. Cyclic voltammograms on Al and Ni from 2.5 to 4.2V of the solid polymer Electrolytes MX3, MX23, and MX22 given in Table 3. Sweep rate was 0.5 mV/s.

Stability of MEOX-containing electrolytes on Al in this anodic regime is immediately recognizable in Figures 17a through 17c, where the decomposition currents remain below 1$\mu A/cm^2$ at 4.2V. These data reaffirm the suitability of Al as the anodic current collector. It appears in Figure 14e and Figures 17a through 17c that the onset and peak currents for the decomposition of the electrolytes shift to more anodic potentials as the amount of MEOX in the electrolyte increases. This shift may be the result of the gradual decrease in the concentration of an impurity present in EC and/or PC as their ratios in the SPE change from 73 m/o in SPE BC19 to 0 m/o in SPE MX22 or it may be a simple oxidation/passivation process involving the electrode surface itself. Reduction of water in EC or PC may not be the cause for this shift because all plasticizers used in SPE preparation contained a water content of about 18 ppm. During the second cycle the anodic response of all three electrolytes becomes insignificant and the onset of decomposition currents shift towards 3.8V. As discussed earlier, the oxidative response for Ni starting from around 3.5V involves oxidation of the metal itself. The latter also accounts for the anodic currents of the order of 50 $\mu A/cm^2$, occurring around 3.5V, as shown in Figures 17d and 17f. Yet, increased amount of MEOX in the SPE seems to inhibit Ni oxidation to the extent that the electrochemical behavior of Ni can be made to approach the behavior of Al within this narrow potential window as the SPE composition changes to MX22. In this case, the oxidation current at 5.0V remains around 11 $\mu A/cm^2$. We observed a similar trend even in a wider potential window of 2.5V-5.0V. The oxidation current on Al remained below 2 $\mu A/cm^2$ even at 5.0V, while that on Ni remained an order of magnitude smaller than currents shown in Figure 15d. This suggest that MEOX not only inhibits the oxidation of Ni but it also decreases the overall electrochemical activity of the metal surface itself. Significantly higher anodic currents observed on Pt at about 4.5V in MEOX-containing electrolytes compared to those in Figure 15b suggest that Pt surface is electrocatalytic towards oxidation of such electrolytes.

Figure 18 shows the voltammograms of MEOX-containing electrolytes on carbon and Ni electrodes between -0.3V to 2.5V.

The overall CV features appear to be similar to those of BC-containing electrolytes. However, as the ratio of MEOX in the plasticizer increases from 11.5 m/o in MX3 to 73 m/o in MX22 the CV response on both electrodes diminishes. Since all these SPEs have similar conductivities at room temperature, differences in electroactivity may be due to modification of the electrode surface by MEOX, possibly through an adsorption process. For the MX3 electrolyte on carbon (Figure 18a), waves for Li deposition/stripping and intercalation/deintercalation processes are clearly visible. On the other hand, Li intercalation appears to be the predominant process for the MX22 electrolyte (Figure 18c) and Li deposition is insignificant even at potentials as low as -0.3V. The CV of MX23 (Figure 18b) holds a middle ground between these two cases. In a related study, we observed a decrease in electrochemical activity with increasing amount of MEOX in the SPE for Li alloy formation on Al and Pt.

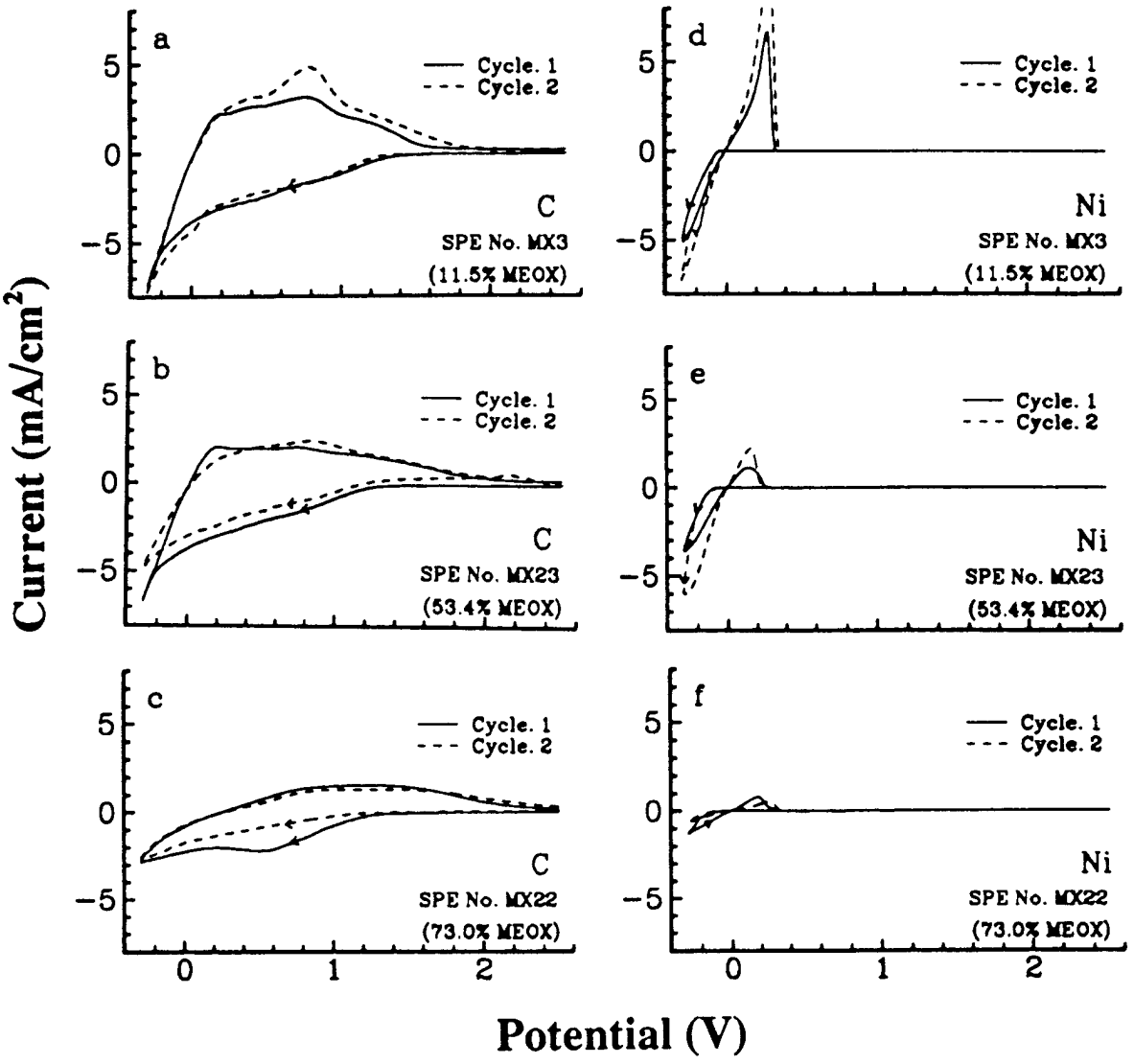

Figure 18. Cyclic voltammograms within a potential span of 2.5 and -0.3V on carbon and Ni in contact with the solid polymer electrolytes MX3, MX23, and MX22 given in Table 3. Sweep rate was 0.5 mV/s.

3.1.9 The Behavior of Li/Polymer Electrolyte Interface. Charge transfer at Li/electrolyte interface is expected to be influenced by the dynamics of Li passivation and other factors such as the morphology of plated Li. The study of the nature of this interface has a direct relevance to the understanding of the rechargeability and the rate capability of Li cells. There have been a number of studies on the electrochemical properties of the Li/liquid electrolyte interface[10-13]. Tafel characteristics of the Li/organic liquid electrolyte interface has been shown to depend intimately on the thickness of the solid electrolyte interface (SEI),[14,15] and any attempt to use Tafel plots to evaluate kinetic parameters of such an interface is valid only under rigorously controlled conditions, such as short overpotential measurement times to preserve the thickness of the SEI layer. Considering the relatively not so perfect contact between the Li/SPE interface coupled with its possible correlation with the morphological changes occurring on the Li surface especially during long term polarization, use of Tafel plots to extract any kinetic parameters may be highly questionable despite a recent report on such measurements.[16] Our own preliminary measurements with Li//SPE//Li cell based on MEOX-containing SPEs have shown that in a galvanostatic overpotential measurement (e.g., at 0.36 mA/cm^2) the potential of the working electrode never reached a steady value regardless the duration of the measurement. In a related experiment, a sequence of anodic and cathodic galvanostatic steps of the same magnitude (e.g., at 0.36 mA/cm^2) and duration (i.e., 300 sec.) have failed to show a consistency in the final overpotential attained in each successive cathodic or anodic step. Nevertheless, some relevant information on the charge transfer resistance at the Li/SPE interface in contact with a particular SPE can be obtained from AC impedance measurements. In a three electrode solid-state cell an approximate value for the charge transfer resistance of the working electrode can be obtained from the diameter of the semicircle in the Cole-Cole plot of the AC impedance data for the electrode.[17] We have noticed that the charge transfer resistance extracted in this fashion for the Li/SPE interface reaches a pseudo-steady-state value after about 24 hours following a few initial galvanostatic anodic/cathodic cycles. The solid electrolyte interface (SEI) re-formed following this perturbation may be characteristic of the composition of the SPE in contact with the Li electrode. We investigated the evolution of the charge transfer resistance at the Li/SPE interface as a function of the SPE's MEOX content. All Li//SPE//Li cells underwent three anodic/cathodic cycles with a passage of 0.1C/cm^2 charge in each step. Following this SEI "shuffling", the cell was allowed to rest for 24 hours, under open-circuit, before measuring the impedance. In the PAN/EC-PC-MEOX/$LiAsF_6$ electrolytes used for this study, MEOX content in the plasticizer varied form 0.0 to 100 mole % all having a common ratio of EC/(EC+PC) = 70. The observations are shown in Figure 19. As the ratio of MEOX in the plasticizer increases, the charge transfer resistance seems to increase and reaches the highest value when the SPE contains only MEOX. These observations are consistent with MEOX retarding the electrochemical activity of the electrolytes seen in Figures 17 and 18 on electrodes other than Li. It is useful to note that in a recent study similarities have been established in the structure and properties of surface films formed on Li and noble metals in propylene carbonate electrolytes at low potentials.[18]

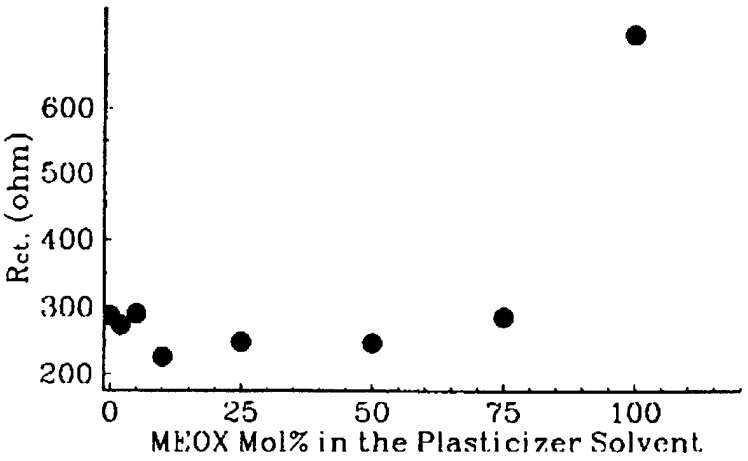

Figure 19. Effect of the content of MEOX on the charge-transfer resistance of Li/solid electrolyte interface.

3.2 Li//SPE//$Li_xMn_2O_4$ Cells

3.2.1 Discharge Capacity and Cycling Behavior. Low voltage lithiated manganese oxides were characterized in solid polymer electrolyte (SPE) cells of the type Li//SPE//$Li_xMn_2O_4$. Capacity utilization and cycle life of these cells were of primary interest. The cells of two or three electrode configuration were typically cycled between 3.75V to 2.0V. Composition of some of the key solid polymer electrolytes used are given in Table 7.

Table 7. SPE Compositions used in Solid Polymer Electrolyte Cells.

	Electrolyte	
Number	PAN:EC:PC:BC:$LiAsF_6$ (m/o)	PAN:EC:PC:BC:$LiAsF_6$ (w/o)
BC5X	21.0:43.2:26.2:3.7:6.0[a]	12.1:41.4:29.1:4.6:12.8
BC15	21.0:37.8:22.9:12.3:6.0[b]	11.9:35.4:24.9:15.3:12
BC18	21.0:71.0:0.0:0.0:8.0[b]	12.5:70.0:0.0:0.0:17.5
#3	23.0:38.5:33.2:0.0:5.4	13.5:37.5:37.5:0.0:11.6
Number	PAN:EC:PC:MEOX:$LiAsF_6$ (m/o)	PAN:EC:PC:MEOX:$LiAsF_6$ (w/o)
MX3	21.0:33.8:27.7:11.5:6.0	12.1:32.1:30.6:12.6:12.7
MX23K[c]	19.0:11.1:9.0:54.8:6.2	12.5:10.2:9.5:57.4:12.5
SA92	21.0:36.5:0.0:36.5:6.0	12.1:35.0:0.0:40.1:12.8.
Number	PAN:EC:BL:$LiAsF_6$ (m/o)	PAN:EC:BL:$LiAsF_6$ (w/o)
ECBL1	21.0:36.5:36.5:6.0	12.9:37.2:36.3:13.6
ECBL6	21.0:29.2:43.8:6.0	12.9:29.8:43.7:13.6
Number	PAN:EC:BL:$LiPF_6$ (m/o)	PAN:EC:BL:$LiPF_6$ (w/o)
ECBL2	21.0:36.5:36.5:6.0	10.9:38.3:37.5:13.3
ECP1	13.0:72.9:0.0:14.1	
Number	PAN:EC:DPC:$LiPF_6$ (m/o)	PAN:EC:DPC:$LiPF_6$ (w/o)
DPC2	20.0:68.0:7.0:5.0	12.0:67.8:11.6:8.6
DPCX	0.0:57.0:38.0:5.0	0.0:44.3:49.0:6.7

[a]The plasticizer composition corresponds to 5 X_{BC}.

[b]The plasticizer composition corresponds to 17X_{BC} (BC15 in Table 6).

[c]This SPE is related to MX23 (Table 3) except that it has lower PAN content.

Figures 20 and 21 depict the capacity and cycling performance of $Li_{0.9}Mn_2O_{4.2}$ in test cells employing the Electrolytes BC15 and BC5X, respectively, from Table 7.

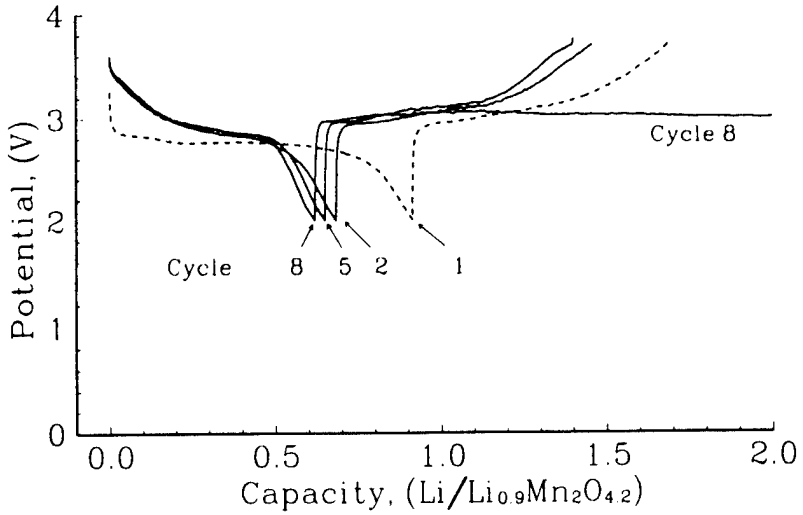

Figure 20. Cycling curves at room temperature for Li//SPE//$Li_{0.9}Mn_2O_{4.2}$ Cell LMN12. Theoretical capacity was 21.7 mAh. Solid polymer electrolyte was BC15 (Table 7). The cathode was 51.0 w/o $Li_{0.9}Mn_2O_{4.2}$:8.0 w/o Chevron Carbon:14.5 w/o EC:10.2 w/o PC:6.3 w/o BC:4.9 w/o PAN:5.1 w/o $LiAsF_6$. Cathode geometric area was 10 cm^2. Charge/discharge current density was 0.1 mA/cm^2.

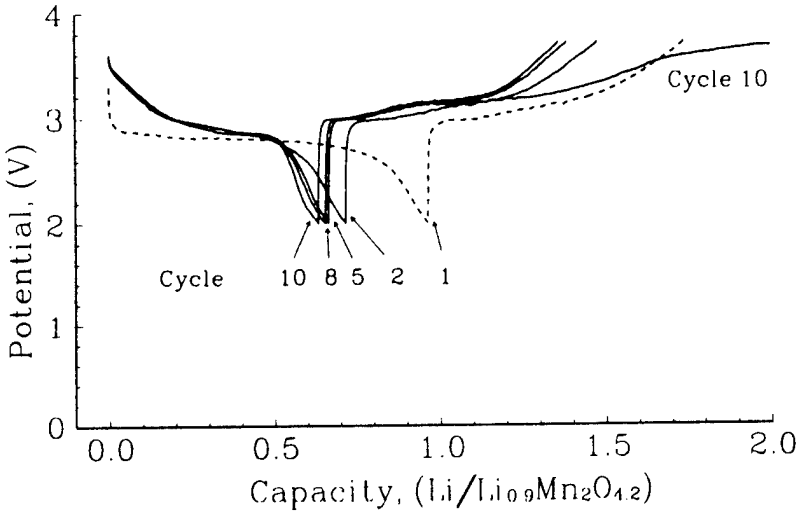

Figure 21. Cycling curves at room temperature for Li//SPE//$Li_{0.9}Mn_2O_{4.2}$ Cell LMN21. Theoretical capacity was 21.8 mAh. Solid polymer electrolyte was BC5X (Table 7). The cathode was 50.3 w/o $Li_{0.9}Mn_2O_{4.2}$:7.9 w/o Chevron Carbon:17.3 w/o EC:12.2 w/o PC:1.9 w/o BC:5.1 w/o PAN:5.4 w/o $LiAsF_6$. Cathode geometric area was 10 cm^2. Charge/discharge current density was 0.1 mA/cm^2.

In both cases the reversible capacity declined slowly at first and then reached a constant value corresponding to an intercalation of 0.6 moles Li per $Li_{0.9}Mn_2O_{4.2}$. As indicated in Figure 20, the irreversible capacity observed between the first discharge and the first charge amounts to nearly 0.15 Li per $Li_{0.9}Mn_2O_{4.2}$. The Li utilization in the first two cycles is as summarized below.

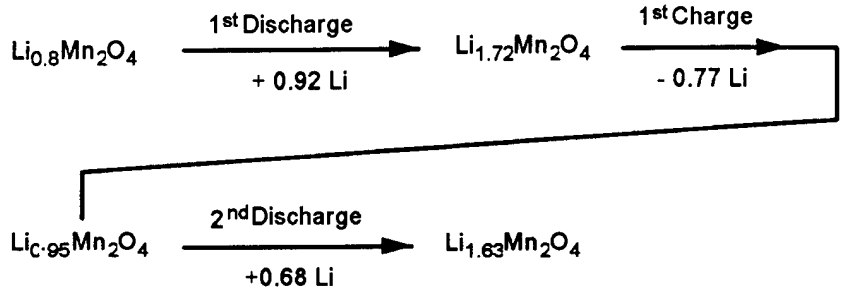

The end of the useful cycle life was indicated by greater disparity between the capacity observed in a charge and the following discharge. This capacity difference is due to the growth of Li dendrites through the SPE forming an electrical shunt (called soft short) between the active electrodes. A number of charge/discharge runs identical to those shown in Figures 20 and 21 were undertaken. Even though they all showed efficient rechargeability, the cycle life in all cases did not exceed dozen or so cycles. However. one noticeable feature was that the cells based on the SPE BC15 consistently ran fewer cycles compared to its counterpart with lower BC content (BC5X). A test cell that failed was opened and examined under the microscope, and the cathode was found to have delaminated from its aluminum backing. Li growth through the SPE was clearly visible and it had the appearance of a "leopard skin" with a distinctive black pattern limited to the region where the two active electrodes contacted the SPE. The perimeter of SPE away from that region did not show any evidence of lithium growth through the electrolyte film.

Shown in Figure 22 is the cycling performance of a Li//SPE//$Li_{0.9}Mn_2O_{4.2}$cell based on SPE #3 (Table 7) which does not contain BC plasticizer. A cycle life longer than either of the cells shown in Figures 20 and 21 was consistently observed. Although electrochemical activity of SPE based on EC-PC-BC ternary mixtures was not different from those without BC, SPE containing BC seem to have the disadvantage of promoting the growth of lithium through the SPE layer, thereby shortening the cycle life of the cell.

Cycling behavior shown above indicates a capacity gap of nearly 0.2 Li/$Li_{0.9}Mn_2O_{4.2}$ between the first discharge and the first charge. This difference is consistent with the conversion of $Li_{0.9}Mn_2O_{4.2}$ to $Li_{1.1}Mn_2O_4$ during the first discharge followed by the extraction of 0.8 Li during the first charge. However, since Li is present in large excess in these cells, capacity during the second discharge and subsequent charge/discharge steps should be equivalent to one Li/Mn_2 corresponding to the reversible conversion of $LiMn_2O_4$ to $Li_2Mn_2O_4$. In contrast, the discharge capacity in the second cycle remains close to 80% of that of the first discharge. The different discharge profiles between the first and the second discharge, however, suggest a possible change of the crystal structure of the cathode material during the fist discharge.

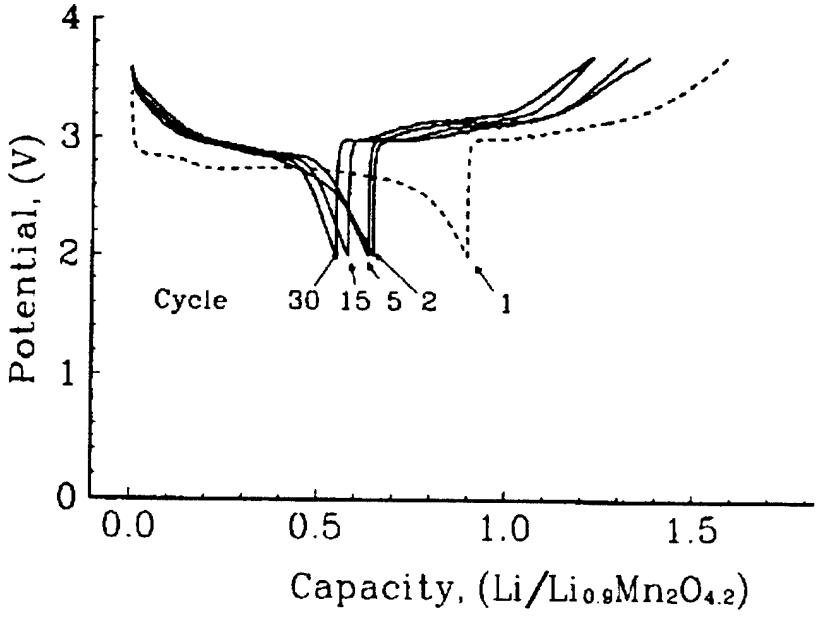

Figure 22. Cycling curves at ambient temperature for Li//SPE//$Li_{0.9}Mn_2O_{4.2}$ Cell LMN23. Theoretical capacity was 24.7 mAh. Solid polymer electrolyte was #3 (Table 7). The cathode was 51.0 w/o $Li_{0.9}Mn_2O_{4.2}$:8.0 w/o Chevron Carbon:15.4 w/o EC:15.4 w/o PC:5.5 w/o PAN:4.8 w/o $LiAsF_6$. Cathode geometric area was 10 cm^2. Charge/discharge current density was 0.1 mA/cm^2

Two types of low voltage lithiated manganese oxides, $Li_{0.9}Mn_2O_{4.2}$ and $Li_{1.0}Mn_2O_{4.7}$ were characterized in PAN-based solid polymer electrolytes containing MEOX containing ternary plasticizers. Figures 23 through 26 compare the voltage versus capacity profiles and the long-term cycle life of the two cathode materials in Li//SPE//$Li_xMn_2O_4$ cells containing the MX3 electrolyte from Table 7.

According to Figure 23, the first and the second cycle discharge capacities correspond to the utilizations of 0.87 and 0.63 mol Li per $Li_{0.9}Mn_2O_{4.2}$. In contrast, the corresponding utilizations for $Li_{1.0}Mn_2O_{4.7}$ were 0.96 and 0.75 Li/Mn_2 in the same electrolyte (Figure 25). The gap between the first and the second discharge capacities, however, remains at about 0.20 Li/Mn_2 for both materials. The discharge capacity of $Li_{1.0}Mn_2O_{4.7}$ remains above that of $Li_{0.9}Mn_2O_{4.2}$ until cycle 100, at which point the utilization of both materials approaches 0.5 Li per Mn_2. From cycle 50 to cycle 100, the fade rate of $Li_{1.0}Mn_2O_{4.7}$ was about 0.13% per cycle. The fade rate of $Li_{0.9}Mn_2O_{4.2}$ however, was a significantly low 0.01% per cycle within the same span of charge/discharge cycles. Beyond cycle 100, utilization of $Li_{0.9}Mn_2O_{4.2}$ was slightly better than that of $Li_{1.0}Mn_2O_{4.7}$. The voltage versus capacity profiles shown in Figures 23 and 25 indicate little change from the second cycle onwards. Because of its overall excellent charge/discharge reversibility (Figure 26), longer cycle life and appreciably higher Li utilization during the most of its cycle life, $Li_{1.0}Mn_2O_{4.7}$ appears to be the superior of the two cathode materials.

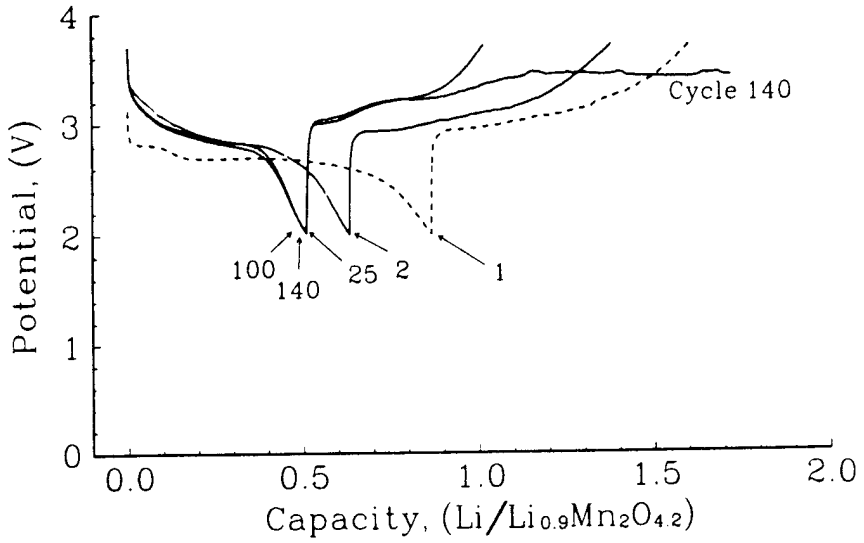

Figure 23. Cycling curves at room temperature for Li//SPE//$Li_{0.9}Mn_2O_{4.2}$ Cell BMX4. Theoretical capacity was 17.6 mAh. Solid polymer electrolyte was MX3 (Table 7). The cathode was 50.0 w/o $Li_{0.9}Mn_2O_{4.2}$:8.0 w/o Chevron Carbon:15.3 w/o EC:14.6 w/o PC:6.0 w/o MEOX:3.1 w/o PAN:3.1 w/o $LiAsF_6$. Cathode geometric area was 10 cm^2. Charge/discharge current density was 0.1 mA/cm^2.

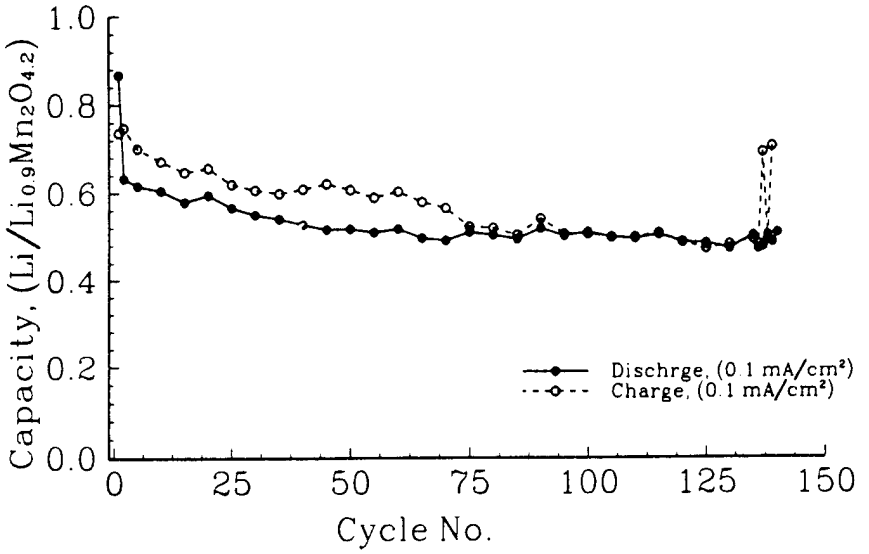

Figure 24. Capacities as a function of cycle number for the cell shown in Figure 23.

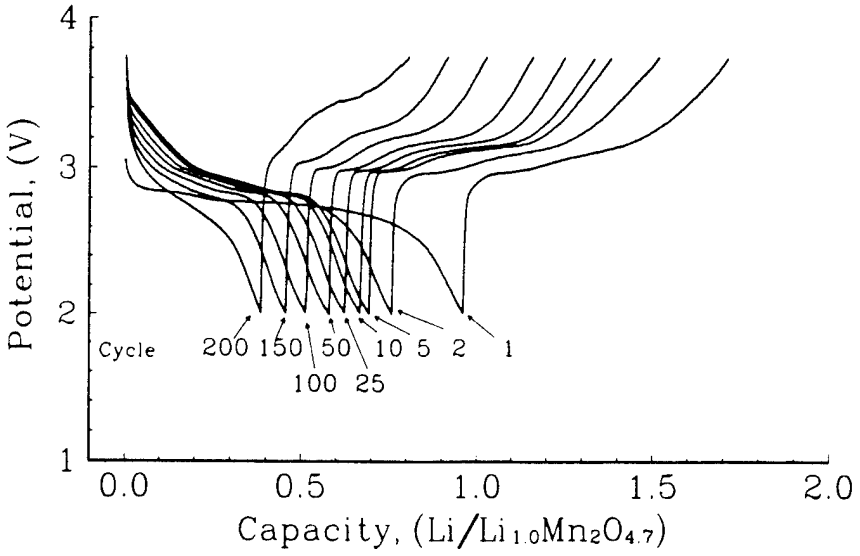

Figure 25. Cycling curves at room temperature for Li//SPE//$Li_{1.0}Mn_2O_{4.7}$ Cell No. BMX34. Theoretical capacity was 12.1 mAh. Solid polymer electrolyte was MX3 (Table 7). The cathode was 51.0 w/o $Li_{1.0}Mn_2O_{4.7}$:8.0 w/o Chevron Carbon:14.9 w/o EC:14.2 w/o PC:5.9 w/o MEOX:3.0 w/o PAN:3.0 w/o $LiAsF_6$. Cathode geometric area was 10 cm^2. Charge/discharge current density was 0.1 mA/cm^2.

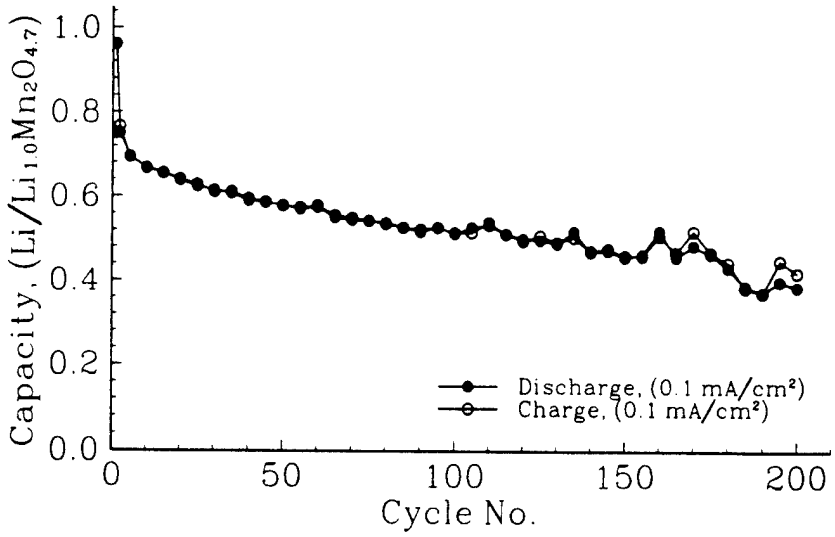

Figure 26. Capacities as a function of cycle number for the cell shown in Figure 25.

Data in Table 3 indicate that SPE compositions suitable for low temperature applications can be found in high MEOX (MX23) regions of the ternary composition diagram. Capacity and long-term performance depicted in Figure 27 are for a $Li/Li_{0.9}Mn_2O_{4.2}$ cell utilizing the polymer Electrolyte MX23K (Table 7) which is related to the SPE MX23 in Table 3.

The first cycle discharge capacity shown in Figure 27 is close to 68% of the theoretical capacity. Despite this slightly inferior cathode utilization in the first cycle of the cell BMX9, the overall capacity and long-term cycling performance of this cell is similar to the one shown in Figure 24 for the same cathode material (i.e., $Li_{0.9}Mn_2O_{4.2}$) in a cell utilizing the SPE MX3. Figure 29 depicts the capacity as a function of cycle number of $Li_{1.0}Mn_2O_{4.7}$ in a cell utilizing SPE MX3 at C/6 and C/3 rates.

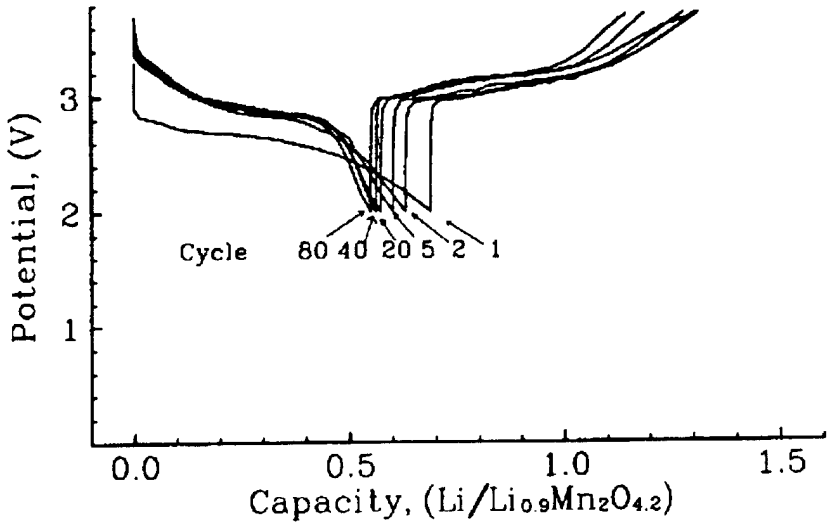

Figure 27. Cycling curves at room temperature for $Li//SPE//Li_{0.9}Mn_2O_{4.2}$ Cell BMX9. Theoretical capacity was 12.2 mAh. Solid polymer electrolyte was MX23K (Table 7). The cathode was 51.0 w/o $Li_{0.9}Mn_2O_{4.2}$:8.0 w/o Chevron Carbon:4.6 w/o EC:4.3 w/o PC:26.1 w/o MEOX:3.0 w/o PAN:3.0 w/o $LiAsF_6$. Cathode geometric area was 10 cm^2. Charge/discharge current density was 0.1 mA/cm^2.

Both cells were charged at C/6 rate. Following a steep decline in capacity during initial cycles, utilization during discharge has leveled off at 0.5 and 0.4 Li per $Li_{1.0}Mn_2O_{4.7}$ for C/6 and C/3 rates, respectively, indicating this material's ability to sustain long-term cycling at higher discharge rates.

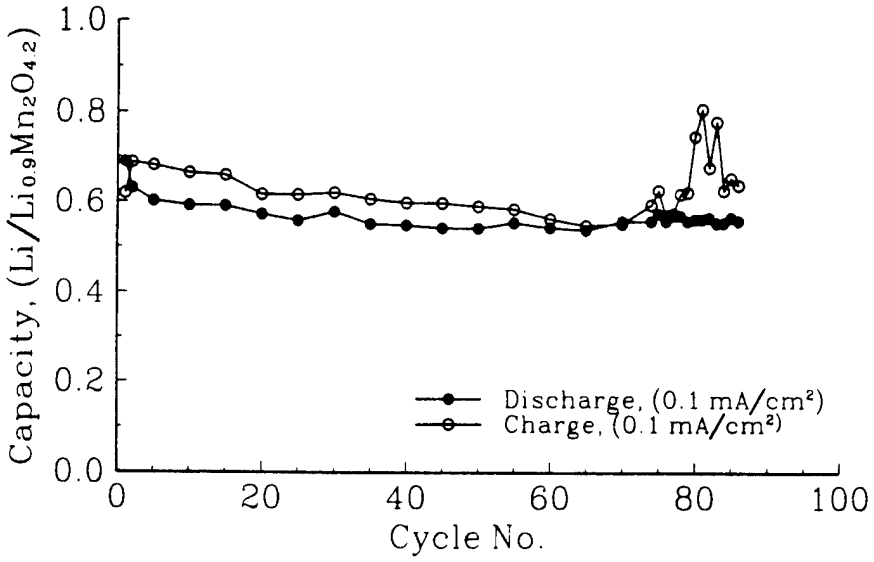

Figure 28. Capacities as a function of cycle number for the cell shown in Figure 27.

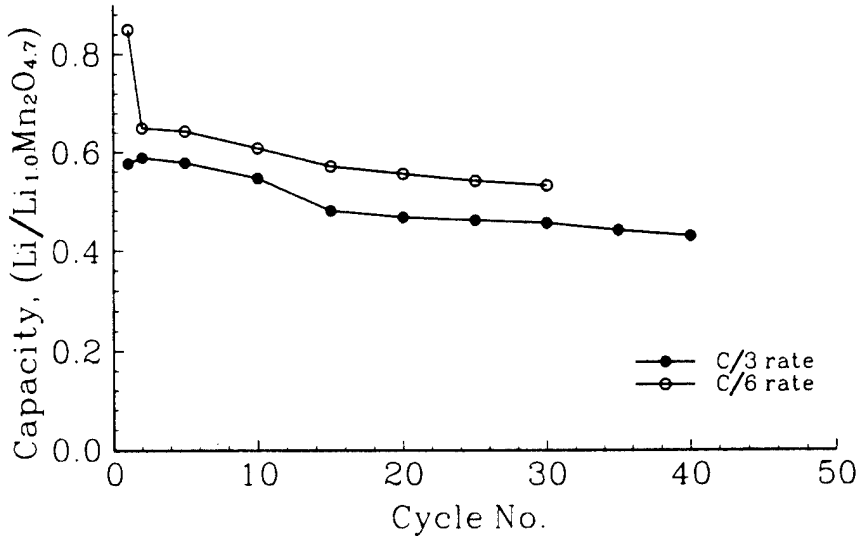

Figure 29. Capacities at room temperature as a function of cycle number for Li//SPE//$Li_{1.0}Mn_2O_{4.7}$ Cell BMX51 at C/6 rate (open circles) and Cell BMX52 (dark circles) at C/3 rates. The solid polymer electrolyte is MX3 (Table 7). Cathode capacities were 12.33 mAh (BMX51) and 12.9 mAh (BMX52). Charge/discharge current densities were 0.2/0.2 mA/cm^2 (BMX51) and 0.2/0.4 mA/cm^2 (BMX52). The cathode was 51.0 w/o $Li_{1.0}Mn_2O_{4.7}$:8.0 w/o Chevron Carbon:14.9 w/o EC:14.2 w/o PC:5.9 w/o MEOX:3.0 w/o PAN:3.0 w/o $LiAsF_6$. Cathode geometric area was 10 cm^2.

Figure 30 depicts the voltage versus capacity curves for $Li_{0.9}Mn_2O_{4.2}$ at various discharge rates at room temperature. At the rate of 0.2 mA/cm^2 (C/5 rate), a capacity of 0.55 mol Li per $Li_{0.9}Mn_2O_{4.2}$ was obtained. Figure 31 displays cycling curves at -10°C for $Li_{1.0}Mn_2O_{4.7}$ at various cycling rates.

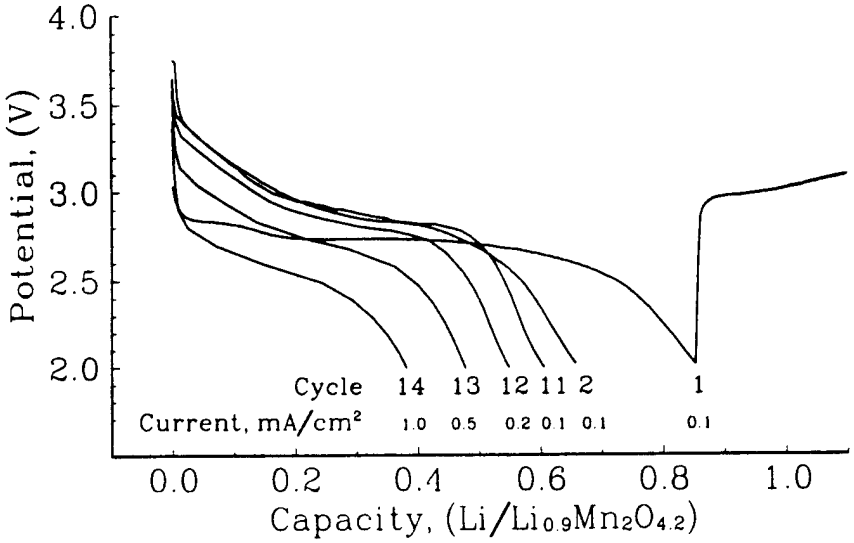

Figure 30. The voltage versus capacity profiles at room temperature for Li//SPE//$Li_{0.9}Mn_2O_{4.2}$ Cell BMX8 at different discharge rates. Charging was done at 0.1 mA/cm^2. Theoretical capacity was 11.1 mAh. Solid polymer electrolyte was MX3 (Table 7). The cathode was 51.0 w/o $Li_{0.9}Mn_2O_{4.2}$:8.0 w/o Chevron Carbon:14.9 w/o EC:14.2 w/o PC:5.9 w/o MEOX:3.0 w/o PAN:3.0 w/o $LiAsF_6$. Cathode geometric area was 10 cm^2.

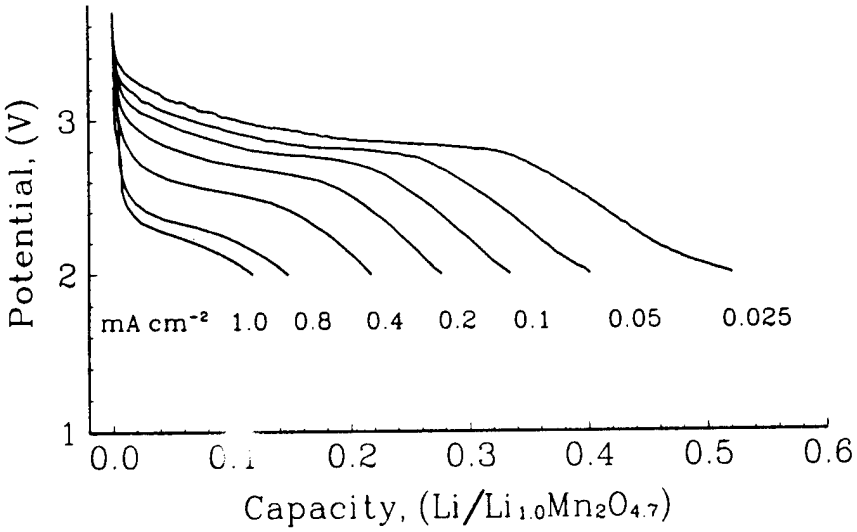

Figure 31. The voltage versus capacity profiles at -10°C for Li//SPE//$Li_{1.0}Mn_2O_{4.7}$ Cell BMX55 at different discharge rates. Charging was done at 0.1 mA/cm^2 (~C/10). Theoretical capacity was 9.8 mAh. Solid polymer electrolyte was MX3 (Table 7). The cathode was 51.0 w/o $Li_{1.0}Mn_2O_{4.7}$ 8.0 w/o Chevron Carbon:14.9 w/o EC:14.2 w/o PC:5.9 w/o MEOX:3.0 w/o PAN:3.0 w/o $LiAsF_6$. Cathode geometric area was 10 cm^2.

Before cycling at -10°C the cell was cycled three times at the room temperature at which a reversible capacity of 0.62 mol Li per $Li_{1.0}Mn_2O_{4.7}$ was observed at the end of the third cycle. In this case charge/discharge was done at 0.2 mA/cm^2 (~C/5 rate). Discharge capacities observed at -10°C are on the order of 50% of that observed at room temperature at comparable current densities. For example, the utilization at 0.2 mA/cm^2 was close to 0.3 mol Li per $Li_{1.0}Mn_2O_{4.7}$. At -20°C the Li utilization dropped to roughly 50% of those observed at -10°C. In this case, the discharge capacity at the same current density was approximately 0.15 mol Li per $Li_{1.0}Mn_2O_{4.7}$. Figure 32 compares the cycling performance at -10°C and -20°C of Li//SPE//$Li_{1.0}Mn_2O_{4.7}$ Cell No. BMX55 utilizing SPE MX3 at a charge/discharge rate of 0.12 mA/cm^2. The first three cycles were performed at room temperature.

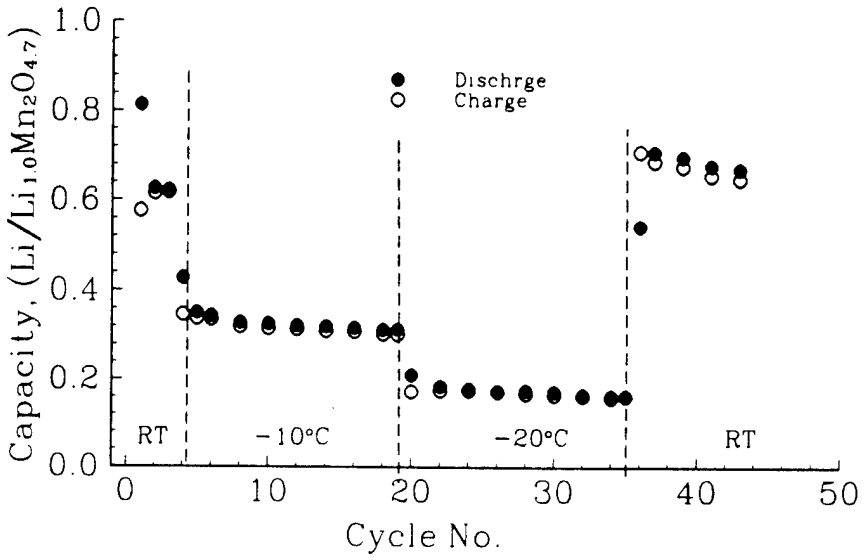

Figure 32. Discharge/charge capacities at different ambient temperatures (noted on the figure) as a function of cycle number for Li//SPE//$Li_{1.0}Mn_2O_{4.7}$ Cell BMX54 at 0.12 mA/cm^2. Theoretical capacity was 10.7 mAh. Solid polymer electrolyte was MX3 (Table 7). The cathode was 51.0 w/o $Li_{1.0}Mn_2O_{4.7}$:14.2 w/o PC:5.9 w/o MEOX:3.0 w/o PAN:3.0 w/o $LiAsF_6$. Cathode geometric area was 10 cm^2.

Diminished Li utilization at sub ambient temperatures is evidenced by the data in Figure 31. Prior to changing the temperature almost 100% reversibility between the charge/discharge capacity was observed. A noticeable feature however, is the nearly 20% difference between the discharge/charge capacities of the first cycle at each temperature despite a nearly three hours stay at each temperature prior to start cycling. Origin of this recurrent irreversible capacity remains unclear. Renewed growth of the passivation layer (and associated over potential) may not be the probable reason because, the Li utilization is restored back to original levels when the temperature is returned to room temperature (Figure 32). Satisfactory low ambient temperature conductivity without freezing was demonstrated for the solid polymer Electrolyte MX3 during electrolyte development. Therefore, extensive polarization of the Li//SPE//$Li_{1.0}Mn_2O_{4.7}$ cell at low ambient temperatures shown in Figure 32 may not be due to a severe drop in electrolyte conductivity due

to freezing. Other possible reasons are the concentration polarization of a practical cell under load due to diminished mass transport and sluggish heterogeneous charge transfer at the solid/polymer electrolyte interface. Since convection is virtually absent, a polymer electrolyte can sustain stable long range concentration gradients that may extend over the entire width of the electrolyte phase. This situation may be critical, specially at low temperature, for the electrolyte confined into narrow channels inside a composites electrode. For such an electrolyte concentration polarization becomes a very complex issue and it was not addressed in this study. However, we investigated the effect of temperature on the charge transfer resistance at the interface between polymer electrolyte and $Li_{1.0}Mn_2O_{4.7}$ electrode by AC impedance measurement.

3.2.2 Impedance Behavior of Li//SPE//Low Voltage $Li_xMn_2O_4$ Cells. In the presence of a reference electrode and a large counter electrode, the impedance measurement can be employed to study the working electrode/electrolyte interfacial behavior alone. Impedance data is usually interpreted in terms of an equivalent circuit representing the interfacial processes occurring at various time domains. Impedance measurement of a composite electrode is seriously prone to problems arising from surface roughness, imperfect contacts at the electrolyte/electrode interface, and variable local charge carrier concentration. As a result, only a qualitative comparison of impedance response of different electrodes is feasible. Evolution of the impedance behavior of a single electrode/electrolyte interface may still be used, however, as a valuable tool to draw important conclusions on the stability of the interface, the passivation phenomenon, and the corrosion of electrode contacts.

Depicted in Figure 33 is the impedance response of the $Li_{1.0}Mn_2O_{4.7}$ working electrode of a Li//SPE//$Li_xMn_2O_4$ cell versus Li reference electrode. It typically exhibits only one distinct feature; a single semicircle displaced along the Z' axis. The impedance response is similar to that originated from a parallel combination of a capacitor, C_{dl} and a resister, R_{ct}, both in series with another resistor R_b. R_b identified with the combined resistance of the solution and electrode leads. C_{dl} is the double layer capacitor of the solution/electrode interface and R_{ct} is the charge transfer impedance. The spur extending from the low frequency end (on the right) of the semicircle may be associated with diffusion of Li^+.

Figure 34 depicts how $\ln(1/R_{ct})$ for the cathode/electrolyte interface vary against the inverse of ambient temperature (K°) for Li//SPE//$Li_{1.0}Mn_2O_{4.7}$ Cell No. BMX53 in three electrode configuration. Figure 34 also includes a comparison of the bulk resistance R_b observed for Cell No. BMX53 and the approximate ohmic resistance of the SPE laminate inside the cell estimated from the conductivity data for SPE MX3 (Table 3). Parallel variation observed for R_b and the estimated SPE resistance indicates that at low temperatures variation of R_b of the cell mainly originates from the solid electrolyte film and there is no evidence for any phase change involving the electrolyte contained in an actual Li//SPE//$Li_{1.0}Mn_2O_{4.7}$ cell. Figure 34 also reveals a linear Arrhenius type relationship between $\ln(1/R_{ct})$ and 1/T(K°). Actual data for Cell No. BMX53 are given in Table 8.

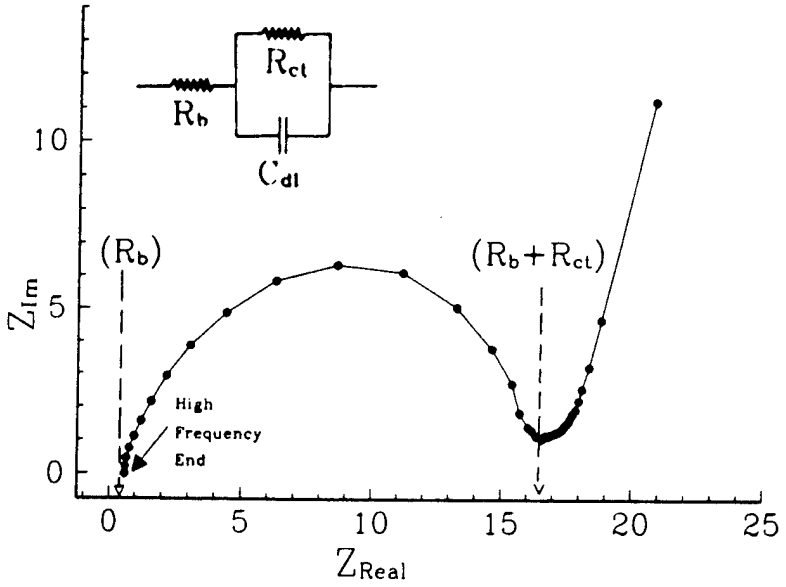

Figure 33. Impedance response of a typical Li//SPE//$Li_xMn_2O_4$ cell in three electrode configuration. Shown in the inset is the network corresponding to this impedance response. R_b is the bulk resistance. C_{dl} is the double layer capacitance. R_{ct} is the charge transfer resistance.

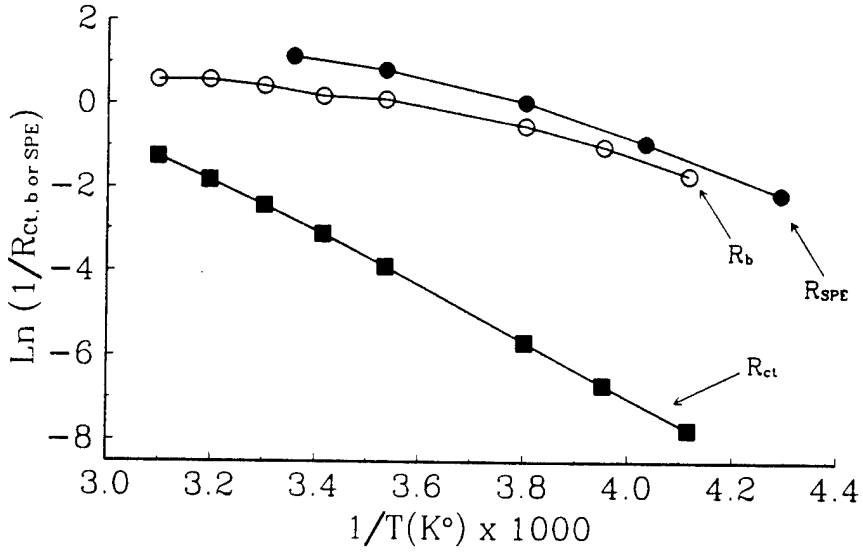

Figure 34. The Arrhenius plots for the inverse of the interface resistance R_{ct}, bulk resistance R_b and the estimated resistance of the SPE laminate included in Cell BMX53 in three electrode configuration

Table 8. Variation of R_b and R_{sc} with Temperature for Li//SPE//$Li_{1.0}Mn_2O_{4.7}$ Cell No. BMX53.

Temperature °C	R_b (Ω)	R_{ct} (Ω)
+50	0.56	3.53
+40	0.56	6.17
+30	0.65	11.38
+20	0.83	22.70
+10	0.89	49.04
-10	1.66	291.48
-20	2.72	795.58
-30	5.38	2301.9

The data in Table 8 suggest that the low Li utilization observed earlier (Figures 31 and 32) for Li//SPE//$Li_{1.0}Mn_2O_{4.7}$ cells may be due to the exponential increase in charge transfer resistance at the $Li_{1.0}Mn_2O_{4.7}$ electrode/polymer electrolyte interface with the decreasing temperature. It should lead to high over-potentials at low temperatures even at moderate current densities and as a result, voltage cutoff limits are reached prematurely prior to the utilization of the full electrode capacity. This effect is further enhanced in a two electrode cell due to any charge transfer difficulty arising at the Li counter electrode.

Interfacial resistance of a cell under open-circuit can be used as a probe to assess the stability of a polymer electrolyte/electrode interface. Any chemical reaction between the electrode and the electrolyte that could alter the general makeup of the interface (e.g., deposition of a secondary film) may result in substantially changed interfacial resistance or the appearance of a another semi-circle in the impedance diagram. A Li//SPE//$Li_{1.0}Mn_2O_{4.7}$ Cell No. BMX29 containing MX3 electrolyte (Table 3) was stored at 25°C and the impedance spectra of the cathode were monitored over an extended period of time. Impedance spectra depicted in Figure 35 were taken at the beginning and following 12 and 106 days of aging, respectively. All impedance spectra appeared similar to that in Figure 33 with a single semicircle and a spur at the low frequency end.

The fact that the appearance of the spectrum remained unchanged indicates the stability of the electrolyte/electrode interface. Nearly constant R_b value is consistent with the lack of any corrosion in the electrical contacts. Variation of R_{ct} is presented as a function of time elapsed in Figure 36. Gradual increase in the R_{ct} value may be the result of a continual growth of the primary passivation layer. Following an initial decrease the open-circuit voltage, V_{oc} has promptly reached a steady state value. Some of these data are tabulated in Table 9.

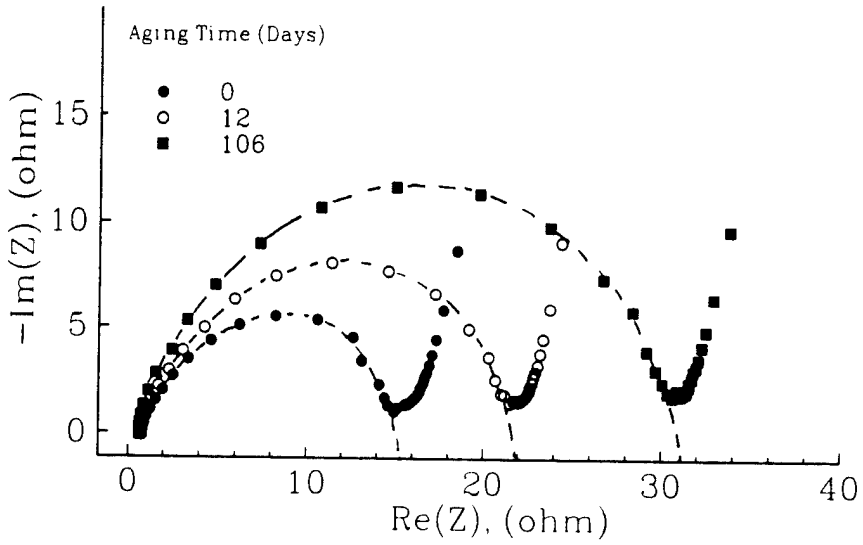

Figure 35. Impedance spectra of the $Li_{1.0}Mn_2O_{4.7}$ cathode in the Li//SPE//$Li_{1.0}Mn_2O_{4.7}$ Cell BMX29 relative to the Li reference taken at the beginning, 12 days and 106 days of storage at 25°C

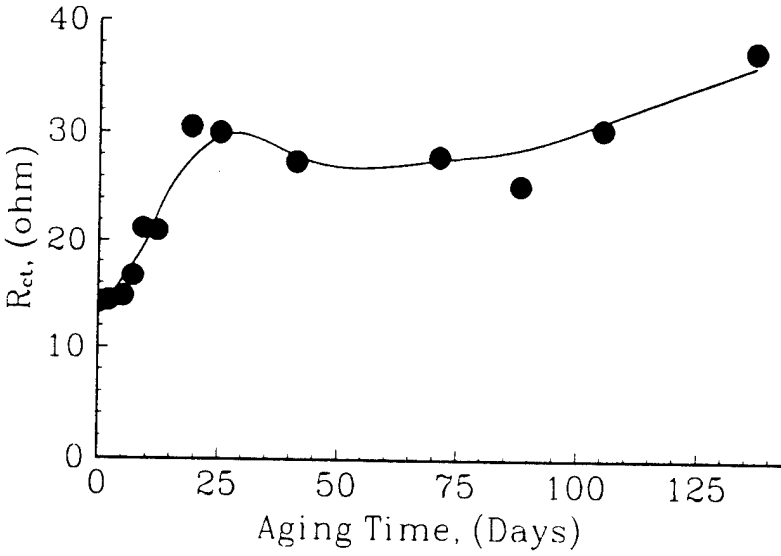

Figure 36. Charge transfer impedance, R_{ct} for the cathode/electrolyte interface versus aging time for Li//SPE//$Li_{1.0}Mn_2O_{4.7}$ Cell BMX29 in three electrode configuration.

Table 9. Impedance Data for the Cathode/Electrolyte Interface of an Aging Li//SPE//$Li_{1.0}Mn_2O_{4.7}$ Cell BMX29.

Days of Storage	R_b (Ω)	R_{ct} (Ω)*	V_{oc} (Volt)
0	0.8	14.2	3.255
5	0.6	14.8	3.255
12	0.6	21.0	3.245
25	0.6	35.0	3.195
106	0.6	30.0	3.195
137	0.6	36.9	3.195

*Visually estimated values.

Impedance spectra of a Li//SPE//$Li_{1.0}Mn_2O_{4.7}$ solid state cell No. BMX35 employing MX3 electrolyte were taken intermittently during long-term cycling at the end a full charge. Cycling was done at room temperature within a potential window from 3.75V to 2.0V. Variation of R_{ct} for the cathode/electrolyte interface is depicted as a function of the cycle number in Figure 37.

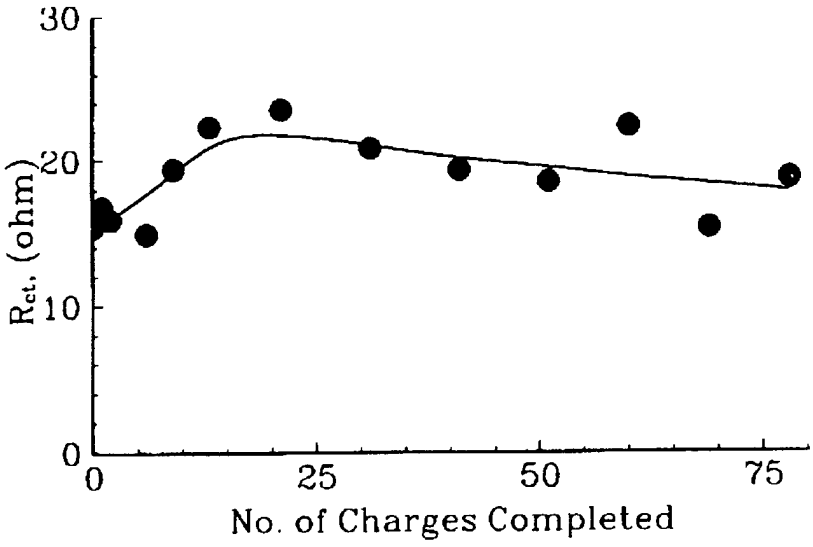

Figure 37. Charge transfer impedance, R_{ct} for the cathode/electrolyte interface versus the number of charges completed for Li//SPE//$Li_{1.0}Mn_2O_{4.7}$ Cell No. BMX35 utilizing the SPE MX3 in three electrode configuration. Cathode area was 10 cm^2, and the charge/discharge current density was 0.1 mA/cm^2.

R_{ct} decreased slightly at first, than increased and eventually leveled off upon further increase in number of charges. Appearance of the spectrum was similar to that in Figure 33 which remained unchanged during the entire investigation. The variation of R_{ct} in Figure 37 may be the net result of an initial activation followed by a gradual build up of the primary passivation layer. The examination of an opened cell revealed a completely delaminated cathode composite and no visible corrosion of the electrical contacts. The cell components are held together tightly by the external atmospheric pressure and delamination does not seem to have a significant effect on R_b which remains relatively unchanged. During the later part of cycling, however, delamination appears to increase R_b slightly with cycling. Charge transfer resistance for the anode/electrolyte interface remained low at all times during cycling. R_{ct} and R_b values for few selected cycles are tabulated in Table 10.

Table 10. Impedance Data for the Cathode/Electrolyte Interface of a Li//SPE//$Li_{1.0}Mn_2O_{4.7}$ Cell BMX35 following Charge.

No. of Charges	R_b (Ω)	R_{ct} (Ω)*
1	0.6	17.4
6	0.7	15.3
21	0.7	23.8
51	0.7	18.6
69	0.9	16.1
87	1.3	20.3

*Visually estimated values.

3.3 Cells Utilizing Spinel $Li_xMn_2O_4$ (4V)

Because of safety concerns associated with the use of metallic lithium in lithium cells, development of rocking-chair lithium-ion batteries is gaining momentum. In this case a lithium ion host such as carbon is used as the anode, and a high voltage cathode material is essential to offset the otherwise lower cell potential that results from the replacement of lithium metal anodes. The high voltage cathode material $Li_xMn_2O_4$ was synthesized for this purpose.

3.3.1 Capacity and Cycling Behavior of Li Cells. Figure 38 depicts the selected cycling and long-term performance of the Li//SPE//$Li_{1.1}Mn_2O_4$ Cell No. HVMX9 containing the Electrolyte MX3 (Table 7) and a composite cathode made with high voltage $Li_{1.1}Mn_2O_4$ composite cathode cycled over the 3.0V-4.25V potential range at a current density of 0.1 mA/cm^2. A utilization of only 78% of the theoretical capacity was observed during the first charge. The capacity continued to fade at an accelerated rate with cycling and at cycle 40 an internal short appeared as indicated by a jump in the charge capacity. The cell shorted within the

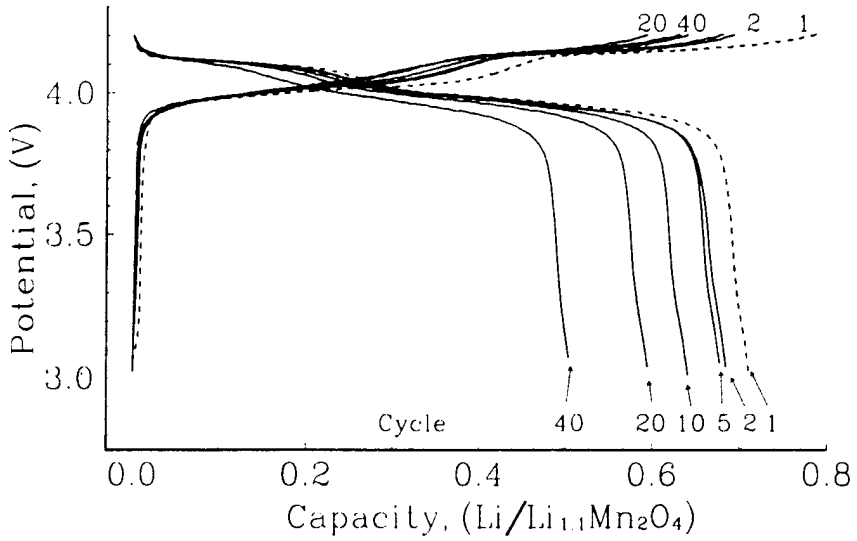

Figure 38. The voltage versus capacity profiles at room temperature for Li//SPE//$Li_{1.1}Mn_2O_4$ Cell HVMX9. Theoretical capacity was 15.5 mAh. Solid polymer electrolyte was MX3 (Table 7). The cathode was 51.0 w/o $Li_{1.1}Mn_2O_4$ 8.0 w/o Chevron Carbon:14.9 w/o EC:14.2 w/o PC:5.9 w/o MEOX:3.0 w/o PAN:3.0 w/o $LiAsF_6$. Cathode geometric area was 10 cm^2, and the charge/discharge current density was 0.1 mA/cm^2.

next two cycles. A cell to cell variation in the charge/discharge capacity was observed and the cycle life was consistently limited to 15-40 cycles. Such variation may be related to differences in dendrite growth through the SPE. Examination of a failed cell revealed a lithium growth through the SPE layer that may have created a soft short.

High voltage lithiated manganese oxide $Li_xMn_2O_4$ was also characterized in solid polymer electrolyte cells utilizing PAN- based electrolytes based on EC-γ BL binary plasticizers. Capacity and long-term cycling performance of a typical high voltage (4V) $Li_{1.1}Mn_2O_4$ cathode in a Li/SPE/$Li_{1.1}Mn_2O_4$ solid state cell (Cell HVBL2) employing ECBL6 (Table 7) electrolyte are presented in Figures 39 and 40. This electrolyte was chosen because it was the most conductive of the PAN/EC-γ BL/$LiAsF_6$ electrolytes at ambient temperature. The cycling was done at room temperature within the potential range from 4.2V to 3.0V. Theoretical capacity of the cathode was 13.8 mAh based on a cathode utilization of one Li per $Li_xMn_2O_4$.

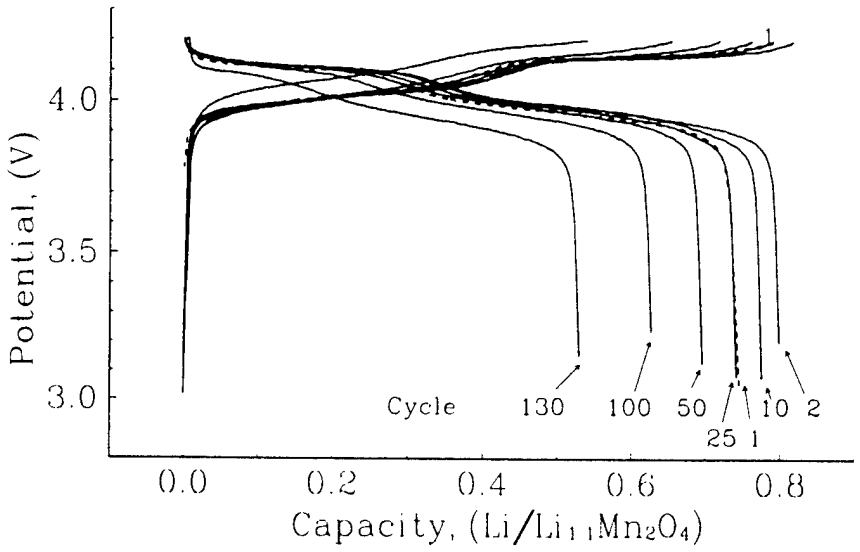

Figure 39. Cycling curves at room temperature for Li//SPE//$Li_{1.1}Mn_2O_4$ Cell HVBL2. Theoretical capacity was 13.8 mAh (1.0 mol Li/$Li_{1.1}Mn_2O_4$). Solid polymer electrolyte was ECBL6 (Table 7). The cathode was 53.2 w/o $Li_{1.1}Mn_2O_4$:8.0 w/o Chevron Carbon:13.3 w/o EC:19.6 w/o λ-BL:3.0 w/o PAN:3.0 w/o $LiAsF_6$. Geometric area of the cathode was 10 cm^2, and the charge/discharge current density was 0.1 mA/cm^2 (~C/14 rate).

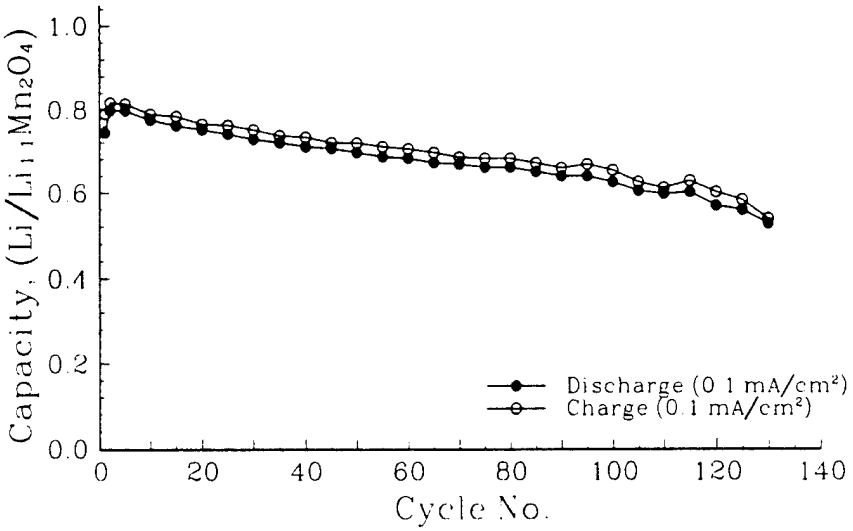

Figure 40. Discharge/charge capacities as a function of cycle number for the cell shown in Figure 39.

As shown in Figure 39, the initial reversible capacity was close to 0.8 mol of Li per $Li_{1.1}Mn_2O_4$. Even though the cell demonstrated long term rechargeability, the data shown in Figure 40 on the capacity *vs.* cycle number agree with a fade rate of 0.17% per cycle within the range from cycle 20 to cycle 120.

A higher capacity consistently observed during charge may be due to electrolytic oxidation at high cathode potentials. If the observed discharge to charge capacity ratio of 97% solely came from a real capacity loss it should result in almost zero rechargeable capacity at cycle 140. For the cell depicted in Figure 39 the discharge was restricted to 3V so that only the high voltage capacity is utilized. The material can be reduced (lithiated) further to reach a lower voltage plateau at ~2.7-2.8V.

Figures 41 and 42 allow us to see the capacity and long-term cycling performance of a typical high voltage (4V) Li_xMnO_4 in a $Li//SPE//Li_xMn_2O_4$ solid state cell employing ECBL6 (Table 7) electrolyte. The cell was cycled at a current density of 0.1 mA/cm^2 between 4.2V to 2.0V to include both upper and lower discharge plateaus.

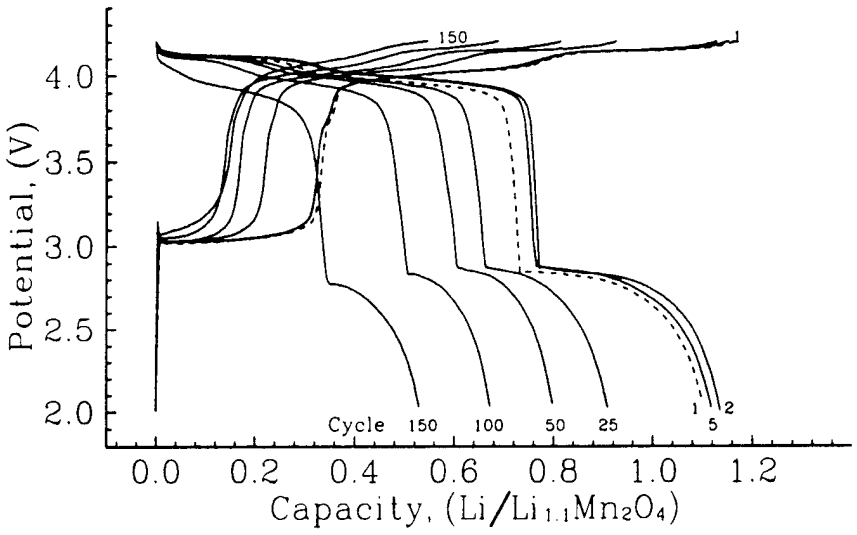

Figure 41. Cycling curves at room temperature for $Li//SPE//Li_{1.1}Mn_2O_4$ Cell HVBL5. Theoretical capacity was 10.7 mAh (1.0 mol $Li/Li_{1.1}Mn_2O_4$). Solid polymer electrolyte was ECBL6 (Table 7). The cathode was 53.2 w/o $Li_{1.1}Mn_2O_4$:8.0 w/o Chevron Carbon:13.3 w/o EC:19.6 w/o λ-BL:3.0 w/o PAN:3.0 w/o $LiAsF_6$. Geometric area of the cathode was 10 cm^2, and the charge/discharge current density was 0.1 mA/cm^2 (~C/11 rate).

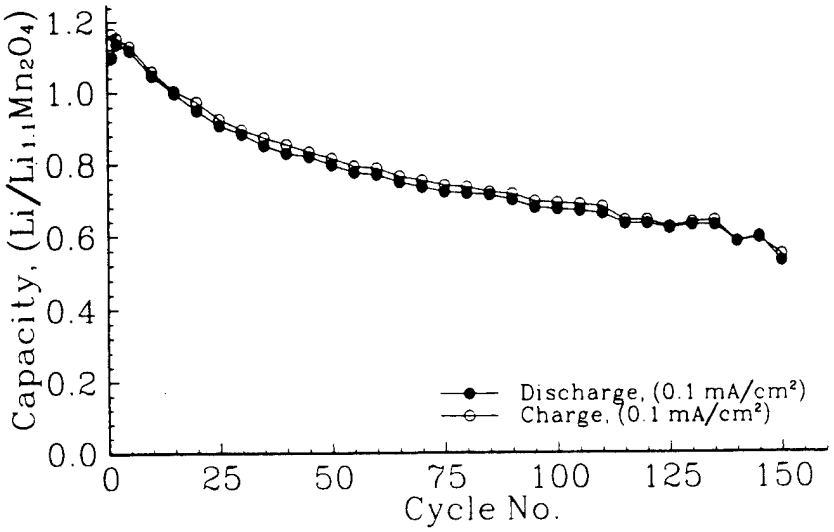

Figure 42. Discharge/charge capacities as a function of cycle number for the cell shown in Figure 41.

Consistently higher capacity during charge and the gradual fading of the overall capacity are evident in Figure 42 and from the 50th cycle onwards the fade rate levels off at 3% per cycle. Cycling over a broader voltage span may have created a great mechanical stress on the electrode causing it to lose electrical contacts among the active particles faster. It explains the relatively higher fade rate of the cell shown in Figure 42 compared to that in Figure 40. The actual cell performance data for a few selected cycles are given in Table 11.

Table 11. Cycling Data for Li//SPE//$Li_{1.1}Mn_2O_4$ Cell HVBL5.

	Specific capacity (mol Li per $Li_{1.1}Mn_2O_4$)						Discharge/Charge
Cycle	Discharge H*	Discharge L*	Charge H	Charge L	Total Discharge	Total Charge	Ratio
1	0.73	0.37	0.84	0.32	1.10	1.17	0.94
2	0.77	0.36	0.84	0.31	1.14	1.15	0.98
5	0.76	0.36	0.82	0.31	1.12	1.13	0.99
25	0.66	0.25	0.72	0.2	0.91	0.93	0.98
50	0.61	0.19	0.67	0.15	0.8	0.82	0.98
100	0.53	0.14	0.57	0.13	0.67	0.69	0.97
150	0.35	0.18	0.42	0.13	0.53	0.55	0.97

*Discharge H and Charge H refers to the capacities corresponding to the upper (~4V) plateau during discharge and charge, respectively. Discharge L and charge L refers to the capacities corresponding to the lower (~2.7V) during discharge and charge, respectively.

During most of its cycle life (>125 cycles) the cell appears to lose it lower plateau capacity faster than its upper plateau capacity. And in later cycles, they both decay at similar rates and the cell capacity declines significantly faster. Comparison of Figures 40 and 42 indicates that cycling over a broader potential span allows for a short term gain in the specific capacity of the cathode. Although, the lower potential plateau is reminiscent of the reduction plateau of the low voltage material where, lithiation up to 1.0 mol Li per $Li_{1.0}Mn_2O_{4.7}$ was possible (Figure 26), the capacity of the high voltage $Li_xMn_2O_4$ in the lower plateau is substantially low, only 37% of the expected capacity. This indicates that the high voltage $Li_{1.1}Mn_2O_4$ remaining at the end of the ~4V reduction plateau is very different in terms of its lithiation behavior from the low voltage $Li_{0.93}Mn_2O_4$. Ironically, the low voltage material $Li_{1.0}Mn_2O_{4.7}$ was found to have insignificant capacity within the potential range from 4.2V to 3.0V (upper voltage plateau).

3.4 Electrochemical Characterization of the Carbon Composite Anode

Investigation of a carbon half-cell is precedent to the development of rocking-chair lithium-ion batteries. Our previous work with PC-containing electrolytes indicated a massive electrolyte reduction producing a potential plateau close to 1V *vs.* Li^+/Li during the galvanostatic discharge of a Li//SPE//graphite cell and also low rechargeability of such cells. This prompted us to exclude PC in our work on the development of electrolytes for carbon based lithium-ion cells. Since both EC and MEOX are capable of acting as stand-alone plasticizer solvents as reported earlier, attention was focused on PAN based electrolytes containing a binary solvent mixture of EC and MEOX.

3.4.1 The Graphite Electrode. First we studied Li intercalation into and deintercalation from graphite in cells containing the Electrolyte BC18. Voltage *vs.* capacity profiles for intercalation and deintercalation (discharge and charge) of graphite are presented in Figure 43 for a typical Li//SPE//Alfa Graphite cell No. AA-6 employing the Electrolyte BC18 (Table 7) and operating at 40°C.

Two voltage plateaus corresponding to the reduction of the electrolyte are positioned around 1V *vs.* Li^+/Li. The total charge capacity observed during the first discharge until the lower cut off voltage of -0.02V *vs.* Li^+/Li corresponds to 1.3 mol Li per C_6. The carbon electrode appears to have passivated following the first discharge step, and its utilization during the first charge and subsequent charge/discharge cycles approximated the expected level of one mol Li per C_6. The capacity equivalent to approximately 0.3 mol Li/C_6 appearing at ~1V is attributed to the passivation reaction. The cell developed an internal short during its fourth cycle. The Li//SPE//Alfa Graphite cell performs poorly at room temperature due to crystallization of EC in the carbon composite resulting in an electrolyte with low conductivity. Therefore, it was of interest to search for binary EC-MEOX/$LiAsF_6$ electrolytes that lead to improved performance at low ambient temperatures.

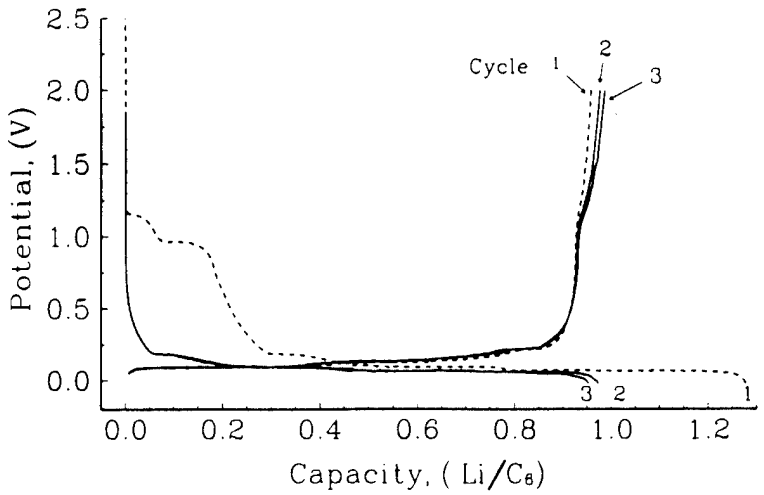

Figure 43. Cycling curves at 40°C for Li//SPE//Alfa Graphite Cell No. AA6. Theoretical capacity was 28.1 mAh. Solid polymer electrolyte was BC18 (Table 7). The cathode was 51.0 w/o Alfa Graphite:43.0 w/o EC:3.0 w/o PAN:3.0 w/o $LiAsF_6$. Cathode geometric area was 10 cm^2, and the charge/discharge current density was 0.1 mA/cm^2 (~C/30 rate).

Figure 44 shows capacity data for Li//SPE//Alfa Graphite cell, BMX17 during its first two charge/discharge cycles. This cell was based on the SPE composition SA92 (Table 7). The first cycle discharge capacity appears to be entirely due to electrolyte reduction and passivation at 1V *vs.* Li^+/Li. The passivation layer appears to offer a formidable barrier to ion conduction and there is hardly any capacity observed for the first charge or any subsequent charges/discharges. *MEOX appeared to interfere with Li intercalation into graphite and in general, a carbon half-cell based on any SPE containing MEOX, was found to have no useful rechargeability.*

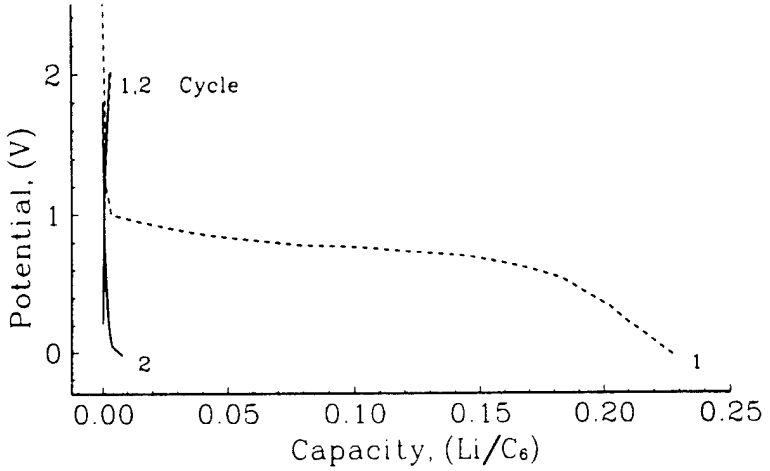

Figure 44. Cycling curves at room temperature for Li//SPE//Alfa Graphite Cell BMX17. Theoretical capacity was 20.3 mAh. Solid polymer electrolyte was SA92 (Table 7). The cathode was 51.0 w/o Alfa Graphite:20.0 w/o EC:23.0 w/o MEOX:3.0 w/o PAN:3.0 w/o $LiAsF_6$. Cathode geometric area was 10 cm^2, and the charge/discharge current density was 0.1 mA/cm^2.

Attention was next focused on PAN-based electrolytes based on EC-γ BL binary plasticizers. Depicted in Figure 45 are selected charge/discharge cycles of a Li//SPE//Alfa Graphite cell performed at a current density of 0.1 mA/cm^2 utilizing the Electrolyte ECBL1 (Table 7) and the corresponding performance data are summarized in Table 12.

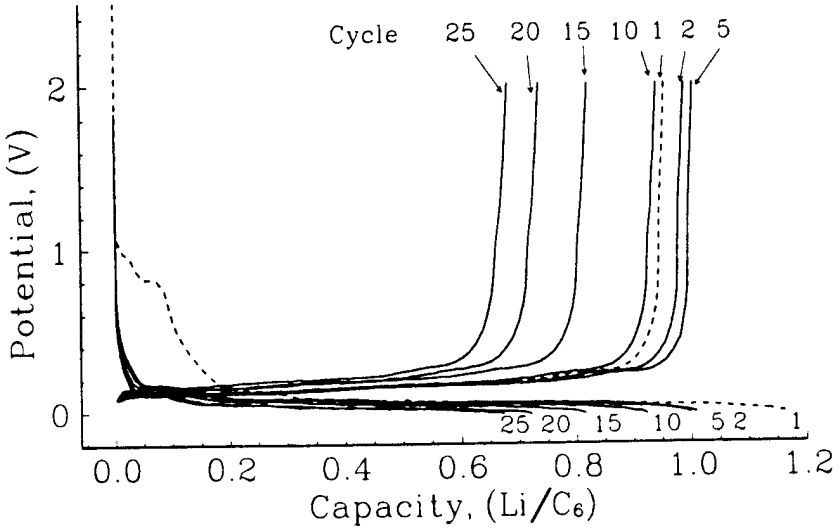

Figure 45. Cycling curves at room temperature for Li//SPE//carbon Cell AA9. Theoretical capacity was 13.7 mAh. Solid polymer electrolyte was ECBL1 (Table 7) The cathode was 51.0 w/o Alfa Graphite:3.0 w/o PAN:21.7 w/o EC:21.3 w/o γ-BL:3.0 w/o $LiAsF_6$ Cathode geometric area was 10 cm^2, and the charge/discharge current density was 0.1 mA/cm^2.

Table 12. Cycling Data for Li//SPE//Alfa Graphite Cell AA9.

Cycle No.	Specific Capacity mol Li per C_6		Specific Capacity Ratio
	Discharge	Charge	Discharge/Charge
1	1.16	0.96	1.21
2	1.01	0.99	1.02
5	1.00	1.01	0.99
10	0.92	0.94	0.98
15	0.82	0.82	0.99
20	0.72	0.74	0.98
25	0.67	0.68	0.99

The cycling was carried out at room temperature. The first cycle discharge capacity equivalent to 1.16 Li/C_6 suggests an even smaller extent of electrolyte reduction compared to cell No. AA6 based on the BC18 electrolyte as described above. A utilization level of 0.96 Li/C_6 is observed for the first charge step. Lack of significant electrolyte reduction has allowed the discharge capacity during the next few cycles to stay close to 1 Li/C_6 with 100%, reversibility during corresponding charges. Beyond cycle 10, however, the level of cathode utilization started to deteriorate rather rapidly and at cycle 25 the Li utilization has declined to 0.65 Li/C_6.

Because of the potential toxicity of $LiAsF_6$, rechargeability of the Alfa Graphite anode in a polymer electrolyte containing $LiPF_6$ would be of significant interest.

Li//SPE//Alfa Graphite cells containing $LiPF_6$ showed low utilization and rapid loss of capacity upon cycling as shown in Figure 46. Rapid deterioration of electrolyte containing $LiPF_6$ may be partially responsible for this poor performance, since a solution of $LiPF_6$ in the EC-γ-BL mixed solvent developed a brown color rapidly and the color became very intense upon heating with PAN at the electrolyte processing temperature of 140°C. The first discharge curve shows a less prominent plateau at around 0.6V attributable to electrolyte decomposition. The discharge capacity to a -20 mV cutoff was equivalent to 0.23 Li/C_6, of which only 0.17 Li/C_6 was reversible. Later cycles showed significantly low utilization.

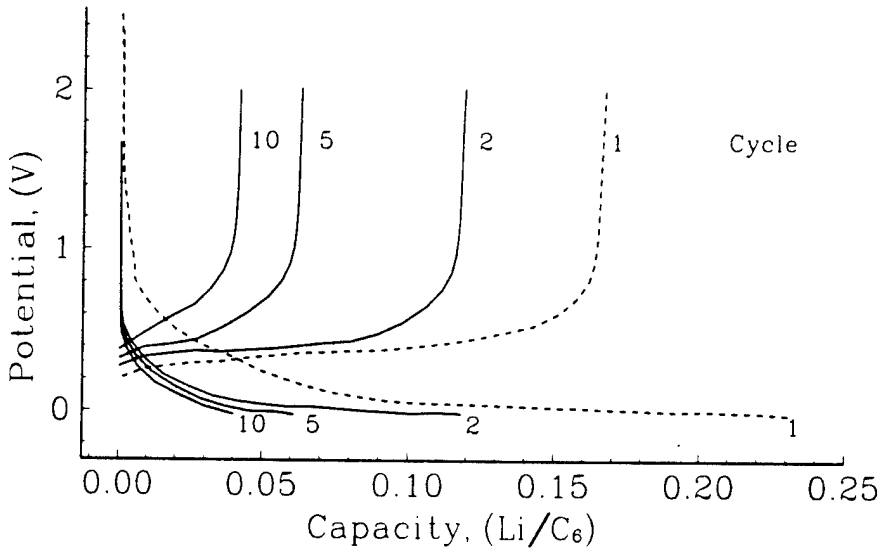

Figure 46. Cycling curves at room temperature for Li//SPE//carbon Cell AA11. Theoretical capacity was 19.2 mAh. Solid polymer electrolyte was ECBL2 (Table 7). The cathode was 51.0 w/o Alfa Graphite:3.0 w/o PAN:21.7 w/o EC:21.3 w/o γ-BL:3.0 w/o $LiPF_6$. Cathode geometric area was 10 cm^2, and the charge/discharge current density was 0.1 mA/cm^2.

Gradual fading of the graphite anode capacity shown by the data in Figure 45 for Cell No. AA9 may be caused either by an irreversible cathodic process (probably electrolyte reduction) taking place parallel to Li intercalation or the loss of contacts between the active graphite particles due to continuous expansion and contraction of the graphite matrix accompanying charge/discharge cycles. Incorporation of acetylene black as a conductivity enhancing additive into the graphite electrode has been suggested in the published literature as a remedial measure mitigating capacity losses due to the second process. Since acetylene black itself is capable of intercalating Li, it was desirable to determine the capacity of acetylene black in a solid state cell with the Li anode. Figure 47 depicts the cycling of a cell (AA17) containing the SPE, ECBL1 (Table 7) based on Chevron carbon cycled between 2.5V-0.0V at a current density of 0.1 mA/cm^2. The first cycle discharge capacity of over 1.5 mol Li per C_6 clearly demonstrate a massive irreversible capacity associated with electrolyte reduction. A reversible capacity of close to 0.25 Li/(C_6) observed from cycle 2 to cycle 10 is consistent with the utilization reported for Chevron type carbons.

According to Figure 47, Chevron carbon has a reversible capacity close to 93 mAh/g, which is nearly 25% of the capacity obtained with Alfa Graphite. Figure 48 compares the capacity as function of cycle number for two Li//SPE//Carbon cells, one with a cathode containing Alfa Graphite, Cell No. AA9 (Figure 44) and another with mixture of graphite and Chevron carbon at a ratio of 7.5:1, cell No. AA19.

Both carbon electrodes in Figure 48 exhibited capacities close to the expected maximum of 1 Li/(C_6) during late cycles. However, the graphite cathode containing Chevron carbon exhibits a comparatively higher first cycle irreversible capacity. Since close to 13% of the carbon matrix is Chevron carbon, and the first discharge capacities for the two components are close to 1.2 Li/C_6 (Figure 45) for graphite and 1.5 Li/C_6 (Figure 47) for Chevron carbon, first discharge capacity for the graphite/carbon electrode shown in Figure 48 should be close to 1.25 Li/C_6. Much larger capacity was, however, observed during the first discharge (~1.7 Li/C_6) and the underlying reason for this *extra* capacity is not understood at the present time. As expected, the reversible capacity of the Cell No. AA19 remained slightly below that of the Cell No. AA9 (Figure 48). Therefore, incorporation of acetylene black in the graphite electrode does not seem to offer a clear advantage at least in the short term and also, the high first cycle irreversibility of the graphite composite containing Chevron carbon can be considered as a deterrent, especially for Li-ion cells with a limited amount of cyclable lithium.

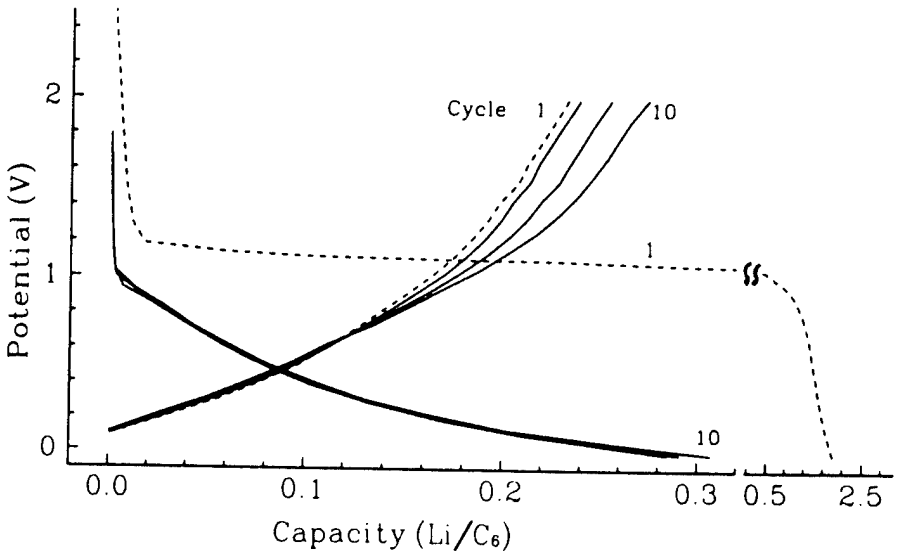

Figure 47. Cycling curves at room temperature for Li//SPE//Chevron carbon Cell No. AA17. Solid polymer electrolyte was ECBL1 (Table 7). The cathode was 20.0 w/o Chevron carbon:5.0 w/o PAN:35.4 w/o EC:34.6 w/o γ-BL:5.0 w/o $LiAsF_6$. Cathode geometric area was 10 cm^2, and the charge/discharge current density was 0.1 mA/cm^2.

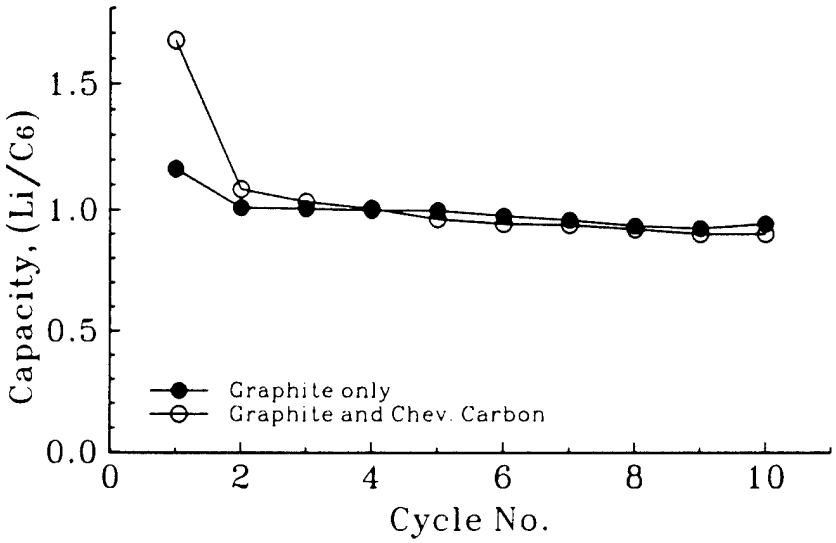

Figure 48. Comparison of capacity versus cycle number for Li//SPE//Alfa Graphite Cells AA-9 (Figure 44) and AA19. Solid polymer electrolyte was ECBL1 (Table 7). The cathode in Cell AA19 was 37.5 w/o Alfa Graphite:5.0 w/o Chevron carbon:3.7 w/o PAN:25.3 w/o EC:24.8 w/o γ-BL:3.0 w/o $LiAsF_6$ Cathode geometric area was 10 cm^2, and the charge/discharge current density was 0.1 mA/cm^2.

The data in Figure 46 demonstrated the efficient rechargeability of Alfa graphite in the Electrolyte ECBL1 (Table 7) with reversible utilization of Li close to 1.0 mol per C_6. The capacity in that case did not decline appreciably until cycle 10 and at cycle 25 it reached about 0.65 Li mol per C_6. However, our continuing effort to improve PAN-based electrolytes based on EC-γ BL binary plasticizers was marred by the inconsistencies in the Li utilization observed in this electrolyte for different lots of synthetic graphite that we purchased from the same vendor (Alfa). Rechecking the performance of several Li//SPE//graphite cells containing freshly prepared ECBL1 revealed that they too failed to reproduce the data shown in Figure 45. Our attempts to correct this discrepancy involved using purer chemicals, drier solvents and also, the effect of possible contaminants. The extent of this data irreproducibility is highlighted in Figure 49 which compares the capacity *vs.* cycle number data for one of these recent Li//SPE//graphite cells (AA72) containing ECBL1 electrolyte with those reported previously for Cell AA9.

We speculate that the irreproducibility highlighted in Figure 49 for graphite half cells may be due to minor lot-to-lot variations of the physical properties of the commercially available graphite

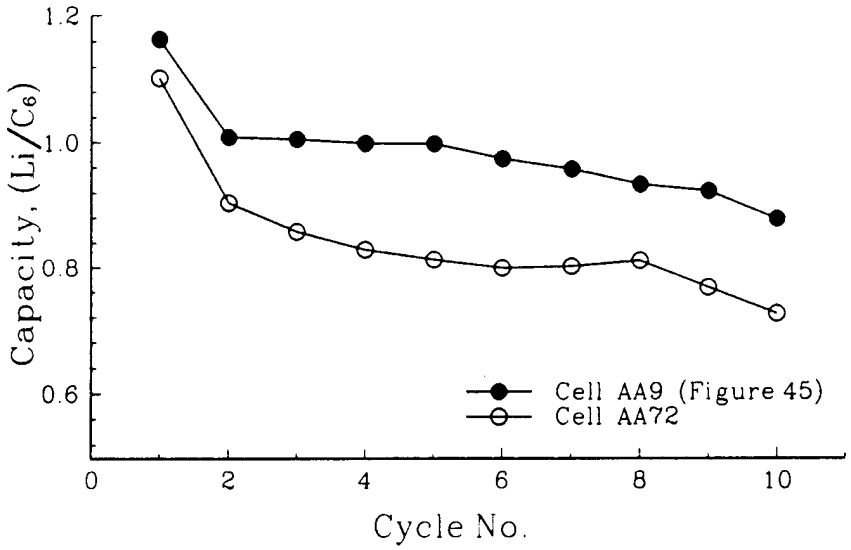

Figure 49. Comparison of capacity versus cycle number data for the Li//SPE//Alfa graphite Cell No. AA72 containing the Electrolyte ECBL1 (Table 7) with those for a similar cell, Cell No. AA9, shown in Figure 45.

3.4.2 Carbon Electrode made by Solvent-Cast Technique. Apart from the nature of the electrolyte used, cycling performance of the carbon electrode appears to be sensitive to other factors such as the binder and the fabrication process used. We have successfully developed fabrication procedures other than the hot-rolling technique which is normally used to make electrode. In one process, carbon was dispersed in a THF solution of a polymer, poly(vinyl chloride-co-vinyl acetate), mixed with the plasticizer solvents to obtain a paste with putty like consistency. The paste was rolled to form a laminate at ambient temperature and the low boiling THF was removed by evaporating under partial vacuum leaving the high boiling plasticizer solvents in the composite. We used this procedure to fabricate graphite and Conoco coke composite electrodes containing EC/$LiPF_6$ plasticizer. Capacity *vs.* voltage curves are presented in Figure 50 for a Li//SPE//Alfa Graphite cell, (AA59) operating at 40°C.

The total capacity observed during the first discharge was about 1.06 Li/C_6. Utilization during the first charge and next few charge/discharge cycles approximated the expected level of one mol Li C_6. The reversible capacity continued to decline slowly and in cycle 20 it reached 0.72 mol Li per C_6. A prominent feature is the low irreversible capacity involved in the first cycle. Specific capacities shown in Figure 50 are comparable to those in Figure 43, even though direct comparison of the two cells is not valid. However, data in Figure 50 clearly demonstrate the utility of the solvent cast technique to fabricate laminated thin film carbon electrodes. Figure 51 depicts the capacity *vs.* voltage curves for a Li//SPE//Conoco Coke cell, (AA65) operating at 40°C.

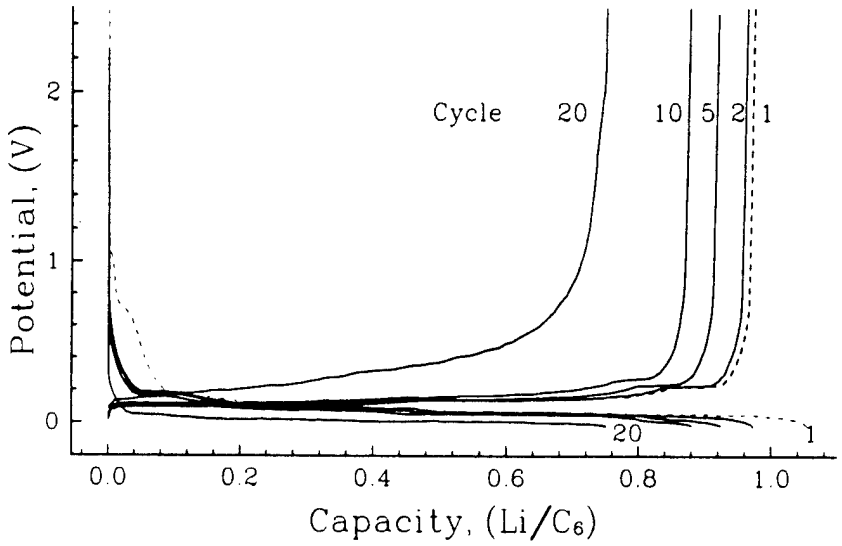

Figure 50. Cycling curves at 40°C for Li//SPE//Alfa Graphite Cell AA59. Theoretical capacity was 16.1 mAh. Solid polymer electrolyte was ECP1 (Table 7 The cathode was 57.0 w/o Alfa graphite:10.0 w/o poly(vinyl chloride-co-vinyl acetate):30.9 w/o EC:2.15 w/o $LiPF_6$ Cathode geometric area was 10 cm^2, and the charge/discharge current density was 0.1 mA/cm^2.

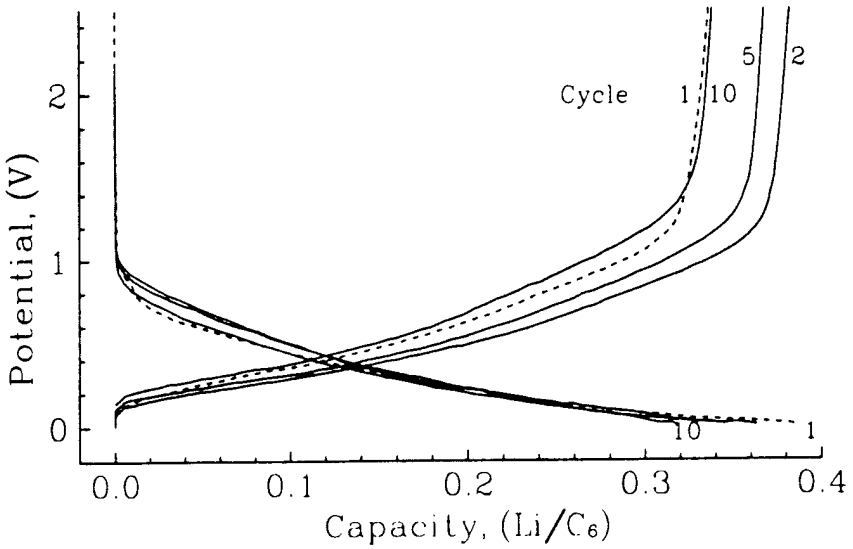

Figure 51. Cycling curves at 40°C for Li//SPE//Conoco Coke Cell AA65. Theoretical capacity was 14.0 mAh (1.0 mol Li per C_{12}). Solid polymer electrolyte was ECP1 (Table 7). The cathode was 80.0 w/o Conoco-Coke:10.0 w/o poly(vinyl chloride-co-vinyl acetate):9.0 w/o EC:1.0 w/o $LiPF_6$. Geometric area of the cathode was 10 cm^2, and the charge/discharge current density was 0.1 mA/cm^2.

In this case only the compositions with low electrolyte content could furnish a paste with adequate consistency to roll because coke absorbs hardly any organic liquids. According to Figure 51, Li intercalation has reached nearly 0.4 Li/C_6 during the first few cycles. Lower than the anticipated utilization of 0.5 Li/C_6 may be due to wettability problems associated with the lower content of the plasticizer used in the formulation.

3.4.3 Carbon Electrode made by Hot-Pressing Technique. Despite the encouraging results discussed above, the carbon electrode containing a polymer electrolyte binder appears to have certain inherent limitations. Because of the absence of convection and low carrier mobility solid polymer electrolytes are different from their liquid counterparts and they are susceptible to problems arising from concentration polarization. As pointed out earlier, this situation may be prevalent to the polymer electrolyte binder present within the electrode composite. A potential way to circumvent this problem is to use using thin electrodes with high materials loading and to avoid using the polymer electrolyte binder all together. Instead, a liquid electrolyte made up of low molecular weight, high permittivity and, low viscosity solvents can be supported inside the empty channel of a composite electrode. A solid polymer electrolyte is still be used as the ion conductive separator. Such a process was successfully developed to fabricate carbon composite electrodes with substantially better electrochemical properties and endurance. Capacity *vs.* voltage curves are presented in Figure 52 for a Li//SPE//Alfa Graphite cell, (AA81) cycling at ambient temperature.

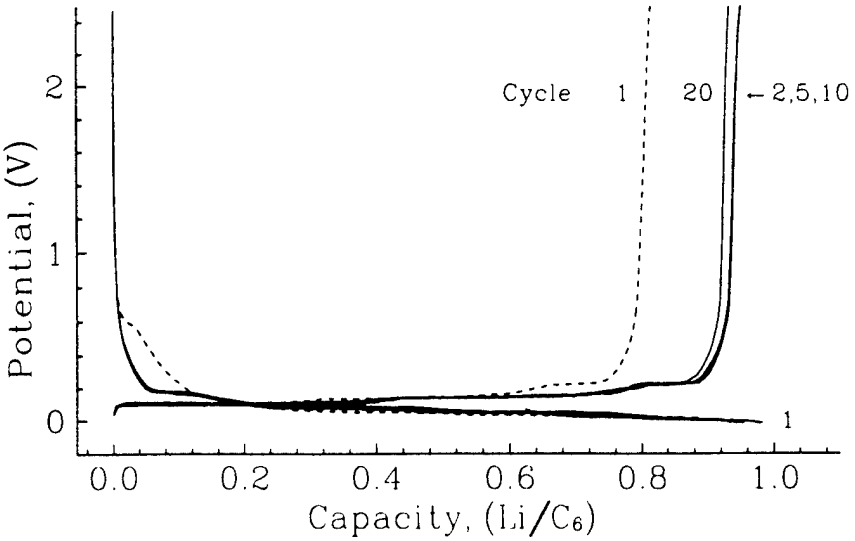

Figure 52. Cycling curves at room temperature for Li//SPE//Alfa Graphite Cell AA81. Theoretical capacity was 46.8 mAh. Solid polymer electrolyte was DPC2 (Table 7). The cathode (dry) was 93.0 w/o Alfa graphite:2.0 w/o Chevron carbon:5.0 w/o poly(vinylidene fluoride). Soaking electrolyte was DPCX (Table 7). Cathode area was 10 cm^2, and the charge (discharge) current density was 0.1 (0.2) mA /cm^2.

Efficient utilization of Li is evident in Figure 52 with a reversible capacity of nearly 0.9 Li/C_6 up to the cycle 20 at a discharge rate close to C/20. Unlike the previous observations for cells based on Alfa Graphite (Figures 45 and 50), the first cycle discharge capacity was relatively low (~1 Li/C_6). The first charge capacity of nearly 0.8 Li/C_6 indicates that as much as 0.2 mol of Li per C_6 has been used up for irreversible reactions in agreement with the other Alfa Graphite cells discussed thus far (Figures 45 and 50). Parallel information for Li//SPE//Conoco Cell No. AA81 is depicted in Figure 53.

Reversible Li utilization better than 0.4 mol Li per C_6 shown for the first 20 cycles in Figure 53 is quite satisfactory compared to the maximum reported capacity of 0.5 Li/C_6 for coke. At present, the cell has cycled over 45 cycles and the capacity is maintained at 0.4 Li/C_6.

3.4.4 Capacity Fade in Li//SPE//Carbon Cells. The capacity and the cyclability of carbon in a cell are dependent on a variety of factors. These are: type of carbon, source, thermal history, nature of the electrolyte, electrochemical parameters maintained during discharge/charge, compatibility among the electrolyte and electrode materials, and the process used to fabricate electrodes. In addition to that, all carbon containing half cells share some common problems, such as irreversible capacity in the first discharge and fading of the capacity during repeated cycling. Irreversible capacity has been correlated with the effective surface area of a particular carbon and is therefore related to both electrochemical properties of the electrolyte and the surface chemistry of carbon. Capacity fading on the other hand, may be a consequence of the loss of electrical contacts among active particles due to lattice expansion and contraction during cycling, loss of contact between the active material and current collector due to delamination or the gradual build up of a passivation layer on the carbon surface. All these factors elevate the impedance of the

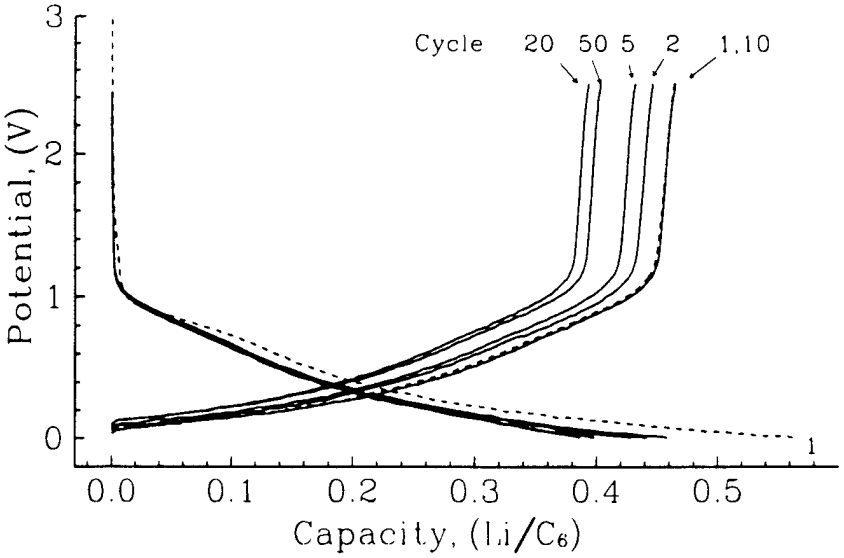

Figure 53. Cycling curves at room temperature for Li//SPE//Conoco Coke Cell AA80. Theoretical capacity was 38.5 mAh. Solid polymer electrolyte was DPC2 (Table 7). The cathode (dry) was 95.4 w/o Conoco Coke:2.1 w/o Chevron carbon:2.6 w/o poly(vinylidene fluoride). Soaking electrolyte was DPCX (Table 7). Cathode geometric area was 10 cm^2, and the charge (discharge) current density was 0.1 (0.2) mA /cm^2.

electrode that results in an over-potential causing the electrode to reach its voltage limits prematurely during cycling. Therefore, development of a successful carbon electrode relies on our ability to understand and manage the causes that contribute to irreversible capacity and capacity fading. Data included in Table 13 were derived from the impedance spectra of a carbon electrode in a three electrode Li//SPE//Alfa graphite Cell No. AA74 taken at the end of different discharges during repeated cycling from -0.020V to 2.5V.

Table 13. Impedance Data for the Graphite Electrode in a Li//SPE// Graphite Cell taken at the End of a Discharge[a].

No. of Discharges	R_b	R_{ct}[b]
0	0.5	8.4
1	0.6	13.6
2	0.6	22.1
5	0.6	32.0
8	0.6	40.0
12	0.6	~53

[a]The Li//SPE//Alfa Graphite Cells AA74 is based on a hot-rolled cathode. Theoretical capacity was 16.3 mAh. Solid polymer electrolyte was ECBL1 (Table 7). The cathode was 51.0 w/o Alfa Graphite:3.0 w/o PAN:21.7 w/o EC:21.3 w/o γ-BL:3.0 w/o $LiAsF_6$. Cathode geometric area was 10 cm^2, and the charge/discharge current density was 0.1 mA/cm^2.

[b] Visually estimated values.

While the bulk impedance (R_b) of the electrode remains virtually constant, the charge transfer resistance (R_{ct}) increases steadily with cycling. Delamination and loss of contact among carbon particles due to mechanical deformation of the carbon lattice should appear in R_b as well as R_{ct} values for the electrode. The latter reflects the changing area of interfaces across which charge transfer takes place and the former is related to the increase in the spatial dimensions of the conducting phase. An increasing passivation layer, however, mainly influences the R_{ct} feature of the impedance spectra. According to the data presented in Table 13, during the early part of cycling at least, delamination or the loss of contacts among active particles doesn't seem to be the source of continuing capacity loss seen, for example, in Figure 45. Gradual increase of the R_{ct} value suggests a continually growing passivation layer. Since the discharge curve for carbon is essentially flat during the latter part of the discharge, any small increment in the over-potential due to passivation corresponds to a significant loss of capacity. This translates into a lower amount of recyclable Li entering the carbon lattice. This aspect is further highlighted by the fact that during the long term cycling of a carbon half cell, efficiency of the charge/discharge process (ratio of capacities) remains close to one even though the capacity continues to fall. Therefore proper management of the passivation layer on carbon appears to be an essential initiative for combating the capacity loss of carbon electrodes.

Figure 54 presents further evidence for a continually growing passivation layer on the carbon electrode in a Li//SPE//Alfa Graphite Cell No. AA-77 containing ECBL1 electrolyte. The carbon capacity was 16.1 mAh. The first discharge/charge cycle was carried out at 0.1 mA/cm^2 within a potential span of -0.020V to 2.5V *vs.* Li^+/Li. Capacities observed during the first discharge and the first charge were 16.4 and 12.4 mAh, respectively. Starting from the second cycle the discharge limit was preset to a constant depth of 12.2 mAh while the charging was allowed up to a cell potential of 2.5V. As shown in Figure 54 the discharge curve has shifted towards more negative potentials with each discharge and in just 4 cycles it has begun to overlap with the plateau corresponding to the Li deposition. A negatively shifting discharge curve is strongly indicative of a growing passivation layer. If the discharge was potential limited as is done usually, the growing passivation causes the over-voltage to elevate forcing the cell to reach its lower cutoff faster during each discharge and as a result, to lower the utilization.

3.4.5 Carbon/Aluminum Composite Anode. Gravimetric and volumetric capacities of Li_xAl alloy ($0<x<1$), 993 mAh/g and 1340 mAh/cm^3, respectively, are higher than the corresponding values for lithiated graphite, 372 mAh/g and 837 mAh/cm^3. Therefore a composite containing graphite and Al will have higher specific capacity than graphite alone. Such composites are useful in a cell of the configuration Carbon,Al//polymer electrolyte/$Li_xMn_2O_4$. Intercalation of aluminum is characterized by a potential profile that has plateaus corresponding to three major alloy phases namely; i) +0.38V for $\alpha + \beta$; ii) +0.12V for $\beta + \gamma$; and iii) +0.05V for $\gamma + \delta$. These are reminiscent of the plateaus observed for graphite that correspond to the coexistence of pairs of nearby stage compounds. The voltage profile in this case, is essentially flat and stays below 80 mV *vs.* Li^+/Li. Although more positive voltage profile for Li-Al involves a slight voltage penalty, substantially higher capacity of Li-Al ensures higher energy density for cells with Li-Al anodes. Poor capacity retention is evident in reported data on the ambient temperature rechargeable batteries employing pure Al during repeated cycling over a large compositional range. The main reason for this drawback was the result of chemical and mechanical degradation

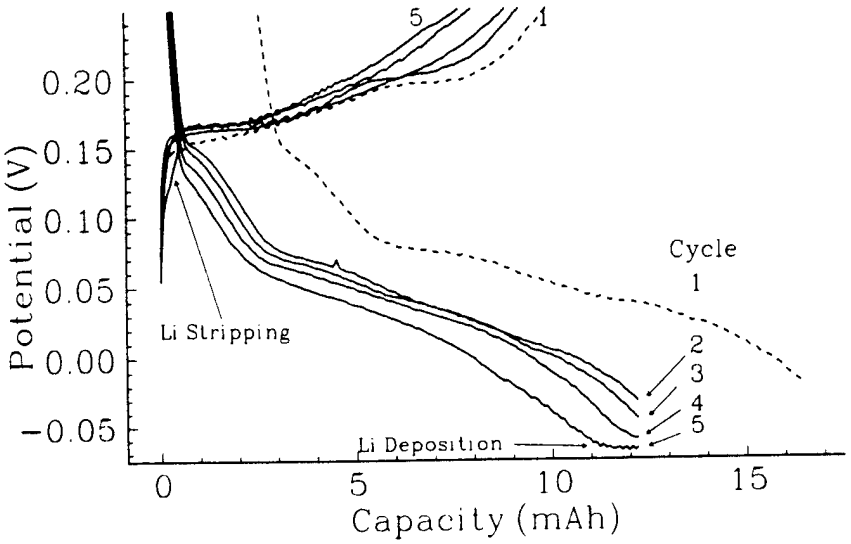

Figure 54. An expanded portion of the cycling curves for Li//SPE//Alfa Graphite Cell AA77. Theoretical capacity was 16.1 mAh (1.0 mol Li/(C_6)). Solid polymer electrolyte was ECBL1 (Table 7) The cathode was 51.0 w/o Alfa Graphite:3.0 w/o PAN:21.7 w/o EC:21.3 w/o γ-BL:3.0 w/o $LiAsF_6$. First cycle limits were 0.020V to 2.5V Li^+/Li. Starting from the second cycle the discharge was capacity limited at 12.2 mAh while, the upper limit was still 2.5V. Geometric area of the cathode was 10 cm^2, and the charge/discharge current density was 0.1 mA/cm^2.

processes that stemmed from poor diffusion of Li into the alloy bulk. We have attempted to circumvent these mechanical and other constraints relating to poor Li diffusion by using a composite of fine Al powder (<20 μm) dispersed mechanically in graphite and bound by an ion conductive SPE. The SPE binder was considered to provide an elastic matrix in which Al can always stay in contact with rest of the composite through significant changes in its size associated with deep cycling. Few selected results on this Al containing graphite composites are discussed next.

Depicted in Figure 55 are selected charge/discharge cycles of the Li//SPE//Composite half cell based on the Al/graphite/Chevron carbon binder composite and ECBL1 electrolyte (Table 7) performed at a current density of 0.1 mA/cm^2. A prominent plateau close to 0.4V on the charge profile is characteristic of the delithiation of Li-Al (α-β equilibria). Cell performance data corresponding to Figure 55 is presented in Table 14.

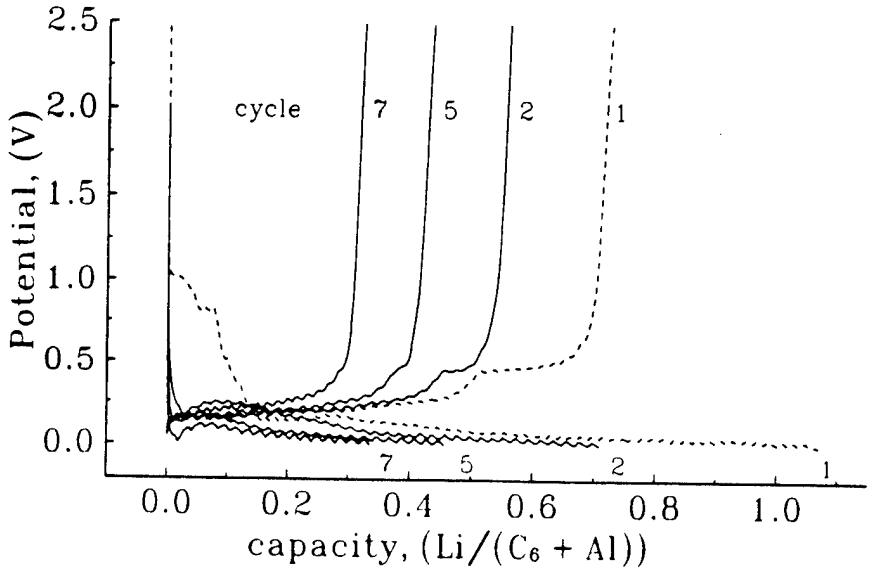

Figure 55. Cycling curves for Li//SPE//Al,Graphite Composite Cell AA31. Theoretical capacity was 19.0 mAh (10.0 mAh for graphite, 9.0 mAh for Al). Solid polymer electrolyte was ECBL1(Table 7). The cathode was 38.4 w/o Alfa Graphite:12.8 Al:1.3 w/o Chevron Carbon:3.2 w/o PAN:20.8 w/o EC:20.3 γ-BL:3.2 w/o $LiAsF_6$. Cathode geometric area was 10 cm^2, and the charge/discharge current density was 0.1 mA /cm^2.

Table 14. Cycling Data for Li//SPE//(Al,Graphite, Chevron Carbon Composite) Cell AA-31.

Cycle	Discharge (mAh)	Charge (mAh)	Specific Capacity Li/(C_6 + Al) Discharge/Charge	Ratio of Charge* Capacity/Initial Graphite Capacity
1	20.33	13.8	1.07/0.73	1.38
2	13.47	10.64	0.71/0.56	1.06
5	8.67	8.27	0.46/0.44	0.83
7	8.07	7.69	0.43/0.41	0.77
9	6.37	6.15	0.34/0.32	0.62
10	0.13	0.16	0.01/0.01	0.02

*Theoretical capacities of Alfa graphite and Al in the composite are 10.0 mAh and 8.9 mAh, respectively

Theoretical capacities corresponding to graphite and Al in the composite are close to 10.0 mAh and 8.9 mAh, respectively. These capacities were calculated by considering the actual electrode composition and the maximum capacities of each component, 1 Li/(C6) and 1 Li/(Al). Assuming a utilization of 1 mol Li per C_6 on the first charge, the capacity observed for the first charge (13.8 mAh) corresponds to about 43% first cycle reversibility for Al. On the 7th charge plateau around 0.4V has disappeared and the overall utilization has declined to about 80% of the expected graphite capacity. Utilization during charge continued to go down and from the 10^{th} cycle, the cell simply began to polarize repeatedly between the two preset voltage limits resulting in almost zero cell capacity. This behavior was consistently observed in repeated attempts. A failed cell was opened and examined under the microscope, and no defect other than the complete delamination of the composite layer was discovered. AC impedance spectroscopy of a failed cell however, showed a substantial increase in the intercept of the mid-frequency semicircle with the real axis indicating an increase in the charge transfer resistance. This is consistent with a serious passivation process involving both Al and graphite and it may very well be the cause for the cell to lose its capacity during latter part of cycling.

We also compared these results with those obtained for carbon/Al composite electrodes prepared by the solvent cast technique using the soluble polymer binder, poly(vinyl chloride-co-vinyl acetate). Fabrication procedure was identical to that used for the carbon electrodes discussed earlier in detail. They showed a moderate yet consistent improvement in specific capacity as well as the cycle life. The overall observations however, were parallel to those in Figure 55 and in Table 15. As before, following a steady decline, the rechargeable capacity suddenly dropped to near zero value accompanied by a large increase in the charge transfer resistance. The most significant finding is the fact that these carbon/aluminum composite electrodes have a significant potential to boost the overall specific capacity of the carbon anode.

3.5 Carbon//SPE//$Li_{1.1}Mn_2O_4$ Cells

3.5.1 Solid State Cells containing Electrodes made of Composites Hot-rolled onto Current Collectors. Having studied the rechargeability of the high voltage cathode material $Li_xMn_2O_4$ and the carbon anode separately we now have the opportunity to discuss the cycling behavior of Li-ion cells incorporating these electrodes. These cells are assembled in discharged state and they minimize the disadvantages of using a Li metal negative electrodes such as safety hazards and shorter cycle life associated with the use of pure metallic Li. Capacities of the anode and cathode are chosen by considering the first cycle charge/discharge characteristics of both $Li_{1.1}Mn_2O_4$ and carbon half-cells. For example, as shown in Figure 37 utilization of the cathode material remains at about 80% during the first charge (deintercalation) and the first discharge (intercalation) of the carbon half-cell shown in Figure 44 involves an equivalent capacity of about 1.2 mol Li per C_6 or 1.2 times the theoretical capacity of carbon. For a given carbon anode, the corresponding cathode capacity for a *balanced cell* can be calculated after allowing additional capacity to satisfy the irreversible capacity at the anode and also, to allow for its own maximum available charge depth of about 0.80%. Therefore, the calculated cathode capacity amounts to 1.5 times (1.2/0.80) that of the anode and the expected reversible capacity of the cell becomes equal to the

Table 15. Cycling Data for Li//SPE//Carbon Cell AAF1.

Cycle No.	Charge (mAh)	Discharge (mAh)	Charge/ Discharge Ratio	Specific Capacity Li/C_6 Charge/Discharge	Mid Capacity Voltage (Volt)	Energy Density (Whr/Kg)
1	21.12	16.32	1.29	1.20/0.92	3.855	68.5
2	15.76	15.44	1.02	0.89/0.88	3.855	64.8
5	14.40	14.32	1.01	0.81/0.82	3.857	60.2
25	11.46	11.65	0.98	0.64/0.66	3.827	48.6
50	9.16	9.41	0.97	0.52/0.53	3.745	38.4
120	7.59	7.59	0.99	0.43/0.43	3.765	3.1.

Pertinent Data for Calculating the Energy Density

Weight, g	Cathode laminate	0.325
	Anode laminate	0.093
	Ni shim (anode current collector)	0.275
	Al shim (cathode current collector)	0.075
	Solid polymer electrolyte (thickness - 4.5 mil, area - 10 cm^2 and density 1.3 g cm^{-3})	0.150
	Total	0.918

theoretical capacity of the anode. In practice, however, the cathode and the anode are chosen so that their capacity ratio remains within the range from 1.3 to 1.5 and as a result, the cell configuration will be slightly cathode limited. Capacity and cycling characteristics of a Alfa Graphite//SPE//$Li_{1.1}Mn_2O_4$ lithium-ion cell are shown in Figures 56 and 57. The cell was cycled between upper and lower limits of 4.25 and 2.65V, respectively, at 0.1 mA/cm^2. The anode and the cathode capacities were 17.7 mAh and 24.5 mAh, respectively, corresponding to a cathode to anode capacity ratio of 1.4.

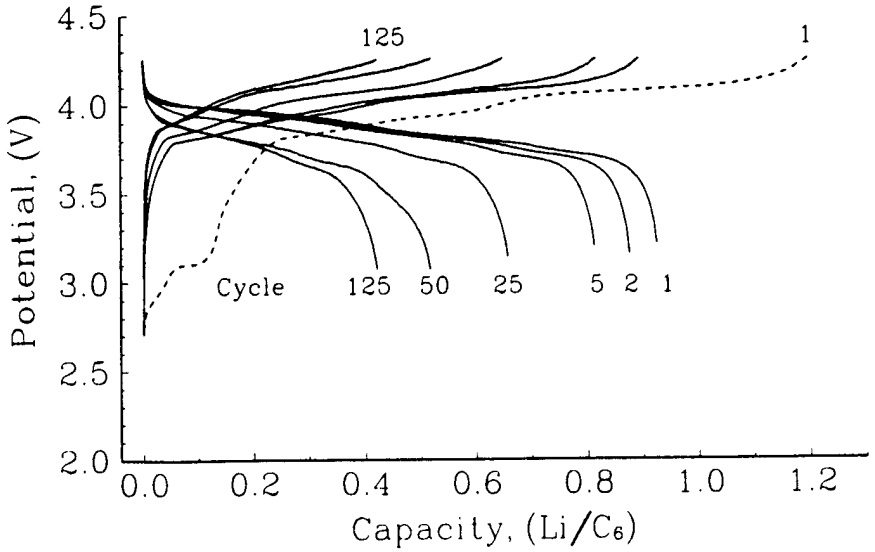

Figure 56. Cycling curves at room temperature for Alfa Graphite//SPE//$Li_{1.1}Mn_2O_4$ Cell AAF1. Respective cathode and anode capacities were 24.5 mAh (1 mol Li per $Li_{1.1}Mn_2O_4$) and 17.7 mAh (1 mol Li per C_6) corresponding to a cathode/anode capacity ratio of 1.4. Solid polymer electrolyte was ECBL1 (Table 7). The cathode was 51.0 w/o $Li_{1.1}Mn_2O_4$:3.0 PAN:17.7 w/o EC:17.3 w/o γ-BL:3.0 w/o $LiAsF_6$. The anode was 51.0 w/o Alfa Graphite:3.0 w/o PAN:21.7 w/o EC:21.3 w/o γ-BL:3.0 w/o $LiAsF_6$ SPE binder. Geometric area of both electrodes was 10 cm^2, and the charge/discharge current density was 0.1 mA/cm^2.

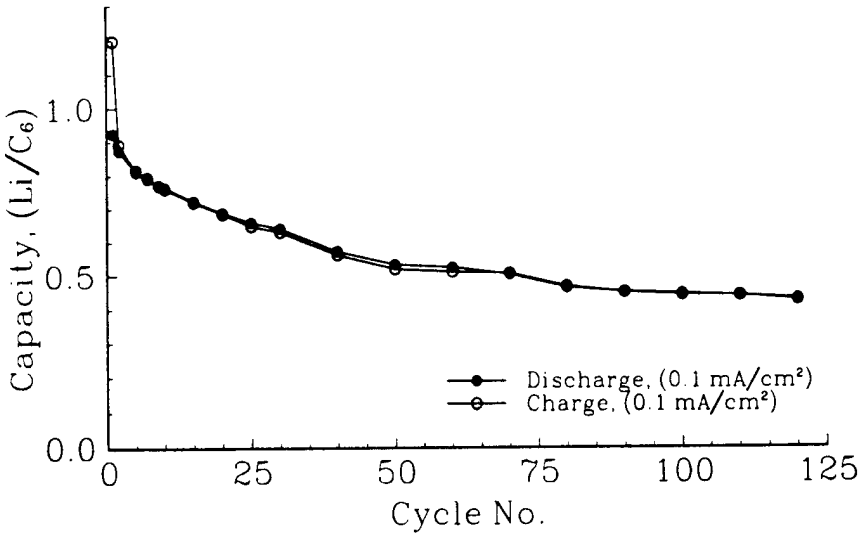

Figure 57. Capacity versus cycles for the cell shown in Figure 56.

Cell performance data corresponding to Figure 56 are summarized in Table 15. The first cycle charge capacity of 1.2 mol Li per C_6 corresponds close to 100% utilization of the carbon anode as expected for a balanced cell. Steady decline in the Li utilization observed for the individual cathode (Figure 39) and for the anode (Figure 45) in γ-BL containing electrolyte contributes to the steady fade in capacity depicted in Figure 56. Energy density of a cell can be optimized by the adjustment of a few key parameters such as the weight ratio of electroactive to electro-inactive materials, weight of the electrolyte film and, weight of the current collectors. No such effort was made in the present study.

3.5.2 Solid State Cells containing Compressed Electrodes Soaked in a Liquid Electrolyte. Capacity and cycling characteristics of a Alfa Graphite//SPE//$Li_{1.1}Mn_2O_4$ lithium-ion cell are shown in Figures 58 and 59. The cell was cycled between upper and lower limits of 4.25 and 2.65V, respectively, at 0.1 mA/cm^2. The anode and the cathode capacities were 31.15 mAh and 44.66 mAh, respectively, corresponding to a cathode to anode capacity ratio of 1.4.

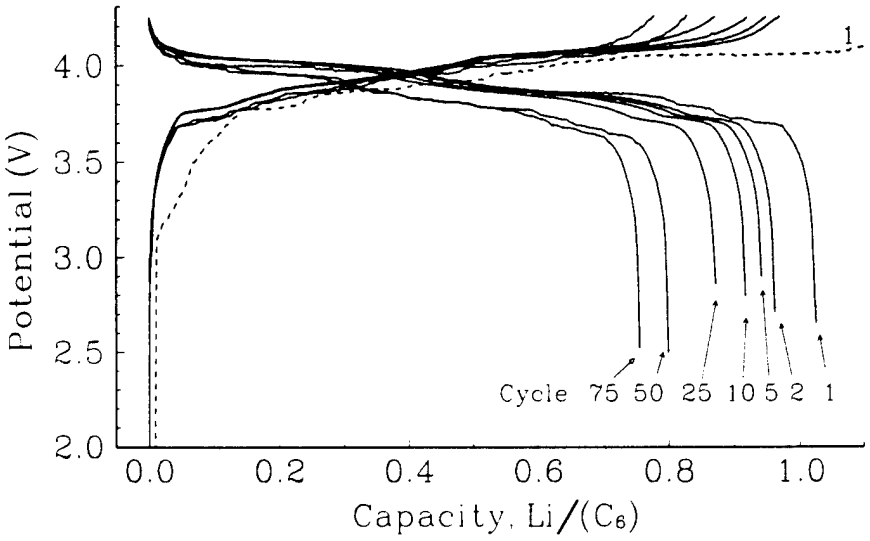

Figure 58. Cycling curves at room temperature for Alfa Graphite//SPE//$Li_{1.1}Mn_2O_4$ Cell AAF9. Cathode and anode capacities are 44.66 mAh (1 mol Li per $Li_{1.1}Mn_2O_4$) and 31.15 mAh (1 mol Li per C_6) corresponding to a cathode/anode capacity ratio of 1.4. Solid polymer electrolyte was DPC2 (Table 7). Dry cathode was 93.5 w/o $Li_{1.1}Mn_2O_4$:2.5 w/o PE:4.0 w/o Chevron Carbon. The dry anode was 93.0 w/o Alfa Graphite:5.0 w/o PVDF:2.0 w/o Chevron carbon. Soaking electrolyte was DPCX (Table 7). Respective geometric areas of the cathode and anode were 10 and 11.3 cm^2 and the charge/discharge current density was 0.1 mA/cm^2.

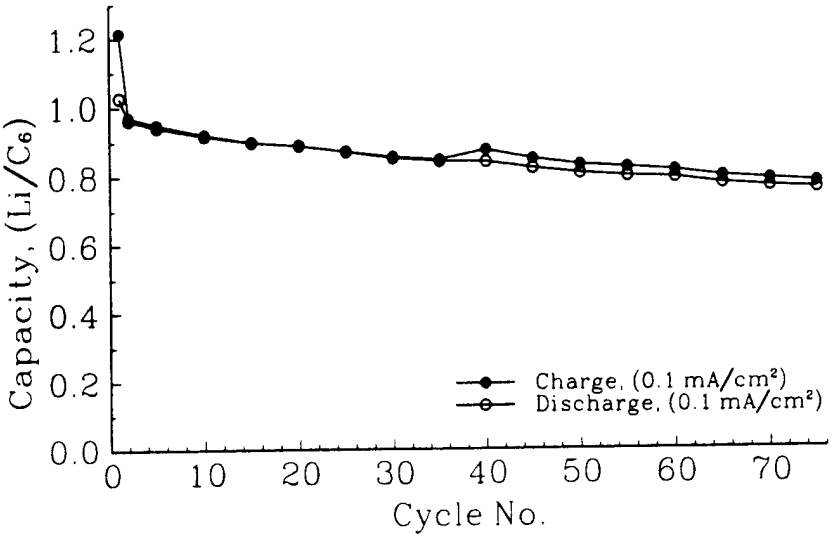

Figure 59. Capacity versus cycles for the cell shown in Figure 58.

Figures 58 and 59 illustrate a cell with good Li reversibility and cycle life. Relatively sharp potential change at the end of a charge step (Figure 58) indicates the full utilization of the cathode charge capacity. A ratio of cathode to anode capacities of 1.4 implies that the cell is properly balanced in terms of the initial capacities of each electrode. Cycling was done close to C/30 rate relative to the original anode capacity. The Li utilization corresponds to the first charge through the second charge is as summarized below. Li_x^{IRR} is the first cycle irreversible loss of Li at the anode which is close to 0.2 mol Li per C_6 as anticipated.

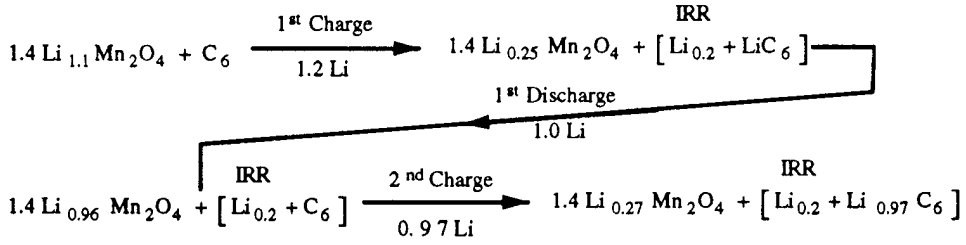

The cell appeared to be cycling normally through Cycle 50. From Cycle 2 onwards the capacity fade rate was uniform and approached 0.3% per cycle. Judging from the amount of Li transferred in and out from an electrode during each cycle, Li irreversibility appears to be greater at the cathode. The advantage of using dense (compressed) electrodes supporting a liquid electrolyte in a Li-ion cell is clearly evident from the data in Table 16. Characteristics of a similar cell at higher current density is depicted in Figures 60 and 61 and Table 17.

Table 16. Cycling Data for Alfa Graphite//SPE//$Li_{1.1}Mn_2O_4$ Cell, AAF9 at Low Rate.

Cycle No.	Charge (mAh)	Discharge (mAh)	Charge/Discharge Ratio	Specific Capacity Li/C_6 Charge/Discharge	Mid Discharge Voltage (Volt)	Energy Density (Whr/Kg)
1	37.02	31.92	1.16	1.21/1.03	3.890	141.9
2	30.22	29.97	1.01	0.97/0.96	3.915	134.1
5	29.56	29.31	1.01	0.95/0.94	3.912	131.0
10	28.66	28.53	1.00	0.92/0.92	3.905	127.3
25	27.13	27.13	1.00	0.87/0.87	3.902	121.0
50	25.79	25.01	1.03	0.83/0.80	3.827	109.4

Pertinent Data for Calculating the Energy Density

Weight, g	Cathode laminate (dry, 5.0 mil thick)	0.313
	Anode laminate (dry, 1.9 mil thick)	0.085
	Soaked in liquid electrolyte (anode estimated)*	0.018
	Soaked in liquid electrolyte (cathode estimated)*	0.054
	Cu mesh (anode current collector)	0.163
	Al mesh (cathode current collector)	0.092
	Solid polymer electrolyte (Thickness - 4.0 mil, Area - 2.7X4.2 cm^2 and Density 1.3 g cm^{-3})	0.150
	Total	0.875

*Weight of the soaked-in electrolyte was calculated from the difference between the total volume of each component and the actual volume of each electrode laminate. Composition of the composites are as given in the figure caption. Densities used were 4.26 g/cm^3 ($Li_xMn_2O_4$), 2.25 g/cm^3 (Carbon), 0.92 g/cm^3 (PE), 1.77 g/cm^3 (PVDF), 1.30 g/cm^3 (solid polymer electrolyte) and, 1.38 g/cm^3 (soaked-in liquid electrolyte). Thickness of the electrode laminate was the difference between the actual electrode thickness and that of the uncompressed shim itself. Weight of the electrodes leads and the cell cover was not included). Densities of Chevron carbon and Alfa graphite were taken as 2.25 g/cm^3 instead of the measured values of 1.42 and 1.6 g/cm^3, to account for the electrolyte incorporated in the pores of each carbon material.

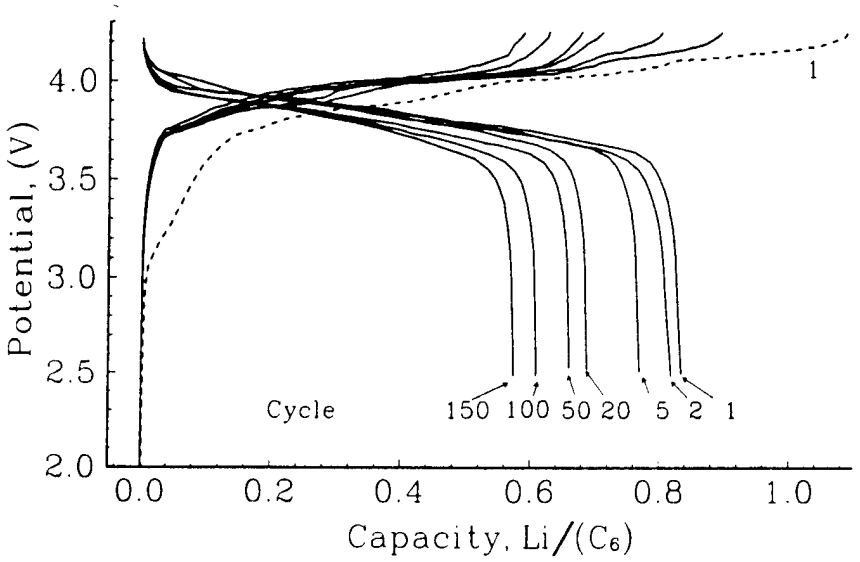

Figure 60. Cycling curves at room temperature for Alfa Graphite//SPE//$Li_{1.1}Mn_2O_4$ Cell AAF22. Cathode and anode capacities are 39.7 mAh (1 mol Li per $Li_{1.1}Mn_2O_4$) and 28.7 mAh (1 mol Li per C_6) with a cathode/anode capacity ratio of 1.4. Solid polymer electrolyte was DPC2 (Table 7). Dry cathode was 93.5 w/o $Li_{1.1}Mn_2O_4$:2.5 w/o PE:4.0 w/o Chevron Carbon. The dry anode was 93.0 w/o Alfa Graphite:5.0 w/o PVDF:2.0 w/o Chevron carbon. Soaking was DPCX (Table 7). Respective geometric areas of the cathode and anode were 10 and 11.3cm^2 and the charge (discharge) current density was 0.4 (0.8) mA/cm^2.

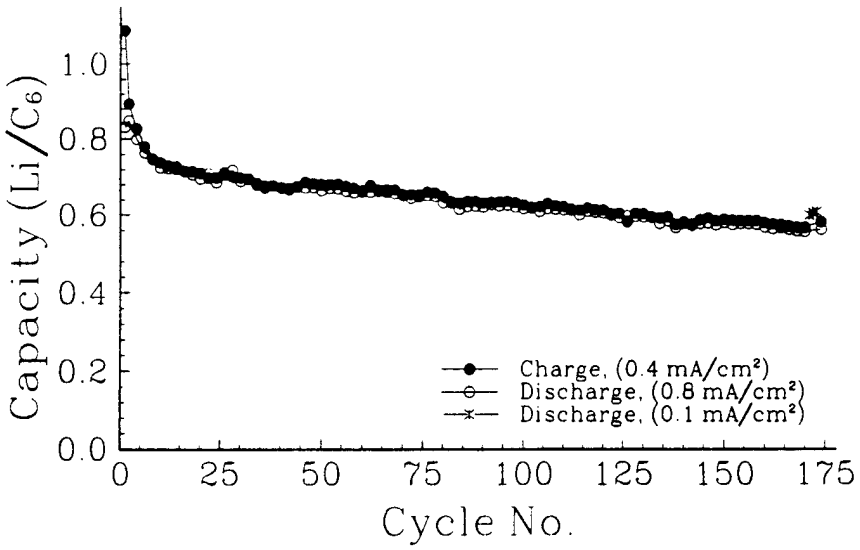

Figure 61. Capacity versus cycles for the cell shown in Figure 60.

Table 17. Cycling Data for Alfa Graphite//SPE//$Li_{1.1}Mn_2O_4$ Cell AAF22 at C/3 Discharge rate

Cycle No.	Charge (mAh)	Discharge (mAh)	Charge/Discharge Ratio	Specific Capacity Li/C_6 Charge/Discharge	Mid Discharge Voltage (Volt)	Energy Density (Whr/Kg)
1	31.12	23.85	1.30	1.08/0.83	3.806	106.5
2	25.62	24.33	1.05	0.89/0.85	3.827	109.3
5	23.01	23.57	0.98	0.80/0.82	3.834	106.1
20	20.37	19.95	1.02	0.71/0.70	3.849	90.1
50	19.52	19.05	1.02	0.68/0.66	3.815	85.3
100	17.99	17.61	1.02	0.63/0.61	3.823	79.0
150	16.89	16.64	1.02	0.59/0.58	3.815	74.5

Pertinent Data for Calculating the Energy Density

Weight, g	Cathode laminate (dry, 4.8 mil thick)	0.287
	Anode laminate (dry, 1.7 mil thick)	0.083
	Soaked in liquid electrolyte (anode estimated)*	0.016
	Soaked in liquid electrolyte (cathode estimated)*	0.061
	Cu mesh (anode current collector)	0.163
	Al mesh (cathode current collector)	0.092
	Solid polymer electrolyte (Thickness - 4.0 mil, Area - 2.7X4.2 cm^2 and Density 1.3 g cm^{-3})	0.150
	Total	0.852

See footnote below Table 16.

The cell was charged at C/6 and discharged at C/3 rate with respect to the initial anode capacity. Capacity fade, substantial during the few initial cycles, slowed down to a very low 0.1% per cycle and remained constant until the cycling was terminated intentionally. Lowering the charge/discharge rate to 0.1 mA/cm^2 in the 170th cycle resulted in a very modest (~6%) increase in the Li utilization. This suggests that the capacity decline observed in the cell was of materials origin and not related to a polarization phenomenon occurring at high rate. Despite the slow capacity fade, the cell demonstrates important attributes such as efficient and reversible utilization of Li at high rate, high energy density and the potential to achieve a long cycle life.

Shown in Figures 62 and 63 are the cycling performance at high rate of a Li-ion cell based on Conoco Coke.

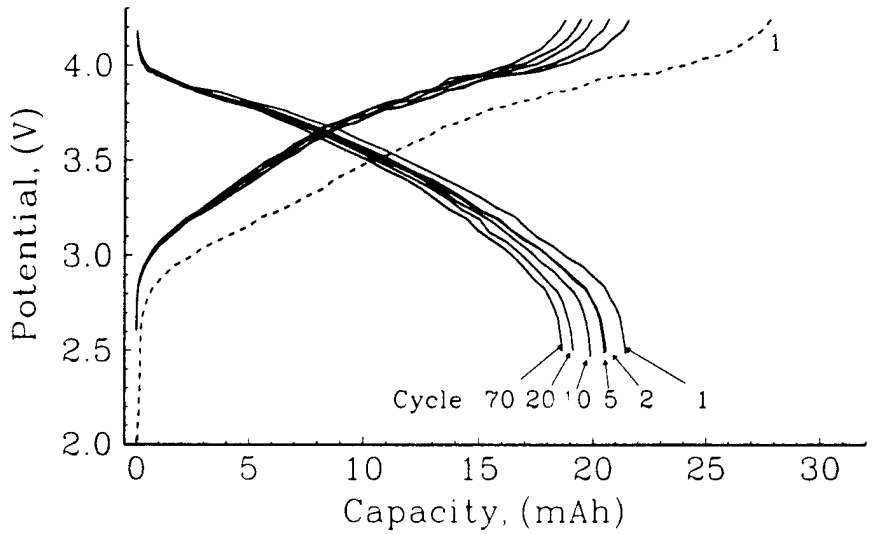

Figure 62. Cycling curves at room temperature for Conoco Coke//SPE//$Li_{1.1}Mn_2O_4$ Cell AAF25. Cathode and anode capacities are 34.9 mAh (1 mol Li per $Li_{1.1}Mn_2O_4$) and 30.4 mAh (1 mol Li per C_{12}) with a cathode/anode capacity ratio of 1.15. Solid polymer electrolyte was DPC2 (Table 7). Dry cathode was 93.5 w/o $Li_{1.1}Mn_2O_4$:2.5 w/o PE:4.0 w/o Chevron Carbon. The dry anode was 95.4 w/o Conoco Coke:2.6 w/o PVDF:2.1 w/o Chevron carbon. Soaking electrolyte was DPCX (Table 7). Respective geometric areas of the cathode and anode were 10 and 11.3 cm^2 and the charge (discharge) current density was 0.4 (0.8) mA/cm^2.

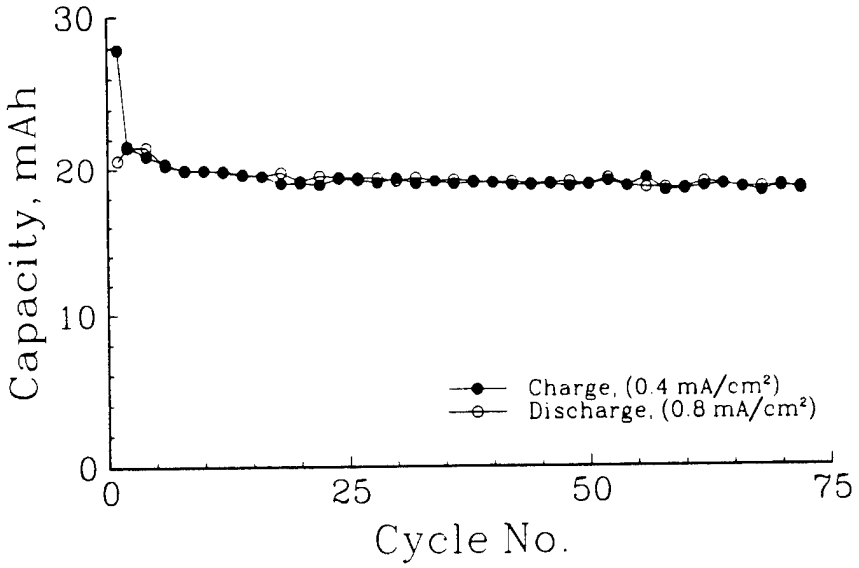

Figure 63. Capacity versus cycles for the cell shown in Figure 61.

Low cathode to anode capacity ratio of 1.15 featured in Cell No. AAF25 represents a severely cathode limited configuration. Assuming a cathode utilization of 0.8 mol Li per $Li_{1.1}Mn_2O_4$ during the first charge and a first cycle irreversible capacity of 0.2 mol Li per C_{12} for the anode, the first cycle discharge is expected to be about 0.7 mol Li (1.15x0.8 - 0.2) per C_{12} or close to 21 mAh. Data in Figure 63 agrees with this expected Li utilization during the first discharge. A very low capacity fade, potentially high cycle life and a high rate capability are featured in Figure 63.

4.0 CONCLUSIONS

PAN-based electrolytes with improved low temperature conductivity can be prepared with the use of carefully selected plasticizer compositions from ternary solvent mixtures consisting of propylene carbonate (PC), ethylene carbonate (EC) and butylene carbonate (BC) or PC, EC and 3-methyl-2-oxazolidinone (MEOX). All of the electrolytes were prepared as free standing films with a thickness of ~4.5 mil. A number of solid polymer electrolytes (SPE) compositions potentially important for ambient temperature applications were identified. The SPE composition with 21.0 m/o PAN:37.8 m/o EC:22.9 m/o PC:12.3 m/o BC:6.0 m/o $LiAsF_6$ exhibited conductivities of 1.1 x 10^{-4} ohm^{-1} cm^{-1} at -40°C and 2.9 x 10^{-3} ohm^{-1} cm^{-1} at 25°C. Two other electrolytes contained MEOX; one with 21.0 m/o PAN:33.8 m/o EC:27.7 m/o PC:11.5 m/o MEOX:6.0 m/o $LiAsF_6$ showed conductivities of 1.14 x 10^{-4} ohm^{-1} cm^{-1} at -40°C and 2.98 x 10^{-3} ohm^{-1} cm^{-1} at 25°C and the other with 21.0 m/o PAN:10.8 m/o EC:8.7 m/o PC:53.4 m/o MEOX:6.0 m/o $LiAsF_6$ had conductivities of 1.56 x 10^{-4} ohm^{-1} cm^{-1} at -40°C and 3.10 x 10^{-3} ohm^{-1} cm^{-1} at 25°C.

Cyclic voltammetry indicated good stability to oxidation for the electrolytes with small oxidative currents of the order of 0.5 $\mu A/cm^2$ at 4.2V vs. Li^+/Li on Al. The oxidation current was electrode substrate dependent. For example, Pt, Ni and carbon showed oxidative currents of the order of 1, 30 and 60 $\mu A/cm^2$, respectively, at the same potential. Alloy formation and plating were evident on aluminum at 0.15V and -0.20V, respectively. Platinum showed similar behavior with alloy formation at 0.45V and Li plating at 0.05V. Carbon showed an onset of lithium intercalation around 1.5V followed by Li plating at -0.1V. Nickel, on the other hand, showed a simple lithium plating-stripping process at -0.05V and 0.15V vs. Li^+/Li, respectively. Al was found to be the material of choice for the cathode current collector whereas, Ni was suitable for the anode current collector.

Investigation of the rechargeability of the Li//SPE//$Li_{0.9}Mn_2O_{4.2}$ cell showed short cycle life with electrolytes containing BC with cell failure caused by internal "soft shorts" on charge. In contrast, cells with MEOX-containing polymer electrolytes, showed vastly improved cyclability with either of the two low voltage (3V) lithiated manganese dioxides, $Li_{0.9}Mn_2O_{4.2}$ and $Li_{1.0}Mn_2O_{4.7}$. Cycling at room temperature, a typical Li/$Li_{0.9}Mn_2O_{4.2}$ cell retained more than 80% of the second cycle capacity corresponding to ~0.5 Li/$Li_{0.9}Mn_2O_{4.2}$ through 140 cycles at 0.1 mA/cm^2. $Li_{1.0}Mn_2O_{4.7}$ too showed long-term cyclability with a capacity close to 0.5 Li/ $Li_{1.0}Mn_2O_{4.7}$ at the Cycle 200. Long-term cyclability was also demonstrated for Li/$Li_{1.1}Mn_2O_4$ (spinel) cells utilizing solid electrolytes containing MEOX. In this case, a capacity of about 0.8 Li per $Li_{1.1}Mn_2O_4$ was observed. The capacity diminished with repeated cycling at a rate of about 0.17% per cycle from Cycles 20 to 120. The spinel $Li_{1.1}Mn_2O_4$ was able to intercalate additional Li at a lower voltage plateau around 2.8V. Even though the spinel material showed long-term cyclability in a broader voltage window, 4.2V to 2.0V encompassing both higher and lower voltage plateaus, the capacity fade rate was a relatively high 0.3% per cycle.

The Li/$Li_xMn_2O_4$ (3V) cell showed low temperature cyclability with diminished capacity. The utilization at -10°C was close to 0.3 Li $Li_{1.0}Mn_2O_{4.7}$ and at -20°C it dropped to about 0.2 Li/ $Li_{1.0}Mn_2O_{4.7}$. This reduced capacity could be due to the effect of changing charge transfer resistance at the $Li_{1.0}Mn_2O_{4.7}$/electrolyte interface which was found to increase exponentially with decreasing temperature.

Rechargeability of commercially available carbons such as graphite, coke and acetylene black was demonstrated in a variety of electrolytes. Carbons sowed no rechargeability in cells based on SPE containing MEOX. Vastly improved cyclability was observed for all carbons when PAN-EC-BL/$LiAsF_6$ electrolytes were used. For example, a cell with 21.0 m/o PAN:36.5 m/o EC:36.5 m/o BL:6.0 m/o $LiAsF_6$ at room temperature showed an equivalent capacity of 1.15 Li/(C_6) during the first discharge and ~1.0 Li/(C_6) during the first charge and the next few charge/discharge cycles. The cell capacity declined slightly with continual cycling and at Cycle 15 the charge/discharge capacity was equivalent to 0.85 Li/(C_6). Long-term cycling was also possible with the Carbon//SPE//$Li_{1.1}Mn_2O_4$ Li-ion cell employing the PAN-EC-BL/$LiAsF_6$ electrolytes. Slow capacity fading with repeated cycling appeared to be a persistent problem. In this case, the capacity faded from 0.92 mol Li per C_6, observed during the first discharge, to 0.52 in Cycle 50.

Capacity decline was observed on repeated cycling in Li/Carbon cells employing a variety of solid polymer electrolytes. In a three electrode cell, impedance of the composite carbon cathode taken at the end of a full discharge indicated that, no significant change occurs in the bulk resistance of the composite carbon electrode during repeated cycling. Observed increase in the charge transfer resistance, R_{ct} with each discharge was consistent with a growing passivation layer on the carbon surface.

A procedure referred to in the text as *hot-pressing* was developed to prepare electrodes for Li and Li-ion cells. Instead of a usual polymer electrolyte binder, these electrodes contained a liquid electrolyte soaked into them. Significantly improved capacity retention during cycling was observed for hot-pressed carbon electrodes. For example, a Li/graphite cell utilizing the PAN-EC-BL/$LiPF_6$ polymer electrolyte and a hot-pressed graphite electrode which was soaked in the EC-DPC/$LiPF_6$ liquid electrolyte, showed a reversible capacity of nearly 0.9 Li/C_6 at C/20 rate up to the Cycle 20. Likewise, a reversible Li utilization better than 0.4 mol per C_6 was observed through the 50th cycle for a Li/coke cell assembled in a similar fashion. Improved capacity retention, rate capability and cycle life were also observed for Li-ion cells employing hot pressed carbon anodes and $Li_{1.1}Mn_2O_4$ cathodes. A typical graphite Li-ion cell discharged at C/30 rate showed a uniform capacity fade rate from the Cycle 2 onwards approaching 0.3% per cycle with a reversible Li utilization of over 0.8 mol Li/C_6 through the Cycle 50. Initial specific energy of this cell approached 142 Wh/kg. At C/3 discharge rate, the capacity fade rate was a low 0.1% per cycle through the Cycle 170 and the corresponding capacity remained at 0.6 mol Li per C_6. Initial specific energy of this cell was estimated to be close to 106 Wh/kg. Cycling performance at high rate (C/3) of a Li-ion cells based on hot-pressed coke also showed superior capacity retention and a negligible rate of capacity fade through Cycle 75.

5.0 REFERENCES

1. Abraham, Applications of Electroactive Polymers, B. Scrosati, Editor, Chapter 3, Chapman and Hall, London (1993).

2. Alamgir and K. M. Abraham, Lithium Batteries - New Materials, Development and Perspectives, Vol. 5, Industrial Chemistry Libraries, G. Pistoia, Editor, Elsevier, New York (1994).

3. Abraham and M. Alamgir, *J. Electrochem. Soc.*, **136,** 1657 (1990).

4. Practical Lithium Batteries, Y. Matsuda and C. R. Schlaikjer, Editors, JEC Press, Inc., Cleveland, OH (1988).

5. V. R. Koch and S. B. Brummer, *Electrochim. Acta*, **23**, 55 (1978).

6. A. N. Dey, *J. Electrochem. Soc.*, **118,** 1547 (1971).

7. K. M. Abraham, *Electrochim. Acta*, **38**, 1233 (1993).

8. B. M. L. Rao, R. W. Francis, and H. A. Christopher, *J. Electrochem. Soc.*, **124,** 1490 (1977).

9. J. Dahn, A. K. Sleigh, H. Shi, W. J. Weydanz, Lithium Batteries - New Materials, Development and Perspectives, Vol. 5, Industrial Chemistry Libraries, G. Pistoia, Editor, Elsevier, New York (1994).

10. J. C. Cessna, *Corrosion,* **27**, 244 (1971).

11. D. R. Cogley and J. M. Butler, *J. Phys. Chem.*, **72**, 4568 (1968).

12. D. Aurbach, M. L. Daroux, P. Faguy and E. B. Yeager, *J. Electrochem. Soc.*, **134**, 1611 (1987).

13. D. Aurbach, Y. Gofer, M. Ben-Zion and P. Aped, *J. Electroanal. Chem.*, **339,** 451 (1992).

14. E. Peled, *J. Electrochem. Soc.*, **126**, 2047 (1979).

15. Y. Geronov, F. Schwager and R. H. Muller, in *"Proceedings of the Workshop on Lithium Nonaqueous Battery Electrochemistry"*, E. B. Yeager, B. Schumm, Jr., G. Blomgren, D. R. Blankenship, V. Leger and J. Akridge, Editors, P. 115, Cleveland, OH, June 4-6, 1980.

16. G. Nagasubramanian, A. I. Attia and G. Halpert, *J. Appl. Electrochem.*, **24**, 298 (1994).

17. G. E. Lagos, N. Bonanos and B. C. H. Steele, *Electrochimica. Acta*, **28**, 1581 (1983).

18. D. Aurbach and Z. Zaban, *J. Electrochem. Soc.*, **141**, 1808 (1994).

ARMY RESEARCH LABORATORY
PHYSICAL SCIENCES DIRECTORATE
MANDATORY DISTRIBUTION LIST

August 1995

Defense Technical Information Center*
ATTN: DTIC-OCC
8725 John J. Kingman Rd STE 0944
Fort Belvoir, VA 22060-6218
(*Note: Two DTIC copies will be sent from STINFO office, Ft Monmouth, NJ)

Director
US Army Material Systems Analysis Actv
ATTN: DRXSY-MP
(1) Aberdeen Proving Ground, MD 21005

Commander, AMC
ATTN: AMCDE-SC
5001 Eisenhower Ave.
(1) Alexandria, VA 22333-0001

Director
Army Research Laboratory
ATTN: AMSRL-D (John W. Lyons)
2800 Powder Mill Road
(1) Adelphi, MD 20783-1197

Director
Army Research Laboratory
ATTN: AMSRL-DD (COL Thomas A. Dunn)
2800 Powder Mill Road
(1) Adelphi, MD 20783-1197

Director
Army Research Laboratory
2800 Powder Mill Road
Adelphi, MD 20783-1197
(1) AMSRL-OP-SD-TA (ARL Records Mgt)
(1) AMSRL-OP-SD-TL (ARL Tech Library)
(1) AMSRL-OP-SD-TP (ARL Tech Publ Br)

Directorate Executive
Army Research Laboratory
Physical Sciences Directorate
Fort Monmouth, NJ 07703-5601
(1) AMSRL-PS
(1) AMSRL-PS-T (M. Hayes)
(1) AMSRL-OP-FM-RM
(22) Originating Office

Advisory Group on Electron Devices
ATTN: Documents
Crystal Square 4
1745 Jefferson Davis Highway, Suite 500
(2) Arlington, VA 22202

Commander, CECOM
R&D Technical Library
Fort Monmouth, NJ 07703-5703
(1) AMSEL-IM-BM-I-L-R (Tech Library)
(3) AMSEL-IM-BM-I-L-R (STINFO Ofc)

ARMY RESEARCH LABORATORY
PHYSICAL SCIENCES DIRECTORATE
SUPPLEMENTAL DISTRIBUTION LIST
(ELECTIVE)

Deputy for Science & Technology
Office, Asst Sec Army (R&D)
(1) Washington, DC 20310

HQDA (DAMA-ARZ-D/
Dr. F.D. Verderame)
(1) Washington, DC 20310

Director
Naval Research Laboratory
ATTN: Code 2627
(1) Washington, DC 20375-5000

USAF Rome Laboratory
Technical Library, FL2810
ATTN: Documents Library
Corridor W, STE 262, RL/SUL
26 Electronics Parkway, Bldg 106
Griffiss Air Force Base
(1) NY 13441-4514

Dir, ARL Battlefield
Environment Directorate
ATTN: AMSRL-BE
White Sands Missile Range
(1) NM 88002-5501

Dir, ARL Sensors, Signatures,
Signal & Information Processing
Directorate (S3I)
ATTN: AMSRL-SS
2800 Powder Mill Road
(1) Adelphi, MD 20783-1197

Dir, CECOM Night Vision/
Electronic Sensors Directorate
ATTN: AMSEL-RD-NV-D
(1) Fort Belvoir, VA 22060-5806

Dir, CECOM Intelligence and
Electronic Warfare Directorate
ATTN: AMSEL-RD-IEW-D
Vint Hill Farms Station
(1) Warrenton, VA 22186-5100

Cdr, Marine Corps Liaison Office
ATTN: AMSEL-LN-MC
(1) Fort Monmouth, NJ 07703-5033